ANAEROBIC DIGESTER MODELLING FOR PRODUCTION OF BIOGAS FROM WASTE HAZELNUT HUSK

A Thesis Submitted to
the Graduate School of
İzmir Institute of Technology
in Partial Fulfillment of the Requirements for the Degree of

MASTER OF SCIENCE

in Chemical Engineering

by
Ozan DEMİR

July 2022
İZMİR

ACKNOWLEDGMENTS

Although bachelor's degree is the first step of the academia, master's degree can be considered the beginning of being a researcher. Therefore, it is mandatory for me to thank those who have guided and supported me in this special journey of my life. First of all, I have to express my utmost respect to my advisor Prof. Dr. Erol ŞEKER, who has made me gain different point of view and been with me every time I failed. I cannot tell how grateful I am for all he taught me. It would not be possible to make this work without his support, and the values to become a better researcher will always be with me in my latter journeys.

Beside my advisor, I also want to particularly thank my colleagues Cem KARACASULU, Emre DEĞİRMENCİ, Özgür Enes TAYTAŞ and Majid AHMADOV for their supports during this period. It was always valuable to make brainstorming with them, and this study totally reflects their contribution.

Nothing would be possible if I did not have my family's support behind me. Especially my mother's, Hatice DEMİR, belief in me and her endless faith were precious. I have to show my gratitude to her specifically. Also, my father Sait DEMİR, my brothers Engin DEMİR and Muhammet Enes DEMİR, my sister Özlem DEMİR, and lastly, my uncle İsmail DEMİR deserve to be thankful to with their presence every time I needed.

Lastly, I must thank my dear friend, Milica NINKOVIĆ, who has always been with me whenever I struggled, and always believed in me in my hard times. The motivation she has given me made any difficulties small.

ABSTRACT

ANAEROBIC DIGESTER MODELLING FOR PRODUCTION OF BIOGAS FROM WASTE HAZELNUT HUSK

Anaerobic digestion is a degradation process of complex organic matters into methane and carbon dioxide in an oxygen-free environment maintained by microorganisms. An advantage, besides energy production, is it is a waste management technique. Hazelnut husk is a valuable raw material for the anaerobic digestion process with more than 55 % cellulose and hemicellulose content. Anaerobic Digestion Model No. 1 (ADM1) developed by IWA Group was used in this study. This master thesis modeled biogas production by co-digestion of cattle manure and hazelnut husk process in MATLAB. The goal was to evaluate the methane amount of a household bioreactor. Tanks-in-series model with 3 CSTRs was chosen after residence time distribution (RTD) analysis.

Ten different cases were investigated to show the effects of carbon source/manure ratio, temperature, carbon source type, total solid (TS) amount, reactor type, and RTD analysis. The carbon source/manure ratio improves the methane yield as it increases. When the ratio is 1, methane yield is 0.229 L/kgVS whilst yield is 0.224 L/kgVS if the ratio is 0.1. The temperature effect on the process is significant. In the thermophilic case, the methane production is 0.432 L/d which is the highest amount compared to mesophilic and psychrophilic cases. When food waste is used as a carbon source with a ratio of food waste/manure of 0.1, the methane production is 0.410 L/d while it is 0.403 L/d in hazelnut husk digester. When the TS amount is doubled, the methane yield goes down from 0.224 to 0.149 L/kgVS because the residence time is not long enough to digest it as well as in case with lower total organic carbon level. In unmixed, mixed, and Chinese Dome Digester types of reactors, methane productions are 0.403, 0.646, and 0.552 L/d, respectively. In the ideal case, the methane production is 1.525 L/d which indicates the necessity of RTD analysis.

ÖZET

ATIK FINDIK KAPÇIĞINDAN BİYOGAZ ÜRETİMİ İÇİN HAVASIZ ÇÜRÜTÜCÜ MODELLEMESİ

Anaerobik çürütme, mikroorganizmalar tarafından sağlanan oksijensiz bir ortamda karmaşık organik maddelerin metan ve karbondioksite bozunma sürecidir. Enerji üretiminin yanı sıra bir avantajı da atık yönetimi tekniği olmasıdır. Fındık kapçığı, %55'ten fazla selüloz ve hemiselüloz içeriği ile anaerobik çürütme işlemi için değerli bir hammaddedir. Bu çalışmada IWA Group tarafından geliştirilen Anaerobik Sindirim Modeli No. 1 (ADM1) kullanılmıştır. Bu yüksek lisans tezi, MATLAB'da sığır gübresi ve fındık kabuğu prosesinin birlikte çürütülmesiyle biyogaz üretimini modellemiştir. Çalışmanın amacı, bir ev tipi biyoreaktörün metan miktarını değerlendirmektir. Bekleme süresi dağılımı (RTD) analizinden sonra 3 seri bağlı CSTR modelinin uygun olduğu görülmüştür.

Karbon kaynağı/gübre oranı, sıcaklık, karbon kaynağı türü, toplam katı (TS) miktarı, reaktör türü ve RTD analizinin etkilerini göstermek için 10 farklı durum incelenmiştir. Karbon kaynağı/gübre oranı arttıkça metan verimi de artar. Oran 1 olduğunda metan verimi 0.229 L/kgVS, oran 0.1 ise verim 0.224 L/kgVS'dir. Proses üzerindeki sıcaklığın etkisi önemlidir. Termofilik durumda metan üretimi 0,432 L/d ile mezofilik ve psikrofilik durumlara göre en yüksek miktardır. Gıda atığı/gübre oranı 0.1 olan reaktörde, gıda atıkları karbon kaynağı olarak kullanıldığında metan üretimi 0.410 L/d iken fındık kabuğu kullanılan çürütücüde 0.403 L/d'dir. TS miktarı iki katına çıkarıldığında, metan verimi 0.224'ten 0.149 L/kgVS'ye düşer, çünkü kalış süresi onu sindirmek için yeterince uzun değildir. Karışmamış, karışık ve Chinese Dome Digester tipi reaktörlerde metan üretimleri sırasıyla 0.403, 0.646 ve 0.552 L/d'dir. İdeal durumda metan üretimi 1.525 L/d'dir ve bu da RTD analizinin gerekliliğini gösterir.

TABLE OF CONTENTS

LIST OF FIGURES

Figure **Page**

Figure **Page**

LIST OF TABLES

Table **Page**

CHAPTER 1

INTRODUCTION

Energy need has been one of the most substantial concerns of humanity since the discovery of controlled fire. Although many animals have a special interest in fire, only humankind could achieve to control it. They used it against the threats of animals in the wilderness in order to protect themselves and maintain their own existence. However, other than safety problems, they had to survive through harsh conditions such as freezing weather, and fire provided them with a friendly environment. With the controlled fire, people met energy source which was mostly wood. Since the energy source ran out, they had to learn how to manage them, and where to find them. This historical process began with harnessing fire was the first test of mankind in satisfaction of energy needs aspect.

The Discovery of controlled fire speeded up the evolution of humans in many ways such as cooking. Especially more civilized nations had to find new energy sources instead of immigrating into where energy source (i.e., wood) was already present, unlike nomads. It is known that the Chinese people were the first society who used coal for cooking and heating nearly 3,000 years ago (Kentucky Foundation 2007). Although this was a great novelty, coal was not the only energy source in those days. People used to benefit from the power of water in a stream or a river, and they built water wheels in order to obtain energy and for irrigation, too. Around 6,000 years ago, the first water wheel was thought to be built (Bellis 2019). However, the first known water wheel, a.k.a. Noria, was built in nearly 2,400 years ago (Noria Corporation 2008). Other than coal and water energy, people in Iran and Afghanistan found a way to make use of wind. They built the first known windmill in order to grind grain and produce flour, and pump water approximately a thousand years ago (Shahan 2014). Main energy sources around the world were coal, water, and wind energy, however, coal became much more popular than others because, in the last quarter of the 17th century, an enormous amount of coal was discovered in North America by French explorers (Kentucky Foundation 2007). In 1760, a new age called the industrial revolution began in Great Britain, and new manufacturing processes developed such as steam engines (White 2009). Mostly, they used to make use of coal in order to meet their energy needs. Coal had ruled the energy industry for nearly

150 years, but a more efficient energy source which is natural gas unthroned it. A man named William Hart noticed bubble formation on the surface of a creek and thought there might have been a gas source under that waterbody. Then, he dug the first ever natural gas well in Fedonia, New York in 1821 (Natural Gas 2013). The industrial revolution did not slow down because Michael Faraday made a spectacular invention in 1831 which was an electricity generator (Age of Revolution 2019). That simple device is made of a coil of a wire whose electrons are excited by the magnetic field and a magnet that has a magnetic field around. If there is any movement on the magnet, an electrical current is established. Like coal and natural gas deposits examples, an oil deposit was found in the United States, too in 1869, and the first, ever oil refinery was built there in history (Habashi 2000). Thanks to these energy sources, the US has pioneered to development of new technologies. One of these technologies was a solar energy plant. Water and wind had already been used as renewable energy sources till then, and it was time to make use of the Sun. A French inventor, Augustin Mouchot foresaw that fossil fuels were limited, and would all be consumed one day, so he invented a solar concentrator to produce eternal energy in 1869 (Land Art Generator 2012) Even though fossil fuels were more convenient to use, entrepreneurs and scientists did not step back finding new ways to generate energy all over the world, and especially in the USA. Only 13 years later, the first-ever hydroelectric power plant started operating along the Fox River in Wisconsin (Nunez 2019) (Edison Tech Center 2014). Like many other energy sources, geothermal energy was also used in North America in 1882, however, the first geothermal power plant was built in Italy in 1904 (ENERGY.GOV 2013) (eia 2021). People had produced energy from wood, water, wind, Sun, geothermal, coal, natural gas, and petroleum so far, but new energy sources are always appealing, so all those inventions were not enough. Therefore, other than fossil fuels and renewable energy sources, engineers and scientists focused on investigating a new one which is nuclear energy in the early 1900s. During World War II (WWII), a valid process was developed for nuclear fission, and Nobel Prize winner Enrico Fermi built the first ever nuclear fission reactor in Chicago (Argonne 2019). However, this was only a fission reactor. The first power plant to generate electricity in the world was built in the USSR in 1954 (World Nuclear 2020).

The world hasn't calmed down yet after WWII. Instead, tension used to increase day by day during the cold war. Arabic countries were in a war against a new undesired country in the Middle East, Israel. Since the USA was on the same side as Israel, Arab members of the Organization of Petroleum Exporting Countries (OPEC) announced an

embargo on the United States which were an oil-dependent country and a few others such as Netherlands and Portugal. Arab members were confident enough to do so because Saudi Arabia had the largest petroleum deposit in the world at those days. This event is called as Petroleum Crisis of 1973. This crisis caused a dramatic raise in the cost of oil. At first, the price of its barrel doubled, and then, the same thing happened to the new price (Office of the Historian 2020).

There have been too many disasters so far while suppressing the energy thirst of humanity. Some of them can easily be told as catastrophic accidents because of the casualties and detrimental effects on the environment. They are also economically damaging events. An oil spill is an example of these occasions. In 1991, Iraq was at war with Kuwait. Coalition forces attacked to Iraq and a week later, the response of Iraq was to intentionally spill oil into the Persian Gulf. Gulf War oil spill was recorded as the largest oil spill in history with 11 million barrels of crude oil in total spilling into the gulf, and it still leads the worst disasters league in this division (Barber 2018). The latest major oil spill is the Deepwater Horizon oil spill disaster by BP happened in the Mexico Gulf in 2010 with 4 million barrels of oil in total spilled into the gulf. This disaster is the largest oil spill in US history (EPA 2022). Other than oil spill disasters, nuclear power plant explosions are also catastrophic. There is a scale called International Nuclear Event Scale (INES), and the highest level is 7 which refers to major accidents. There are only 2 major accidents in history, Chernobyl, and Fukushima disasters. Chernobyl accident is the worst nuclear power plant explosion in history because it directly killed 30 operators and caused 6,500 thyroid cancers. Although the reactor blew up in USSR, the radiation cloud spread over European countries and caused damage there as well (World Nuclear 2022). The second biggest nuclear disaster is the Fukushima power plant disaster. In 2011, Japan hit the strongest earthquake in Japan's history with a magnitude of 9.1. It created a tsunami, and a 15 m wave flooded the nuclear power plant. After sequences of failures in the power plant, 2 reactors blew up. 2,259 disaster-related deaths have been recorded so far (World Nuclear 2021). In brief, sometimes meeting the energy needs of the world can cause a lifetime problem.

An increase in welfare levels shifts people’s concern about environmental issues. While energy demand is still crucial to satisfy, environmental issues cannot be ignored. Developed countries agreed upon a treaty called the Paris Agreement in 2015. This agreement is the first-ever universal agreement to solve environmental problems. Countries that signed the treatment announced their regulations to reduce greenhouse gas

emissions in order to prevent climate change. Therefore, they limit the use of fossil fuels and support renewable energy technologies while undeveloped countries still burn even huge amounts of coal (European Commission 2015). Environmental concerns accelerate the works in renewable energy technologies. In this way, waste management is also achieved.

Energy has crucial importance in today's world due to the high population of people and the electrical devices and transportation vehicles they need for comfortable lives. Therefore, finding new resources or new ways to generate energy to meet the need is one of the main concerns of researchers whilst the demand is increasing day by day. Following energy consumption and production figures clearly show this increasing trend. As is seen in Figure 1.1 and Figure 1.2, the consumption, and production of energy in 1990 and 2021 all around the world are 8556, 8796 and 14061, 14746 Mtoe, respectively (Enerdata 2022). In 2019, total energy consumption and production are 13975 and 14685, respectively. Is clearly seen the effect of lockdown because of the Covid-19 outbreak in 2020 on the energy need of the world because energy consumption and production during lockdown are 13508 and 14166, respectively. On the other hand, the lockdown effect lasted only 1 year since the energy demand and supply hit new records with 4.1% raise in the subsequent years. Although energy demand has increased everywhere, the most remarkable change happened in Asia. This is not surprising at all because the population in Asia has increased by nearly a billion in the last 30 years (Worldometer 2022). Other than the population, the industrialization of Asian countries is also the main reason for this matter.

Turkey is a growing country with a high population; therefore, its energy need is massive. In 1990, energy consumption was 51 Mtoe while production was 25 Mtoe. Half of the demand was produced, and the rest was imported. This shows that Turkey was an energy-dependent country. In the last 32 years, the highest amount of production is 59.3 Mtoe (in 2021) while the consumption increased to 146.8 Mtoe in the same year which is the highest amount in Turkey's history. The highest production amount can only meet the need of the least consumption amount in the last 32 years. Turkey is still an energy-dependent country; however, this time demand is more than three times of production amount while it was only one time of production amount in 1990. In brief, energy dependency is Turkey's major problem because, without importation, Turkey is starving for energy (Enerdata 2022).

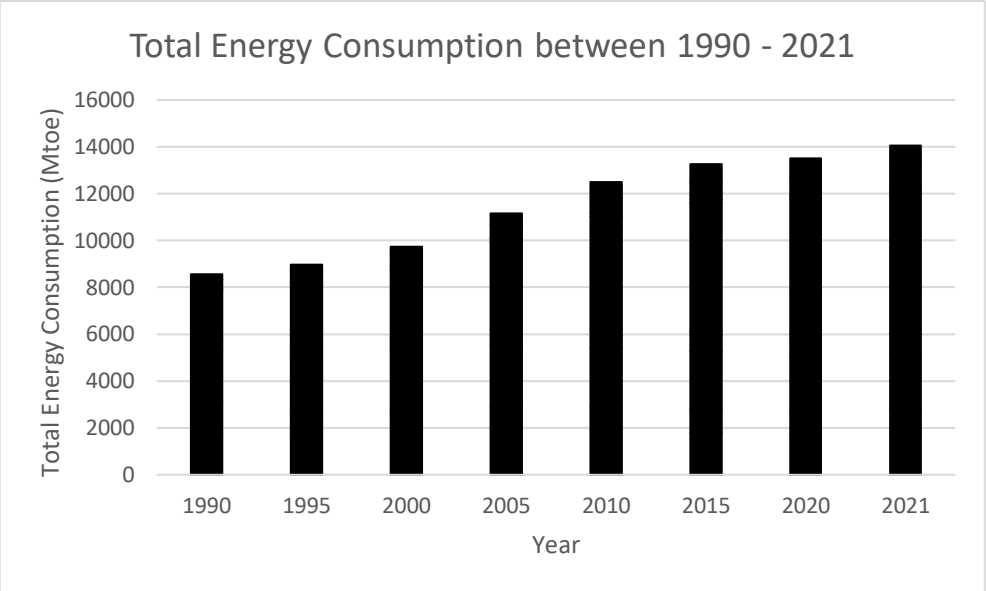

Figure 1.1. Total energy consumption in the world between 1990 and 2021

(Source: Enerdata 2022)

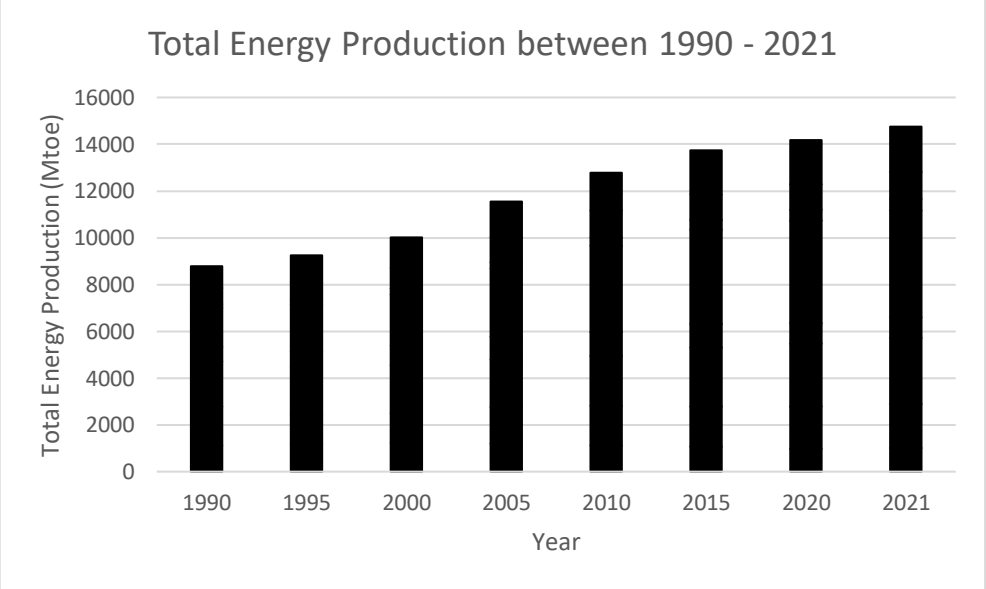

Figure 1.2. Total energy production in the world between 1990 and 2021

(Source: Enerdata 2022)

Renewable energy technologies have been developed since fossil fuels are hazardous to the environment and life, and their amounts are limited as Augustin Mouchot who invented a solar concentrator had foreseen nearly 150 years ago. There are five types of renewable energy technologies which are solar, wind, hydropower, geothermal, and biomass energy technologies.

Solar thermal energy is a type of energy that is produced by absorbing the radiant energy from the Sun and converting it into heat (Pimentel 2008). The surface of the Sun is 6,000 K while Earth's surface is around 300 K. Even though the distance between them is too long, the two-temperature difference creates a great driving force for heat transfer (Twidell and Weir, Solar Radiation 2006). The solar power that reaches to the Earth when the Sun is overhead is 865 W if there is no interruption such as by clouds (Ehrlich and Geller, Solar Radiation and Earth's Climate 2018). Therefore, solar energy is an enormous energy source that can be made use of industrially or directly in houses. Its working principle is to concentrate the sunlight like a magnifying glass and increase the temperature to produce electricity with the help of steam. Mostly, it is useful in Mediterranean countries (Kohl and Dürrschmidt 2013). Another advantage of it is reducing CO_2 emission as the common property of renewable energy sources. Insolation time of Turkey per year is 2,741.07 h which shows Turkey has remarkable potential to benefit from solar energy (Enerji 2022).

Wind occurs when there is a difference in temperature between two regions with the combination of planet rotation. 2 % of solar energy that reaches the world creates wind energy (Enerji 2022). Apart from it having been used for sailing or grinding wheat, it has a great potential to generate electricity. Annual wind energy potential whole around the world is 300 million GWh while the world's electricity need is almost 15 million GWh in a year (Ehrlich and Geller, Wind Power 2018). Different size of wind turbines is available for household or industrial usage. The working principle of a wind turbine is very simple. The wind gets through the blades, and the rotor spins. The generator converts the mechanical energy to electricity (ENERGY.GOV 2013). The wind energy potential of Turkey is 48,000 MW (Enerji 2022).

Hydropower is the most common renewable energy source around the world. Like all renewable energy technologies, hydropower is also eco-friendly technology. They have a lifetime of more than 50 years. The cost of hydropower is almost the initial construction cost of it. Since they are long-life buildings, electricity generated in those plants costs ridiculously cheap (Ehrlich and Geller, Hydropower 2018). The working

principle of hydropower plants is like wind power plants. The stream rotates the turbines, and the generator creates electricity from mechanical energy (Water Science School 2018). Moreover, it is a quite efficient process because today's technology guarantees that around 90 % of the kinetic energy can be converted into electricity (Kohl and Dürrschmidt 2013). Turkey's theoretical hydropower potential is 433 billion kWh (Enerji 2022).

The core of the Earth is about 4,000 °C while the average temperature of the surface is around 25 °C. The heat stored in the core is transferred to the surface by conduction. Also, molten magma creates convective heat transfer. Even though it causes CO_2 emission, it is eco-friendly because a small amount of CO_2 is emitted. 80 % of the heat generated is the decay of radioactive elements such as isotopes of uranium (Twidell and Weir, Geothermal Energy 2006) (Kohl and Dürrschmidt 2013). In a geothermal power plant, steam from hot water is used. It rotates the turbine, and mechanical energy is converted into electricity (NREL 2022). Turkey's geothermal energy potential is estimated 2000 MW for producing 31500 electricity (Enerji 2022).

Any biological material that originated from them is called biomass. There are different classes of biomass sources such as wooden wastes (i.e., wood chips, firewood, etc.), agricultural wastes (i.e., corn, switchgrass, etc.), municipal solid wastes and wastewater, and animal manure. If biomass is processed chemically or biologically to produce energy, the product is called bioenergy. Methane gas, biodiesel, ethanol, etc. are types of bioenergy. Since the sunlight is captured by plants and transferred into glucose by photosynthesis in the first place, solar energy can be considered as the origin of biomass energy (Twidell and Weir, Biomass and Biofuels 2006). Even though fossil fuels were formed from ancient living organisms, they cannot be considered as bioenergy because they are not renewable. The net carbon emission is zero for biomass energy while fossil fuels are risky in this manner. The carbon that is converted into energy is released afterward, therefore; this cycle is proof that it is an eco-friendly energy source (Ehrlich and Geller, Geothermal Energy 2018). Although it is included among renewable energy sources, it is true only if the amount of biomass feedstock that is used is replenished. There are several different ways to make use of biomass to produce energy. Combustion, pyrolysis, gasification, and anaerobic digestion can be given as examples (National Geographic Society 2012). In Figure 1.3, global biofuel demand is shown with a forecast bar. In North America, the biofuel demand is at its highest in all years, however, Asia is expected to have relatively higher growth (eia 2022). In the US, the biomass energy

utilized in 2020 is approximately 115 MTOE which is equal to 5% of primary energy consumption in the United States (eia 2021). The biomass energy potential of Turkey is estimated as 8.6 MTOE while biogas potential is 1.5 – 2 MTOE (Enerji 2022).

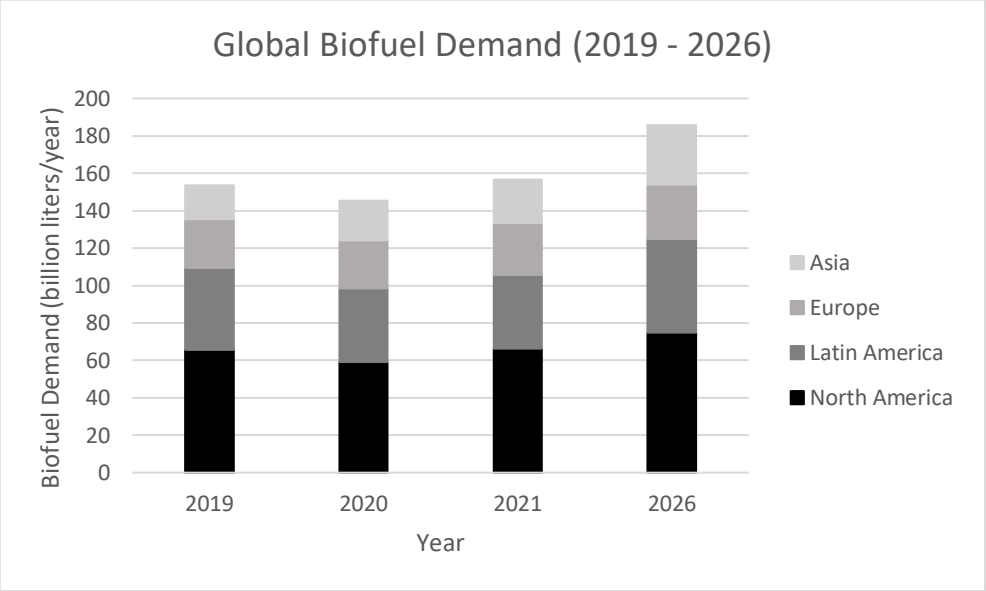

Figure 1.3. Global biofuel demand (2019 – 2026)

(Source: eia 2022)

Anaerobic digestion is a process that a carbon source is consumed by microorganisms in anaerobic conditions. The gas product of the process is called biogas which is mainly a mixture of methane and carbon dioxide and a small portion of other gases. Table 1.1 shows the composition of a typical biogas content. Anaerobic digesters have industrially been processed for 162 years. Since the enthalpy of methane combustion is 192 kcal/mol, any biological material having less heating value than that can be a feedstock. The main feedstocks of this process are municipal wastewater, animal waste (i.e., cow manure, pig manure, etc.), organic waste from industry, agricultural residue, and kitchen waste (Cheng 2018).

Anaerobic digestion, like many other biological processes, is a slow process. Therefore, the size of an industrial digester is gigantic, or/and hydraulic retention time is long in the reactor so that carbon sources are degraded as much as possible. There are

four steps for the degradation of complex organic matter. These are hydrolysis, acidogenesis, acetogenesis, and methanogenesis (Cheng 2018).

Table 1.1. Biogas composition

(Source: Cheng 2018 & Li, et al. 2019)

Biogas Components	**Composition (%)**
Methane	50 – 80
Carbon dioxide	20 – 40
Nitrogen	0 – 5
Hydrogen	0 – 1
Hydrogen Sulfide	0.05 – 1
Ammonia	0.02 – 0.5
Oxygen	0 – 0.5

Hydrolysis is the first step of degradation. In this step, large molecules such as carbohydrates (i.e., cellulose), protein, and lipids are reduced to smaller-sized molecules such as sugar, amino acids, and fatty acids. The bacteria that are assigned for this duty are both aerobic and anaerobic bacteria species. It is an extracellular process, and the responsible microorganisms are facultative and obligate bacteria. The second step is acidogenesis where pH decreases due to the accumulation of volatile fatty acids (VFAs) (i.e., butyric acid and propionic acid). Acetogenesis is the third step. Accumulated VFAs are converted into acetic acid, hydrogen, and carbon dioxide. Mutual bacteria are responsible for acidogenesis and methanogenesis steps. In the last step, methane production is carried out, therefore, it is called methanogenesis. This step is maintained by only archaea bacteria. Methanogens produce methane from hydrogen and carbon dioxide and from directly acetic acid. Hydrogen-utilizing microorganisms are called hydrogenotrophic microorganisms, and acetate-utilizing bacteria are called acetoclastic methanogens. The reactions taking place in this process are shown below. Figure 1.4 shows the degradation of any complex organic material (Cheng 2018) (Manchala, et al. 2017).

$$4H_2 + CO_2 \rightarrow CH_4 + 2H_2O$$

$$CH_3COOH \rightarrow CH_4 + CO_2$$

The microorganisms in the anaerobic digestion process are Clostridium spp., Peptococcus anaerobes, Lactobacillus, Actinomyces, and Escherichia coli for the first three steps while the methanogens are Methanobacteria, Methanosarcina, and Methanothrix. the pH of the sludge should be neutral or slightly higher than 7 because methanogens are quite sensitive to pH values. Even though acetogenins decrease it, inhibition only occurs when there is an imbalance between acidogenesis & acetogenesis and methanogenesis steps because all reactions take place continuously, so the methanogens can tolerate it (Cheng 2018) (Nguyen, Nguyen and Nghiem 2019).

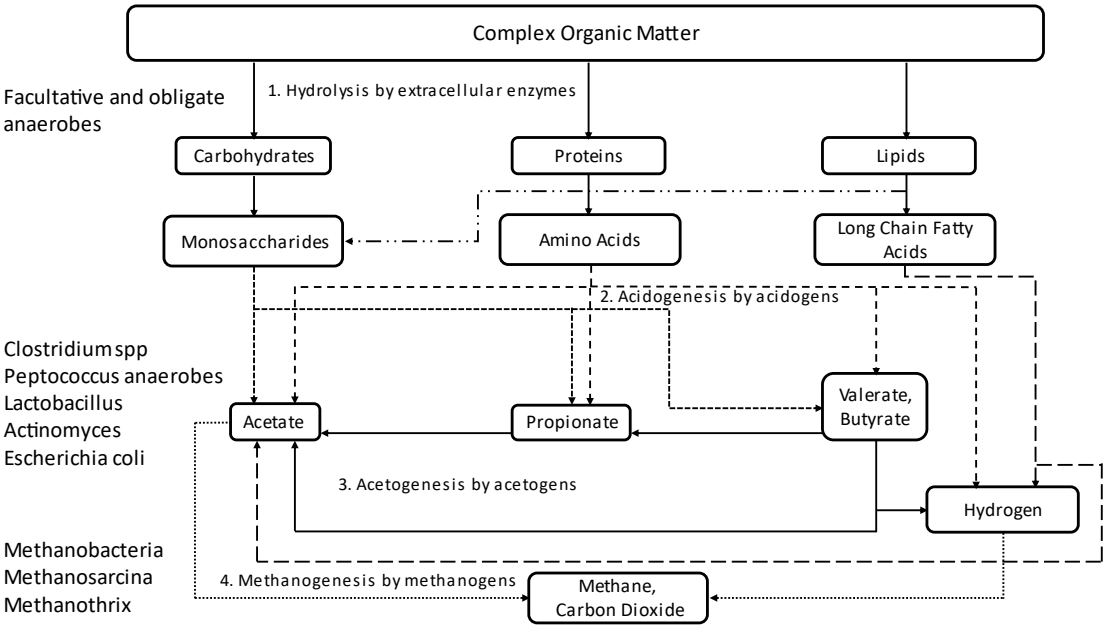

Figure 1.4. Degradation of a complex matter through anaerobic digestion process (Source: Cheng 2018 & Manchala, et al. 2017)

Degradation of many complex organic matters is possible. The following equation shows the stoichiometry of a reaction for any organic matters (Manchala, et al. 2017).

$$C_xH_yO_zN_tS_w + pH_2O \rightarrow qCH_4 + rCO_2 + mNH_3 + nH_2S$$

where t = m, w = n, z + p = 2r, x = q + r and y + 2p = 4q + 3m + 2n.

$$C_xH_yO_zN_tS_w + \left(x - \frac{y}{4} - \frac{z}{2} + \frac{3t}{4} + \frac{w}{2}\right)H_2O \rightarrow$$

$$\left(\frac{x}{2} + \frac{y}{8} - \frac{z}{4} - \frac{3t}{8} - \frac{w}{4}\right)CH_4 + \left(\frac{x}{2} - \frac{y}{8} + \frac{z}{4} + \frac{3t}{8} + \frac{w}{4}\right)CO_2 + tNH_3 + wH_2S$$

The following reaction equations show stoichiometry of reactions from complex organic matters to methane in all steps (Manchala, et al. 2017).

- Hydrolysis
- Carbohydrate:

$$(C_6H_{10}O_5)_{insoluble} \rightarrow Y_c(C_6H_{10}O_5)_{soluble} + (1 - Y_c)(C_6H_{10}O_5)_{inert}$$

where Y_c is fraction of biodegradable carbohydrates.

- Lipids (Glycerol-trioleate):

$$C_{57}H_{104}O_6 + 3H_2O \rightarrow C_3H_8O_3 + 3C_{18}H_{34}O_2$$

- Protein:

$$(Protein)_{insoluble} \rightarrow Y_p(Aminoacids) + (1 - Y_p)(Protein)_{inert}$$

where Y_p is fraction of biodegradable proteins.

- Acidogenesis:
- Simple carbohydrate to acetate, propionate, and butyrate

$$C_6H_{10}O_5 + 0.1115NH_3 \rightarrow$$

$$0.1115C_5H_7NO_2 + 0.744C_2H_4O_2 + 0.5C_3H_6O_2 + 0.4409C_4H_8O_2 + 0.6909CO_2 + 0.0254H_2O$$

where $C_6H_{10}O_5$, $C_5H_7NO_2$, $C_2H_4O_2$, $C_3H_6O_2$, $C_4H_8O_2$ are simple carbohydrate, bacteria, acetate, propionate, and butyrate chemical formula, respectively. 24.8 % of carbohydrate is converted into acetate and 11.5 % of it is converted into carbon dioxide.

- Glycerol to propionate

$$C_3H_8O_3 + 0.04071NH_3 + 0.0291CO_2 \rightarrow 0.04071C_5H_7NO_2 + 0.9418C_3H_6O_2 + 1.09305H_2O$$

where $C_3H_8O_3$ is glycerol.

- Amino acid to volatile fatty acids

$$CH_{2.03}O_{0.6}N_{0.3}S_{0.001} + 0.3006H_2O \rightarrow 0.017013C_5H_7NO_2 + 0.29742C_2H_4O_2 + 0.02904C_3H_6O_2$$

$$+0.022826C_4H_8O_2 + 0.013202C_5H_{10}O_2 + 0.07527CO_2 + 0.28298NH_3 + 0.001H_2S$$

where $C_5H_{10}O_2$ is valerate. 59.5 % of amino acids are reduced to acetate while 7.5 % of them are reduced to carbon dioxide.

- Acetogenesis
- Propionate to acetate

$$C_3H_6O_2 + 1.764H_2O + 0.0458NH_3 \rightarrow 0.0458C_5H_7NO_2 + 0.9345C_2H_4O_2 + 2.804H_2 + 0.902CO_2$$

62.3 % of propionate is reduced to acetate and 30 % of it is reduced to carbon dioxide. Also, 58.2 % of propionate, water and ammonia are converted to hydrogen.

- Butyrate to acetate

$$C_4H_8O_2 + 1.7818H_2O + 0.0544NH_3 + 0.0544CO_2 \rightarrow$$

$$0.0544C_5H_7NO_2 + 1.8909C_2H_4O_2 + 1.8909H_2$$

93.3 % of butyrate is converted to acetate. 32 % of butyrate, water and ammonia are converted into hydrogen.

- Valerate to acetate

$$C_5H_{10}O_2 + 0.8045H_2O + 0.0653NH_3 + 0.5543CO_2 \rightarrow$$

$$0.0653C_5H_7NO_2 + 0.8912C_2H_4O_2 + 0.02904C_3H_6O_2 + 0.4454CH_4$$

32.1 % of valerate is converted to acetate. 8 % of valerate is reduced to methane.

- Long chain fatty acids to acetate

$$C_{18}H_{34}O_2 + 15.2398H_2O + 0.1701NH_3 + 0.25CO_2 \rightarrow$$

$$0.1701C_5H_7NO_2 + 8.6998C_2H_4O_2 + 14.5H_2$$

95.3 % LCFA is converted to acetate. 29.6 % of LCFA, water and ammonia are converted into hydrogen.

- Methanogenesis
- Hydrogen and carbon dioxide to methane

$$2.804H_2 + 0.01618NH_3 + 0.7413CO_2 \rightarrow 0.001618C_5H_7NO_2 + 0.6604CH_4 + 1.45H_2O$$

89 % of carbon dioxide is converted into methane.

- Acetate to methane

$$C_2H_4O_2 + 0.022NH_3 \rightarrow 0.022C_5H_7NO_2 + 0.945CH_4 + 0.945CO_2 + 0.066H_2O$$

47.3 % of acetate is reduced to methane and the same amount of it is used for formation of carbon dioxide.

In the acidogenesis step, degradation of sugars and amino acids takes place because LCFA formed by hydrolysis of lipids is directly processed in the acetogenesis step. Between sugars and amino acids, acetate formation is achieved much better in the degradation of amino acids, and less amount of carbon dioxide is released into the environment. In the acetogenesis step, LCFA is almost completely reduced to acetate. Butyrate degradation to acetate is very similar to LCFA degradation in terms of the formation of acetate and hydrogen. The least efficient one in acetate production is valerate, but it is the only species that produces methane with its reaction. Also, propionate degradation releases the highest percentage of hydrogen. In the methanogenesis step, a high amount of carbon dioxide is used to form methane by hydrogenotrophic bacteria. Acetolactic methanogens create the same amount of methane and carbon dioxide.

The following equations are example reactions in all steps (Clifford 2010).

- Hydrolysis

$$Complex\ Matter + H_2O \rightarrow Monomers + H_2$$

where complex matters are cellulose, starch, sugars, fats and proteins and monomers are glucose, long chain fatty acids and amino acids.

- Acidogenesis

$$C_6H_{12}O_6 + 2H_2 \rightarrow 2CH_3CH_2COOH + 2H_2O$$

$$C_6H_{12}O_6 \rightarrow 2CH_3CH_2OH + 2CO_2$$

In this step, volatile fatty acids and ketones/alcohols are formed.

- Acetogenesis

$$CH_3CH_2COO^- + 3H_2O \rightarrow CH_3COO^- + H^+ + HCO_3^- + 3H_2$$

$$C_6H_{12}O_6 + 2H_2O \rightarrow 2CH_3COOH + 2CO_2 + 4H_2$$

$$CH_3CH_2OH + 2H_2O \rightarrow CH_3COO^- + 2H_2 + H^+$$

$$2HCO_3^- + 4H_2 + H^+ \rightarrow CH_3COO^- + 4H_2O$$

- Methanogenesis

$$2CH_3CH_2OH + CO_2 \rightarrow 2CH_3COOH + CH_4$$

$$CH_3COOH \rightarrow CH_4 + CO_2$$

$$CH_3OH \rightarrow CH_4 + H_2O$$

$$CO_2 + 4H_2 \rightarrow CH_4 + 2H_2O$$

$$CH_3COO^- + SO_4^{2-} + H^+ \rightarrow 2HCO_3 + H_2S$$

$$CH_3COO^- + NO^- + H_2O + H^+ \rightarrow 2HCO_3 + NH_4^+$$

There are several effective parameters in the anaerobic digestion process such as temperature and pH values. One of the most significant influencing parameters is temperature. Three different operating temperature values are classified as psychrophilic,

mesophilic, and thermophilic. Each of them is preferred in different contexts (Zhang, Su, et al. 2014).

The psychrophilic condition is where the temperature is between 10 – 25 °C (Abbas and Rafatullah 2018). In some cases, it can get lower because it is mostly ambient temperature. Therefore, different climate conditions adjust the different temperatures in the system because there is no heat supply to keep the temperature constant at a certain value. Since low temperature slows down the reaction kinetics, the psychrophilic condition is the slowest process. To compensate for this drawback, adjusting high residence time and having a large volume in the digester at once come in handy (Cheng 2018). It is the most common type of household digester because it can still generate biogas at ambient temperature. One of its advantages is it doesn't require as much energy as mesophilic or thermophilic conditions do to run (Rusin, Chamradova and Basinas 2021).

Mesophilic condition is the naturally most preferable process. The temperature range is 30 – 40 °C (Abbas and Rafatullah 2018). Cattle manure is one of the main bacteria sources for the anaerobic digestion process. The rectal temperature of a cattle is 38.4 °C which is in the range of mesophilic circumstances (Godyn, Herbut and Angrecka 2019). Thus, it is the most natural way to create the most comfortable environment for microorganisms by that. It is a faster process than psychrophilic while slower than thermophilic temperature conditions. This process can be improved by co-digestion with different organic materials and two-phase reactors in which the first three steps are held in one phase and methanogenesis is carried out in the latter phase (Ince 1998).

The temperature range is 50 – 65 °C in thermophilic conditions (Abbas and Rafatullah 2018). It is the fastest process because high temperature favors reaction kinetics. Therefore, organic carbon removal is the fastest in thermophilic process (Kim, et al. 2006). It is a common practice because fast processes give the designer a chance to build the digester in small size and the operator to control it easily. One of the major advantages of the thermophilic process is that it is not a suitable environment for hazardous microorganisms. Besides these advantages, sensitivity to the inhibitive parameters is high (Cheng 2018).

pH is as significantly effective as the temperature in the anaerobic digestion process. The most sensitive microorganisms to pH are methanogens, so the pH range should not be lower than 6.5 and higher than 8 if methane production is the goal while the recommended pH range is 6.8 – 7.2 (Cioabla, et al. 2012). The cell membrane is

surrounded by trans-membrane which controls the pathway through the cell. Trans-membrane of methanogenic bacteria has a very small pH gradient in a slightly alkaline environment (Jiang, et al. 2019). This shows that the optimum pH range must surely be adjusted. The byproducts (i.e., phosphates, carbon dioxide, ammonia, hydrogen sulfide, and siloxane) may change pH, so they should be watched out to prevent any pH inhibition (Nghiem, et al. 2017). Chemical reactions of byproducts and water are shown below (Cheng 2018).

$$H_3PO_4 \leftrightarrow H^+ + H_2PO_4^-$$

$$H_2PO_4^- \leftrightarrow H^+ + HPO_4^{2-}$$

$$HPO_4^{2-} \leftrightarrow H^+ + PO_4^{3-}$$

$$H_2CO_3 \leftrightarrow H^+ + HCO_3^-$$

$$HCO_3^- \leftrightarrow H^+ + CO_3^{2-}$$

$$NH_{3,l} + H_2O \leftrightarrow NH_4^+ + OH^-$$

$$H_2S \leftrightarrow H^+ + HS^-$$

$$HS^- \leftrightarrow H^+ + S^{2-}$$

If protein amount in the feedstock is not too high, ammonia concentration is small, too. Also, hydrogen sulfide is not a huge threat although it is an inhibitive compound. However, carbon dioxide composition is at least 20 %, therefore, it might decrease pH value and increase acidity. To keep pH at desired range, alkaline such as lime can be added to the sludge (Cheng 2018).

Inhibition is a big challenge in anaerobic digestion. Since the process is carried out by microorganisms, anything that kills them is considered as inhibitory. Chemical compounds, pH, temperature, and stirring can cause inhibition. Whenever the methane production rate is measured at less than expected value, this tells the operator that inhibition occurs (Cheng 2018).

One of the main inhibitive chemical compounds is ammonia because it can pass the cell membrane and damage the structure of bacteria. Microorganisms need to be provided nitrogen so that they can grow and reproduce. However, if the total of ammonia and ammonium ion is greater than the optimal value, excessive ammonia will prevent methane production. The most sensitive microorganisms are methanogenic bacteria; thus,

ammonia inhibition especially stops methane production (Jiang, et al. 2019). Since bacteria need nitrogen to produce protein, nucleic acid, etc., they utilize ammonia. When the concentration of ammonia is in the range of 50 – 200 mg/L, it is a quite safe environment for microorganisms (McCarty 1964). The highest concentration of total ammonia and ammonium ion (TAN) should not be allowed more than 680 mg/L in order not to deal with ammonia inhibition. When TAN concentration is above 2600 mg/L, the methanogenic activity almost completely stops (Koster and Lettinga 1984). Therefore, the C/N ratio should always be watched out and feedstocks containing protein must be limited since protein is the major source of nitrogen. Microorganisms need both carbon and nitrogen to thrive. However, they do not consume them at an equal rate. Carbon is digested 25 – 30 times faster than nitrogen is by bacteria (Shahbaz, et al. 2020). Hence, the allowable C/N ratio in the process is 20 – 35 (Vivas, et al. 2019). Apart from ammonia inhibiting the process as a chemical compound, it also slows down or completely prevents the methanogenic activity because of the higher pH value it causes than where methanogens can safely be alive and productive. When the basic environment kills the methanogens, the products of the acetogenesis step cannot be converted into methane, so the pH value gets decreased. The accumulation of volatile fatty acids and acetic acid creates an acidic environment where the methanogens that could survive through high basicity cannot process either. When this ratio is ignored and allowed disproportion in their amounts to occur, acidity in the sludge might increase due to the rate of VFAs production that is shifted to a higher value (Shahbaz, et al. 2020). As a result of unbalance, pH inhibition takes place as well because the optimum pH range is not satisfied in the digester. However, bacteria are primitive microorganisms that can adapt themselves to harsh environments regardless of how challenging it is. A way of preventing ammonia inhibition is to make methanogenic bacteria gradually develop durability in such an environment (Cheng 2018). Different studies showed that TAN concentration can be in the range of 3400 – 9000 mg/L after acclimatization (Jiang, et al. 2019). High tolerance to a small C/N ratio is an advantage for the degradation of the protein.

Another inhibitive byproduct is chemical compounds that contain sulfur such as in the forms of sulfate and sulfide. Sulfate-reducing bacteria are in a race against methanogens. Since both bacteria species consume the same substrates (i.e., hydrogen, acetate, etc.), methane production reduces. Thermodynamically, sulfate-reducing bacteria are favored, so acetate and hydrogen are consumed by them faster. Nonetheless, such environments with high acetate concentration are suitable for methanogens to grow faster

while it is vice versa when hydrogen concentration is high (Yoda, Kitagawa and Miyaji 1987) (Robinson and Tiedje 1984). Sulfide is a product of sulfate-reducing bacteria. Sulfide is a chemical compound like ammonia that can penetrate cells and deteriorate their metabolism. H_2S can be given as an example of toxic sulfur-containing molecules. Therefore, sensitive methanogenic microorganisms can easily be interfered with by sulfide (McCartney and Oleszkiwicz 1991). Although sulfur is a required compound, methanogenic microorganisms can tolerate a maximum of 25 mg/L in the sludge (Cheng 2018). It has been shown that sulfide inhibition is observed when its concentration is between 100 and 800 mg/L (Parkin, et al. 1990). It is much less tolerable than ammonia because the toxicity of sulfide is so much higher than ammonia's toxicity. Minerals that create chemical bonds with sulfur form solid particles which are the intruders in anaerobic digestion process. This unclarity is also another way to harm the process if their amount is significant to create unbreakable barriers for microorganisms to reach substrates.

Metal ions are required in the sludge because they are consumed by microorganisms. However, an excessive amount of minerals prevents or slows down methane production as well. Mostly, metal ions are formed when salts dissolve in the liquid. Also, heavy metals are toxic to bacteria (Zha, et al. 2020).

One of the most abundant cations in the digester is sodium. Sodium is consumed by microorganisms; however, it has an inhibitory role when its amount is higher than the tolerable concentration value because it causes dehydration. The most resistant bacteria species to sodium ions are methanogenic bacteria (Cheng 2018). The sodium ion is used to form adenosine triphosphate. When its concentration is in the range of 100 – 200, mesophilic bacteria make use of it without any inhibition. The inhibitive effect of sodium is observed when its concentration is above 3.5 g/L (Anwar, et al. 2016). Methane generation is seriously interfered with when the sodium concentration is around 15 g/L in mesophilic conditions (Patel and Roth 1977) (Anwar, et al. 2016). If the microorganisms are acclimated to the saline environment, the threshold of bacteria for sodium inhibition increases. The inhibition level is 50 % when the sodium ion concentration is around 6 g/L, but it is above 15 g/L when the adaptation process is applied (Feijoo, et al. 1995). Also, cations can mitigate the inhibitory effects of one another, so magnesium sulfate ($MgSO_4$) is added to the digester in order to form Mg^{2+} ions for controlling sodium inhibition (Tharifa, et al. 2020).

Potassium ion is present like sodium ion in the anaerobic digesters because of salts. Microorganisms make use of it to maintain their population and individual vividness. However, its excessive amount is inhibitory (Zha, et al. 2020). When its concentration is lower than 400 mg/L, microorganisms make use of potassium without any inhibition (Cheng 2018). Since there are various VFAs such as propionic acid, acetic acid, etc., there are different methanogenic microorganisms to utilize each. Potassium inhibition does not equally prevent each species to function. Propionic acid utilizers are a more sensitive type of bacteria to potassium ions (Chen and Cheng 2007). In mesophilic conditions, 8 g K^+/L decreases the methane amount produced to its half, and the 12 g K^+/L concentration value is strongly inhibitory while 3 g K^+/L reduces methane production noticeably in thermophilic conditions (Zha, et al. 2020) (Chen and Cheng 2007) (Kugelman and McCarty 1965). This shows that potassium inhibition is a more serious problem when the operating temperature is thermophilic. If there is also calcium in the sludge, a potassium and calcium combination is a much more challenging problem to deal with compared to potassium inhibition alone (Kugelman and McCarty 1965).

Calcium ion is another cation that bacteria need for their growth. However, its drawback is that it causes precipitation as carbonate. Calcium carbonate as an alkalinity source is willingly put into the process as a buffer in order to keep pH constant in the optimum range (Chen, Zhang and Wang 2015) It is a solid material that hardens the mass transfer if its amount is excessive. Therefore, microorganisms that cannot reach the substrate via media and cannot create contact with each other, die, so methane production reduces (Gagliano, et al. 2020). However, it also creates an environment for bacteria to attach and grow on its surface of it. Thus, it causes inhibition, but it is not as problematic as sodium and potassium inhibition (Cheng 2018). When its concentration is between 100 – 200 mg/L, it enhances methane production (McCarty 1964). The calcium inhibition cannot be counted as negligible when its concentration is between 2.5 and 4 because it moderately decreases methane production (Zhou, et al. 2019). In another research, the safe zone with respect to calcium concentration is 3 g/L (Ahn, et al. 2006). Ahn et. al. found out the inhibition is too strong when the calcium concentration is 7 g/L, and McCarty found it is 8 g $Ca2^+$/L.

Microorganisms utilize magnesium like they need other minerals to reproduce. However, a magnesium ion is another cation that inhibits the process when its concentration is high. When the Mg2+ concentration is in the range of 40 – 400 mg/L, inhibition does not occur. As the amount of it increases in the sludge, its inhibitory effects

emerge. 750 mg Mg2+/L is where the inhibition starts slightly, and it is not too severe until 1000 mg Mg2+/L. The methane production is reduced to its half if the magnesium concentration is 2140 mg/L. To avoid magnesium inhibition, a 2 – 4 g/L range must not be allowed in the digester (Romero-Güiza, et al. 2016).

Aluminum is an inhibitive ion that microorganisms do not need for biological activities. It is not a toxic ion to anaerobic microorganisms because of its low solubility (McCarty 1964). Nevertheless, it is not desired in the sludge because it can cause pH instability which can be inhibitive. When its concentration is 2.5 g/L or above, VFA accumulation becomes problematic for the process. Aluminum is not stimulatory and toxic, but it can cause inhibition by changing pH values (Cabirol, et al. 2003).

There is also heavy metal inhibition besides light metal inhibition. Heavy metals do not have any benefit for microorganisms and most of them are toxic. They are iron, zinc, nickel, cobalt, cadmium, chromium, and copper. One of the main reasons that they inhibit the process is heavy metals cannot be degraded through biological processes. Moreover, they damage the structure of enzymes and their functions. Therefore, heavy metals are toxic intruders in the anaerobic digestion process (Cheng 2018). Heavy metals directly damage enzymes, so they cannot function well. This kills the bacteria and inhibits the process (Abdel-Shafy and Mansour 2014). Some heavy metals are too deteriorative because of their high solubility even if their concentration is low. Copper, zinc, and nickel are the most toxic salts. They are also known as antibacterial. Toxicity of the salt changes directly depending on its solubility. Aluminum and iron ions are not too hazardous for the process because of their weak solubility values. The simplest way to prevent or ease heavy metal inhibition is to precipitate them. Sulfide reacts with them and causes precipitation. Therefore, when sulfide and heavy metal are present together, they both mitigate the inhibition of one another (McCarty 1964). Methanogenic bacteria are more sensitive to heavy metal inhibition than acetogenic bacteria. Copper is the first and cadmium is the second most toxic salt for acetogens while it is vice versa for methanogenic microorganisms (Cheng 2018).

The last type of compound inhibition is caused by organic compounds such as alcohols, aldehydes, carboxylic acids, etc. Some of the organic compounds are biodegradable and can be treated at low concentrations. Especially, continuous processes (i.e., CSTR) are very useful to utilize organic compounds even though they are toxic at high concentrations because conversion is accomplished as soon as the feed enters the reactor. For example, methanol can be fed to the continuous digester with a concentration

of 10 g/L although the range of 1 – 2 g/L is toxic (McCarty 1964). The non-soluble organic compounds have inhibitory effects as well. The nonpolar organic compounds accumulate at high concentrations and disrupt the ion balance in microorganisms. This inhibition can be overcome by acclimation like in the other compound inhibition problems (Cheng 2018).

The anaerobic digestion process is a biological process, so there are too many different parameters that should be controlled at the same time because microorganisms are too sensitive to unexpected changes. Modelling the system is one way of evaluating as many as possible scenarios to predict any setbacks in the future to deal with, obtaining reliable data for produced biogas amount in certain operating conditions, and scaling up a laboratory-scale digester to an industrial bioreactor. IWA Group developed a model called Anaerobic Digestion Model No. 1 (ADM1) (Batstone, et al. 2002). The Figure 1.5. Scheme of an anaerobic continuously stirred digester

shows the scheme of a CSTR digester IWA Group researchers modelled. In ADM1, there are 28 processes in total. The first process is the disintegration process. It models the degradation of complex organic matters. Then, reactions in the hydrolysis step are modelled. There are 3 equations for hydrolysis of each macromolecule such as carbohydrate, lipid, and protein. The next 3 processes are for acidogenesis of monomers such as acidogenesis from sugar, acidogenesis from amino acids, and acidogenesis from LCFA. The following 3 processes are for acetogenesis of VFAs such as acetogenesis from butyrate, acetogenesis from valerate, and acetogenesis from propionate. The next 2 processes are for the methanogenesis step. These are aceticlastic methanogenesis and hydrogenotrophic methanogenesis. The last 7 biochemical processes are for the decay of microorganisms that utilize monomers, VFAs, and hydrogen (García, Rodriguez and Cubides 2017).

The kinetics of the reactions are determined in 2 different ways. The first 4 and last 7 processes are first-order reactions while the rest of the 8 processes are modelled as Monod equations. Monod equation is for predicting microbial growth. The equation is a function of substrate. The following equation is the Monod equation (Batstone, et al. 2002) (Rosen and Jeppsson 2006).

$$\mu = \mu_{max} \frac{S}{K_s + S}$$

where μ is microbial specific growth rate, μ_{max} is maximum microbial specific growth rate, K_s is half saturation coefficient, and S is the limiting substrate concentration.

In ADM1, there are biochemical and physicochemical equations, and gas transfer functions. 19 of the equations belong to biochemical functions, 6 of them are physicochemical functions, and 3 of them are gas functions. All the processes are shown in APPENDIX A. STOICHIOMETRIC COEFFICIENTS & RATES, AND COORDINATES as a matrix format. Inhibition is also considered and included in the model. The inhibition reactions are pH, hydrogen, and ammonia inhibition reactions.

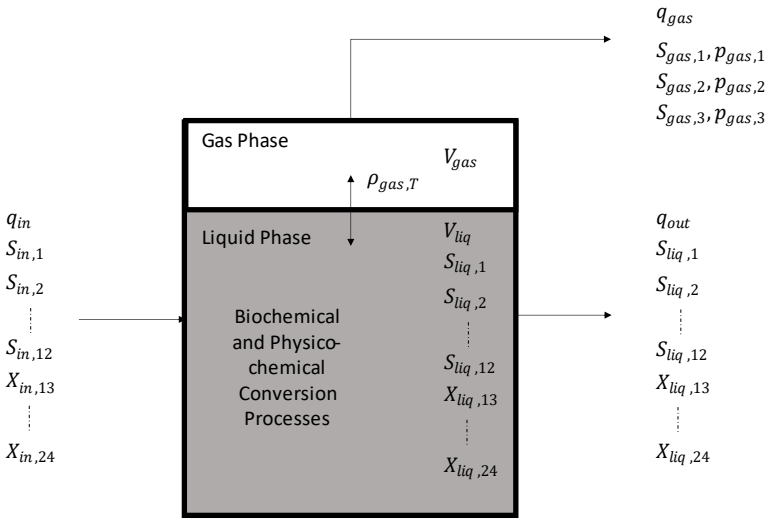

Figure 1.5. Scheme of an anaerobic continuously stirred digester

(Source: Batstone, et al. 2002)

As well as ADM1 has too many advantages, it also has a drawback which is solid transformations such as precipitation are assumed to be non-existent during the process (Manchala, et al. 2017).

In anaerobic digestion, manure is a natural source of energy because there are anaerobic bacteria and incompletely digested lignocellulosic material such as straw. Therefore, manure can produce energy on its own. Also, since a beef cow produces 37 kg of manure every day, the option for gigantic reactors where only mono-digestion of cow manure processing is possible. However, co-digestion of manure and a carbon source makes the process so much more efficient because anaerobes have enough substrate to thrive and populate that way. Agricultural wastes are a good source of complex organic

matters (Pan, et al. 2021). Hazelnut husk has the potential to be used as a co-digestion material in such a process with cow manure. The calorific value of hazelnut husk is not available, but there are other organic matters whose heating values are known and have similar chemical compositions such as wheat straw. The chemical compositions of hazelnut husk and wheat straw are shown in Table 1.2 (Guney 2013) (Mullen, et al. 2015). Hazelnut husk has more lignin than wheat straw does. The heating values of cellulose and lignin are 4,172 and 5,062 kcal/kg (Guney 2013). Thus, hazelnut husk has a greater calorific value than wheat straw. Heating value of wheat straw is 3,845 kcal/kg (Herkowiak, et al. 2018). The calorific value of methane is 11,942 kcal/kg (World Nuclear 2022). Therefore, it is wise to assess hazelnut husk in the anaerobic digestion process.

In Turkey, the production of hazelnut is above 400,000 tons per year. This makes Turkey the prominent country in hazelnut production because this amount is 73 % of hazelnut production all around the world (Şenol, Anaerobic digestion of hazelnut (Corylus colurna) husks after alkaline pretreatment and determination of new important points in Logistic model curves 2020). Nearly half of the crop is waste as husk. Although the amount is remarkable, the harvesting period lasts only 6 weeks, from August to September. It cannot be directly mixed with soil, so farmers firstly compost it, or burn it as a way of waste management. An advantage of the anaerobic digestion process is the sludge as effluent in the digester can be used as a fertilizer. Therefore, hazelnut husk does not require another work to be composted. It can safely be used as an anaerobic digester feedstock because it is lignocellulosic material that cannot be consumed by humans at all (Guney 2013). Thus, it is not a sacrifice of food to produce energy. A disadvantage of hazelnut husk is that it contains a high composition of lignin which can be assumed as inert material because almost none of the microorganisms can digest it.

Table 1.2. Chemical composition of hazelnut husk and wheat straw

(Source: Guney 2013 & Mullen, et al. 2015)

	Hazelnut Husk	**Wheat Straw**
Chemical Compositions	%	%
Cellulose	34.5	28 – 39
Hemicellulose	20.6	23 – 24
Lignin	35.1	16 – 25
Others	9.8	12 - 33

In anaerobic digesters, the sludge has a high viscosity and is challenging to mix. Therefore, there is hydrodynamic analysis to investigate the mixture's behavior whether it is well-mixed or plug flow or not. Well-mixed and plug flow behaviors are ideal hydraulic behaviors. It is called residence time distribution (RTD) analysis. Plug flow means that all the particles enter and leave the reactor at the same time while in CSTR, some particles may never leave the reactor. Therefore, they have different RTD analyses (Fogler 2016).

The experiments are carried out with a specific chemical called tracers such as fluorescein or a radioactive element. The tracer element change depending on the influent of the unit because it must have similar properties to the fluent and it should be mixed with it so that it can behave like it. Since its concentration is aimed to be measured in the effluent, it must be detectable. Moreover, it is chosen as a tracer element if it is thermodynamically inert in that mixture and cannot attach to the walls and remain because the amount of injected tracer should be equal to the collection at the exit to make accurate calculations (Jegede, Zeeman and Bruning 2019). RTD analysis reveals if there is any dead zone, short circuit, or unmixed regions in a tank at the end of the measurements. There are 4 different injection methods which are pulse, step, periodic and random injections. In the pulse injection method, the researcher injects all the tracer into the tank at once and measures its concentration at the exit. If it is a well-mixed sludge, the concentration has its highest value at the beginning, and it gradually decreases over time. If it is a plug flow behavior, pulse output behavior is observed. In step injection, the tracer element is fed to the tank continuously. Pulse and step injections are the easiest and most commonly used ones. In the periodic injection method, the tracer's injection is fluctuating like a wave. In the random injection method the concentration of the tracer is not constant or periodic (Levenspiel, Chemical Reaction Engineering, Third Edition 1999).

RTD curve is created based on the concentration data obtained in the effluent. The results are compared to the possible models if it fits any of them. Well-mixed and plug flow regimes are ideal behaviors, however, the fluid regime does not have to be found ideal. Therefore, there are non-ideal models. These are the compartment model, dispersion model, tanks-in-series model, and convection model for laminar flow in pipes (Levenspiel, Tracer Technology: Modelling the Flow of Fluids(Vol. 96) 2011).

In the compartment model, the behavior of the regimes is modified versions of ideal cases. The differences indicate that there is a dead zone where sludge is not well-mixed or plug flow, or bypassing. Different combinations are possible such as mixed flow

and plug flow in series or parallel, the presence of the recycle stream, etc. The dispersion model and tanks-in-series model are derived from the plug flow model. It is up to the researcher which one is to be used. In the dispersion model, the longitudinal dispersion coefficient is an important parameter. It represents overall spreading. Mostly, it is confused with molecular dispersion coefficient which describes spreading by molecular diffusion only. In Peclet Number, molecular dispersion coefficient is used, but in the dispersion model, longitudinal dispersion coefficient is used because all acting factors such as turbulent or laminar regime and molecular diffusion are taken into consideration. However, in this model, a formula that is the same as Peclet Number's formula is used, only with a longitudinal dispersion coefficient. Therefore, when it is said Peclet Number, a formula with longitudinal dispersion coefficient is meant. Firstly, the Peclet Number is calculated and decided to model as close to plug flow or mixed flow regimes. If the Peclet Number is too high, it is close plug flow and if it is too small, the behavior approaches the mixed flow. Any behavior that fits the dispersion model can be modelled as tanks in series. The advantageous side of the dispersion model is that it is more applicable in different correlations. However, the tanks-in-series model is convenient with any kinetics and it is a simpler model to design. In both models, the length of the vessel is significant. It should be a long vessel. In the convection model for laminar flow in pipes, the dispersion model can be an option as it was said that the dispersion model is a suitable model for different correlations. The other two possibilities in this model are pure convection or pure diffusion regimes. If the vessel is not long enough and the flow has a high rate, the flow's movement is based on convection because molecular diffusion is barely active in such a situation. However, if the vessel is too long, and the fluid's rate is slow, then the movement is mostly based on molecular diffusion (Levenspiel, Tracer Technology: Modelling the Flow of Fluids(Vol. 96) 2011).

The aim of this master thesis is to model a household anaerobic digester whose feedstocks are cow manure and hazelnut husk by using ADM1 mathematical modeling equations and principles while taking RTD analysis into consideration in the model.

CHAPTER 2

LITERATURE SURVEY

2.1. Manure Sources

Cow manure is one of the main manure sources since it is a dairy manure type. It is a carbon source besides it is bacteria and nitrogen-rich because there is still undigested straw. Thus, manure can produce methane without additional carbon intake. In research that was made by D.A. Putri et. al. in 2012, cow manure and water mixture in different ratios were investigated. The manure/water ratios were 1:0, 1:0.25, 1:0.5, 1:0.75, 1:1, 1:2 and 1:3 in reactors R1, R2, R3, R4, R5, R6 and R7, respectively. In a semi-batch reactor where only biogas effluent is the output of the system, the total methane production rate was observed under mesophilic conditions for 90 days. The total volume of methane the researchers recorded at the end of the experiment is 1.75, 1.45, 1.80, 1.75, 2.05, 2.4, and 3 L in R1, R2, R3, R4, R5, R6, and R7, respectively as it is shown in Table 2.1. Highest methane production rate they observed occurred in R7. They also made an inference that water addition improves the efficiency of the process (Putri, Saputro and Budiyono 2012).

Table 2.1. Manure/Water ratio and methane production

(Source: Putri, Saputro and Budiyono 2012)

Reactor	**R1**	**R2**	**R3**	**R4**	**R5**	**R6**	**R7**
Manure/Water Ratio	1:0	1:0.25	1:0.50	1:0.75	1:1	1:2	1:3
Methane Production (L)	1.75	1.45	1.80	1.75	2.05	2.4	3

Pig manure is good nitrogen and bacteria source like cow manure. Therefore, it is a common raw material in the anaerobic digestion process. In 2018, Jie Yang et. al.

investigated the effect of filter media on mono digestion of pig manure in a leach bed coupled with a CSTR. The experimental design is a 15 L tank leach bed connected to CTSR having an active volume of 32 L. Slurry is filtered in the leach bed and fed to methanogenic bacteria. They operated the reactor in mesophilic conditions for 20 days. The filter media they used perlite, ceramsite, and rubber. Table 2.2 shows the biogas and methane yield of filter media. The cumulative biogas yield for perlite, ceramsite, rubber, and control reactor (the one without leach bed reactor) is 230, 245, 220, and 190 mL/gVS, respectively. Cumulative methane yield is 123, 137, 120, and 77 mL/gVS for perlite, ceramsite, and rubber, respectively. Ceramsite was found to be the most efficient filter media, and their discussion about it is that the particles have round, uniform, and rough shapes. They improved the hydrolysis stage with their large specific surface area. However, regardless of which filter media was used, the control digester was the least productive reactor. In the conclusion, they offered the effect of leach bed is that the solid particles remain with the filter media, and more easily digestible leachate is fed to a methanogenic reactor. Their research also showed that pig manure with or without any additional tank such as leach bed reactor is a good resource for methane production (Yang, et al. 2019).

Table 2.2. Biogas and methane yields through filter media

(Source: Yang, et al. 2019)

Filter Media	**Perlite**	**Ceramsite**	**Rubber**	**None**
Biogas Yield (mL/gVS)	230	245	220	190
Methane Yield (mL/gVS)	123	137	120	77

Horse manure is another manure type for the anaerobic digestion process even though it is not as commonly preferred as cattle manure or pig manure. Brian A. et. al. in 2011 investigated horse manure as feedstock with stall waste with softwood bedding in an anaerobic digestion process. In their experiment, they used batch reactors with a

volume of 125 L for solid-state feedstock. Their raw materials in the process are horse manure, stall bedding waste, and sludge from an industrial reactor operating in mesophilic conditions. They measured methane production from co-digestion of horse manure and stall bedding waste and mono-digestion of each. In co-digestion process, the ratios of bedding VS to manure VS are 0.01:1, 0.05:1, 0.1:1, 0.25:1, 0.5:1, 1:1, 2:1 and 4:1. They determined the methane production via 160 mL serum bottles. The experiment lasted for 79 days. Table 2.3 shows the bedding/manure ratio and methane yields obtained in each of the digesters. The cumulative methane yield they obtained from horse manure alone is 133 mL/gVS. Mono-digestion of fresh softwood bedding is a completely inefficient process. The yield of the co-digestion process reduces as the bedding composition increases in the mixture. The inference the researchers made from these results is bedding waste is hard to digest in anaerobic conditions. Moreover, straw's potential was studied as an alternative material for stall bedding in this study, they reached a conclusion that the methane-producing potential of straw is as good as horse manure itself. At the end of the study, the researchers found that horse manure can be used as a feedstock in an anaerobic digester, and stall bedding is not good for methane production in this process. Instead, straw can be replaced as a bedding material (Wartell, et al. 2012).

Table 2.3. Bedding/Manure Ratio and methane yield

(Source: Wartell, et al. 2012)

	Used Softwood Bedding:Horse Manure							**FSB:HM**	
Reactor	R1	R2	R3	R4	R5	R6	R7	R8	R9
Bedding/Manure Ratio	0:1	0.25:1	0.5:1	1:1	2:1	4:1	1:0	1:1	1:0
Methane Yield (mL/gVS)	133	102	88	83	64	60	50	64	1

where FSB is short for fresh soft bedding and HM is short of horse manure.

2.2. Carbon Sources

Anaerobic digestion can be analyzed in under two main headings in terms of raw material diversity. If there is only one feedstock is used in the process, it is called mono-digestion. If there is more than one raw material mixed in a slurry, it is called co-digestion. Mostly, manure and carbon sources are combined so that this additional carbon source will help the bacteria population to grow more than the case they must survive with the undigested straw remaining in the manure.

Agricultural waste is always a good feedstock to produce methane gas through the anaerobic digestion method. Also, it is a waste management method. Corn silage and sugar beet pulp are agricultural wastes that can be efficient. In a study by H. Şenol et. al. in 2019, they were investigated as a mixture and alone. They also pretreated the waste thermally before the experiments were kicked off in order to improve the process. In the experiments, 500 mL batch reactors were used at 39 °C. Slurry whose solid matter was 10 % in all reactors was kept neutral pH while being continuously stirred at 100 rpm. They observed the batches for 30 days. Cattle manure (CM), corn silage (CS) and sugar beet pulp (SBP) ratios were determined as 1:0:0, 0:1:0, 0:0:1, 1:1:1, 2:1:1, 2:2:1, 2:1:2, 1:1:2 and 1:2:1. They, pretreated the wastes at 100, 120, 150 and 180°C for 10, 20, 30, 60 and 120 min. They found the best ratio was in the fourth case with a 2:1:1 ratio of CM:CS:SBP as is seen in Figure 2.1. The methane production yield at the end of the experiments is 180.5 mL/gTS. According to their measurement, mono-digestion of SBP is the least efficient process with a cumulative methane yield of 95.2 mL/gTS. The thermal pretreatment effect on biogas production was investigated by the best raw material ratio. The highest methane yield they found was 362.1 mL/gVS with the pretreated feedstock at 180 °C for 60 min while the least amount of methane per gram total solid was produced with the least heated for the shortest time as it is shown in Figure 2.2. The researchers concluded that thermal pretreatment on agricultural wastes improves the process efficiency. As the temperature in pretreatment increases, methane yield increases, too. The optimum period to subject lignocellulosic material to heat is 60 °C (Şenol, Açıkel, et al. 2020).

It is already proven that food waste is a good source of carbon for the anaerobic digestion process. C. Zang et. al. in 2012 assessed the efficiency of the co-digestion of food waste and cattle manure and mono-digestion of each element. They built two

experimental set-ups, batch, and semi-continuous processes. In both digester types, they adjusted the temperature based on mesophilic conditions and worked with an active volume of 0.8 L.

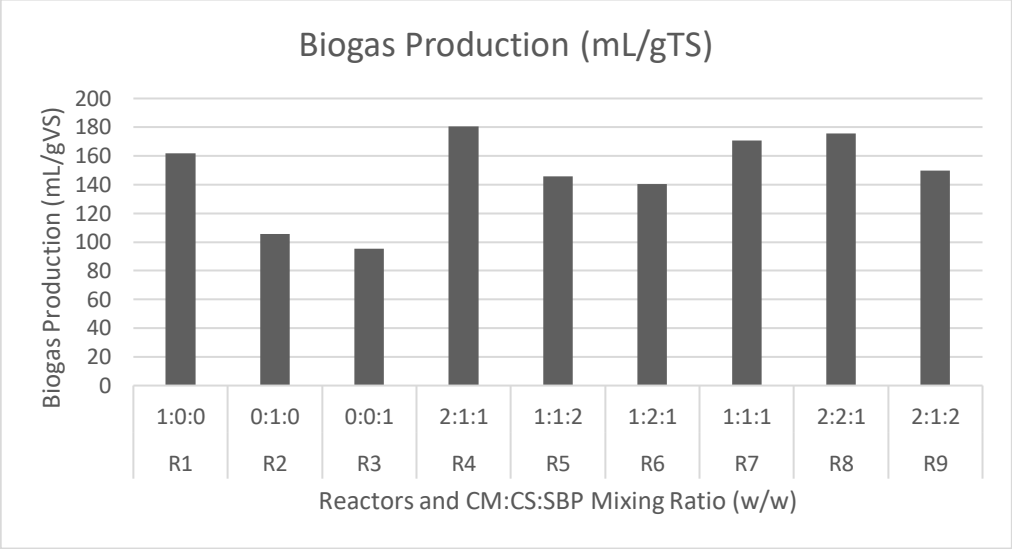

Figure 2.1. Biogas production in different mixing ratio of cattle manure, corn silage and sugar beet pulp (Source: Şenol, Açıkel, et al. 2020)

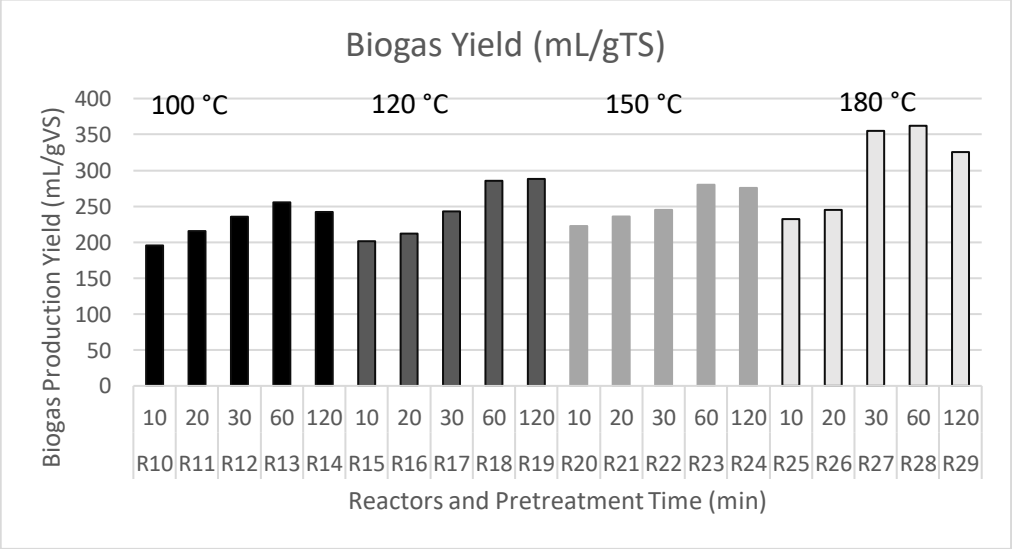

Figure 2.2. Biogas yield at different temperature values and pretreatment times (Source: Şenol, Açıkel, et al. 2020)

They also aimed to find the best food waste (FW) and cattle manure (CM) ratio. They firstly carried out batch experiments so that they could eliminate several trials with different food waste and cattle manure ratios. In batch experiments, they kept the food waste amount constant at 8 gVS/L and changed the amount of cattle manure to have FW/CM ratio at 2, 3, and 4 in co-digestion reactors. In semi-continuous experiments, the most optimal ratio they reached was kept constant and they increased the amount of food waste (i.e., 8, 10, 12 gVS/L/d). Figure 2.3 shows the methane yield in each batch reactor. They measured the highest biogas production at an FW/CM ratio of 2. In that digester, methane yield is 388 mL/gVS. When it is 3 and 4, the methane yield they recorded is 352 and 343 mL/gVS. They found that mono-digestion of food waste showed the best performance in terms of methane yield with 410 mL/gVS, however, the amount of the produced cumulative methane is least when it is compared to any co-digestion process. The increasing amount of manure increases the amount of trace elements such as sodium and magnesium, therefore, it is thought that this improves the methanogenic activity. In semi-continuous processes, the highest methane yield they obtained was when food waste has an organic loading rate of 8 gVS/mL/d with 388 mL/gVS. However, they proposed the total organic loading rate at 15 gVS/mL/d is the most efficient process because methane production was found to be at its highest value at 57.1 L as it is shown in Table 2.4. Mono-digestion of food waste efficiency goes down as the organic loading rate increases. They concluded that co-digestion of food waste with cattle manure was enhanced by 41.1% in terms of methane yield. As organic loading rate is inversely proportional to methane yield (Zhang, Xiao, et al. 2013).

Kitchen waste is to be known as a good carbon source for anaerobic digesters. R. Li et. al. in 2009 investigated the biogas potential of kitchen waste (KW) in a co-digestion process with cattle manure (CM) at different ratios in batch and semi-continuous operations. In batch processes, they adjusted the active volume at 1 L. The experiment was carried out under mesophilic conditions with KW/CM ratios at 0:1, 1:1, 2:1, 3:1, and 1:0 while keeping the total organic loading at 8.4 gVS/L. In semi-continuous operation, they built a two-phase reactor. One phase is the acidic phase and the other one is the methanogenic phase. The working volume of both phases is 0.6 and 3 L, respectively. 2 days after the sludge was fed to the first phase, it was sent to the methanogenic phase to stay there for 10 days. Therefore, they adjusted the organic loading rate to 1.2 gVS/L/d. After 35 days in batch reactors, cumulative methane production was found at 1250 mL in mono-digestion of cattle manure as it is shown in Table 2.5. In the rest of the digesters

where kitchen waste was consumed frankly much more efficiently than in the first reactor. When the KW/CM ratio is 1:1, the methane amount they obtained is 2482 mL.

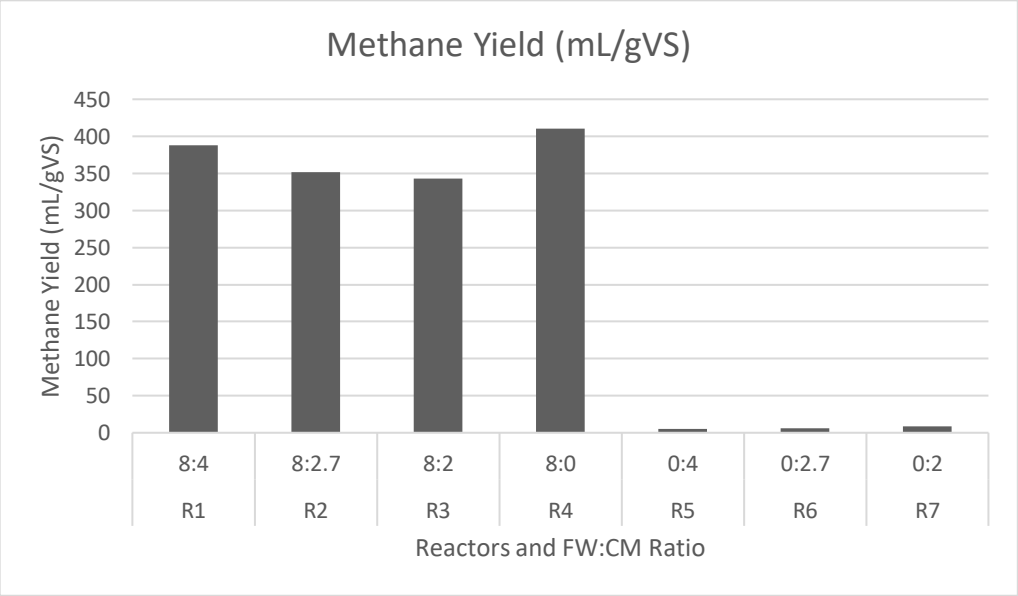

Figure 2.3. Methane yield in different FW:CM ratios

(Source: Zhang, Xiao, et al. 2013)

Table 2.4. Methane production in semi-continuous reactors

(Source: Zhang, Xiao, et al. 2013)

Reactors	**FW:CM**	**Methane Yield (mL/gVS/d)**	**Methane Content (%)**	**Total Methane (L)**
R8	8:0	347	61.2	33.3
R9	10:0	277	58.0	33.2
R10	12:0	96	35.1	5.5
R11	8:4	388	62.3	55.9
R12	10:5	317	60.2	57.1
R13	12:6	139	39.7	14.0
R14	0:4	69	33.5	3.3
R15	0:5	60	32.9	3.6
R16	0:6	55	32.7	4.0

As the kitchen waste amount increases in the digesters, the amount of methane gas enhances, too. Mono-digestion of kitchen waste was recorded as 3022 mL. The explanation of researchers about this difference between mono-digestion of cattle manure and the rest is due to lack of carbon source and high amount of lignin in it, while kitchen waste contains much less lignin, and different kinds of carbon sources such as carbohydrate, fat, and protein. Therefore, they calculated that the biodegradability percentage of sludge in each digester increases as the amount of kitchen waste increases, too. In semi-continuous experiments, they found the least efficient process was mono-digestion of kitchen waste in terms of specific methane potential among the digesters in which kitchen waste is feedstock even though it was the most efficient digester in the batch experiment. Nonetheless, in co-digestion reactors, as the kitchen waste composition increases in mixtures, methane production increases as well as is seen in Figure 2.4. pH value between acidic phase and methanogenic phase was measured the highest in the fourth digester where KW/CM ratio is 3:1, from 4.9 to 7.3. This change is also proof that the researchers achieved the best methanogenic activity in that experiment (Li, Chen and Li 2009).

2.3. Hazelnut Husk as Carbon Source

Hazelnut husk is an agricultural waste. Since it is a lignocellulosic material, it can be a feedstock for the anaerobic digestion process. In 2012, M.S. Guney studied on the potential utilization of hazelnut husk as a type of biomass. As biomass conversion methods, he assessed aerobic and anaerobic digestion, fermentation, enzymatic or acid hydrolysis, combustion, pyrolysis, gasification, and liquefaction methods. He suggests both digestion processes, however, for energy production, anaerobic digestion is a much more favorable process. Moreover, if it is processed as a co-digestion method with manure, the performance of the digester is expected to increase by 50 – 200%. Also, the anaerobic digestion method is the most simple and cheapest method among all except for direct combustion. The chemical composition of hazelnut husk is 55.1% holocellulose (cellulose and hemicellulose) and 35.1% lignin while the rest is ash. Although lignin amount is higher than usual feedstocks for this process, it is a very much suitable raw material that can be benefitted from (Guney 2013).

Table 2.5. Cumulative methane production at different KW:CM ratios

(Source: Li, Chen and Li 2009)

Reactors	KW:CM Ratio	Methane Production (L)
R1	0:1	1.250
R2	1:1	2.482
R3	2:1	2.542
R4	3:1	2.693
R5	1:0	3.022

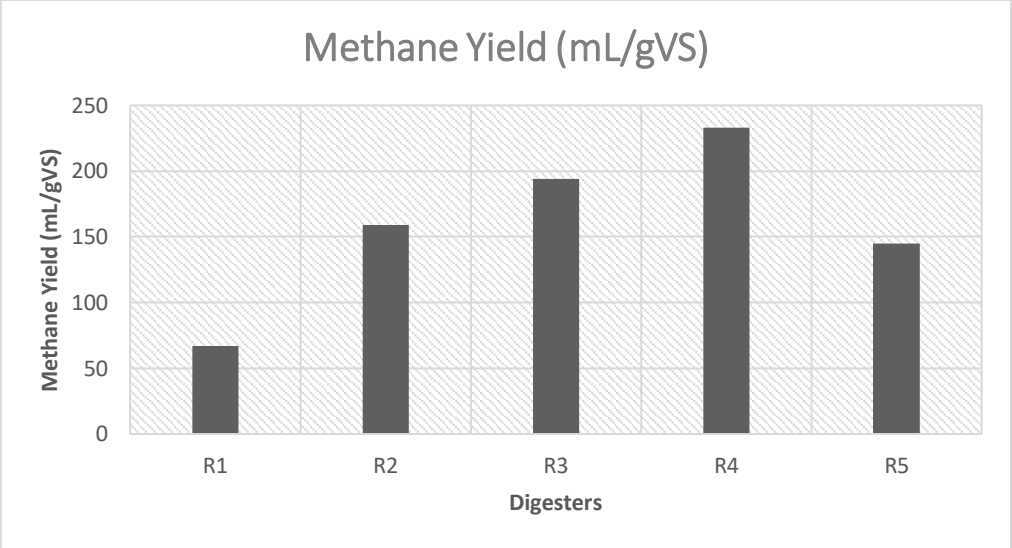

Figure 2.4. Methane yield at different KW:CM ratios in semi-continuous digesters

(Source: Li, Chen and Li 2009)

In 2019, H. Şenol investigated the performance of anaerobic co-digestion of hazelnut husk with cattle manure after alkaline pretreatment and made kinetic modelling based on results obtained. As a novel perception of the cumulative methane yield curve, he determined the critical points in the logistic model in order to understand the bacteria growth. He carried out alkaline pretreatment with NaOH in different concentrations from 1% to 6% and made an experiment for untreated hazelnut husk as a control reactor. The

effective volume in each digester was 0.25 L. The experiments lasted for 30 days while the control reactor lasted 10 more days in mesophilic conditions. He found that alkaline pretreatment increased the solubilization of cellulose, hemicellulose, and lignin by 10.72 – 31.45%, 7.75 – 25.85%, and 12.58 – 45.78% respectively as the concentration of NaOH increases in the solution as it is shown in Figure 2.5. Since lignin is too difficult to degrade by microorganisms, its solubilization improved the most by pretreatment in terms of percentage. According to the methane yield he recorded each day, he showed that each of the pretreated experiments produced much more methane than the control digester. Figure 2.6 shows the methane yield and concentration in reactors. The highest methane yield measured was 278.45 mL/gVS in the fourth experiment where the hazelnut husk was put in 4% NaOH solution while it was 106.19 mL/gVS in the control reactor. Solubilization of the lignocellulosic material increased directly proportionally with NaOH concentration while methane yield decreased after 4%. He explained this seemingly contradictive case as Na+ ions might have been deposited and caused inhibition in the process. The researcher modeled the experiments based on two different modelling equations which are the Logistic model (LM) and the Gompertz model (GM). LM and GM showed that the highest cumulative methane yields were 130 and 114 for the untreated experiment and 277 and 269 for the fourth reactor, respectively (Şenol, Anaerobic digestion of hazelnut (Corylus colurna) husks after alkaline pretreatment and determination of new important points in Logistic model curves 2020).

2.4. Anaerobic Digestion Model No. 1

Anaerobic Digestion Model No. 1 is mathematical modelling for CSTR-type reactors developed by the International Water Association group. The difficulty of ADM1 is that too many concentration data need to be known as input values. In 2008, (Page, et al. 2008) characterized influent and effluent manure in order to evaluate required input values. They also modelled 2 different real-scale PFR digesters and made comparisons between models and measured values from the reactors.

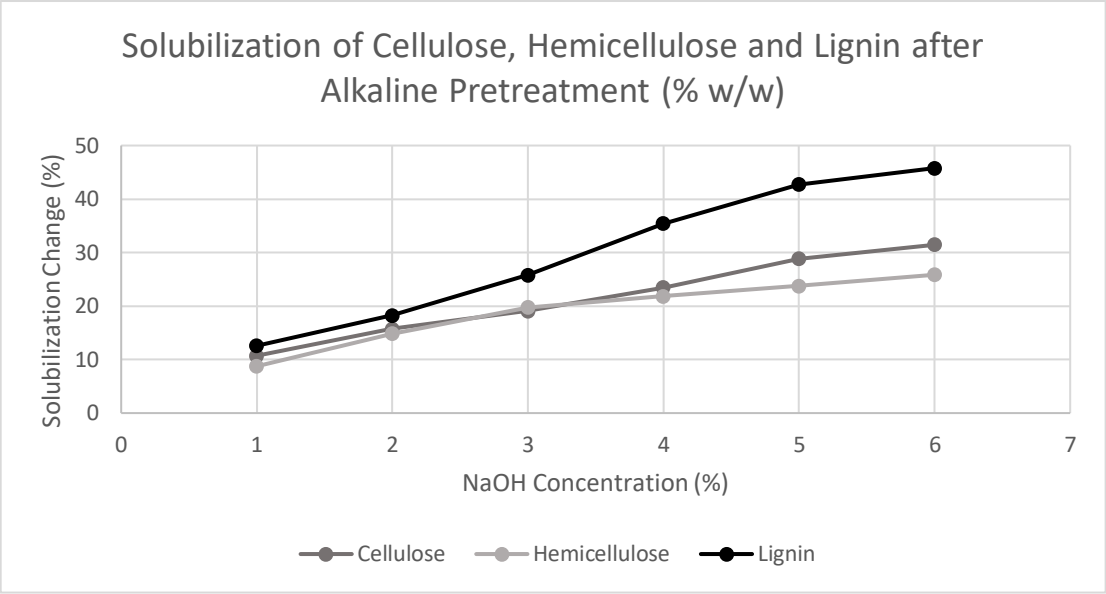

Figure 2.5. Change in solubilization of chemical contents of hazelnut husk compared to untreated sample (Source: Şenol, Anaerobic digestion of hazelnut (Corylus colurna) husks after alkaline pretreatment and determination of new important points in Logistic model curves 2020)

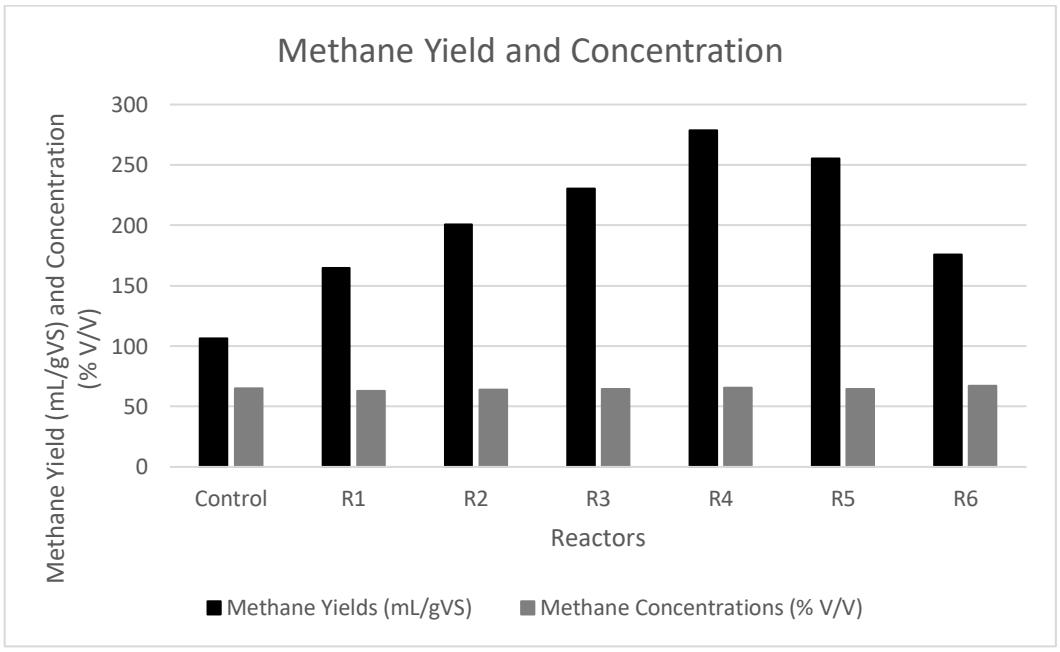

Figure 2.6. Methane yield and concentration data recorded in each of the digesters (Source: Şenol, Anaerobic digestion of hazelnut (Corylus colurna) husks after alkaline pretreatment and determination of new important points in Logistic model curves 2020)

Since ADM1 is for CSTR, they used a tanks-in-series model with 4 equal CSTRs to achieve PFR behavior. They operated experiments in 6.5 L bench-scale digesters under mesophilic conditions with a hydraulic retention time of 20 days. Their models produced more methane than experimental results. The concentration of acetogens had the same problem while they could successfully model methanogen's concentration. They attribute inaccuracies to not well-mixed situations of reactors. Researchers achieved modelling the smaller-sized reactor in terms of biogas production while biogas production was measured higher than modelled one in the larger-sized digester. They suggested this model predict the biogas production performance of a digester even though it might not be accurate all the time. ADM1 is a reliable mathematical modeling system, yet it needs to be improved more (Page, et al. 2008).

2.5. RTD Analysis

Residence time distribution analysis shows the hydrodynamic behavior of the fluid. Thus, it is always beneficial to know it in order to make the most accurate modelling. In an anaerobic digestion process, it is crucial to take it into consideration during designing the digester because it is a highly viscous mixture which is difficult to achieve an ideal profile such as mixed or plug flow. In 2018, A.O. Jegede et. al. evaluated the liquid and solid mixing using the RTD technique in three different types of reactors which were unmixed, mixed, and Chinese Dome Digesters (CDD). They investigated 6 different conditions in a mesophilic environment. Two different total organic carbon (TOC) ratios (i.e., 7.5 and 15 %) were adjusted in each of the digester types. The effective volume they worked with was 39 L. The sludge they formed was a mixture of manure and water. Although their aim was to analyze RTD, they also measured the biogas production to see which process was the most efficient. They applied the pulse injection method and used fluorescein as a tracer. The hydraulic retention time was adjusted to 30 days for the liquid phase. They measured the concentration of tracer in the effluent periodically. Then, they converted the concentration versus time plot into the dimensionless retention time distribution curve. They obtained all the tracer elements injected before 30 days in all cases which shows that none of the operating conditions showed ideal behavior. In each of the digester types, a 7.5% TOC ratio was found to be

mixed better. The dead zone in the TOC ratio of 15% is greater in all digesters. Researchers modelled all 6 cases as non-ideal modelling, tanks in series. Table 2.6 shows the properties of the reactors and methane yields in each of the reactors. Impeller mixed cases fitted 2 tanks in series with R2 of 0.90 and 0.86 for 7.5 and 15 % TOC ratio, respectively. The coefficient of determinations they evaluated were 0.96 and 0.95 for unmixed digesters and 0.93 and 0.85 for CDD, and all 4 of the cases were modelled with 3 tanks in series. Therefore, any digester can be designed with the number of reactors recommended to build as accurately as a possible design under these operating conditions. Methane yields they measured had the highest values when the TOC ratio is lower because they were mixed better, and the dead zone percentage was smaller. Impeller mixed reactor showed the most productive performance with a methane yield of 160 mL/gVS while the least efficient process was unmixed digester with higher solid matter and the methane yield was 90 mL/gVS. The 10 L additional volume of CDD was not included in RTD analysis, but it was effective in methane production, so CDD was found to be a more efficient process than the unmixed reactor. Their conclusion is fewer solid matter in the reactor eases the sludge mixed better while improving the methane yield (Jegede, Zeeman and Bruning 2019).

Table 2.6. The properties of the digesters and methane yield values

(Source: Jegede, Zeeman and Bruning 2019)

Reactors	**TOC (%)**	**t_{min} (day)**	**Number of Tanks**	**R^2**	**Methane Yield (mL/gVS)**
Mixed Digester	7.5	27	2	0.90	160
Mixed Digester	15	25.1	2	0.86	150
Unmixed Digester	7.5	23.6	3	0.96	100
Unmixed Digester	15	20.3	3	0.95	90
Chinese Dome Digester	7.5	25.5	3	0.93	130
Chinese Dome Digester	15	23.2	3	0.85	120

CHAPTER 3

METHODS

This chapter is divided into two sections. Since it is a modeling study, study about the interest of this study which is the anaerobic digestion of hazelnut husk was found in the literature (Şenol, Anaerobic digestion of hazelnut (Corylus colurna) husks after alkaline pretreatment and determination of new important points in Logistic model curves 2020). Its methane yield results were used to find the rate constants of disintegration and hydrolysis reactions. Anaerobic Digestion Model No. 1 (ADM1) was developed and published by the IWA Task Group for Mathematical Modelling of Anaerobic Digestion Processes was used. To solve the ODE set, MATLAB was used as software. 3 packages of MATLAB codes were created that can be checked in APPENDIX C. MATLAB CODES. The solver method used in MATLAB was ode15s for differential equations set. After reaction rate constants were found, operating conditions were decided, so the RTD analysis should have been considered in those conditions because the design was built as a perfect CSTR whilst it might have not reflected the real case. To avoid wrong modelling by assuming it is ideal, a hydrodynamic study with aimed conditions was found in the literature (Jegede, Zeeman and Bruning 2019). RTD analysis was made for different modelling cases and chosen the most suitable one. Then, MATLAB codes were modified with hydrodynamic analysis. The default operating conditions were decided as hazelnut husk as carbon source, mesophilic conditions with 65 days as hydraulic retention time (HRT), 0.1 husk/manure ratio, unmixed reactor, and 7.5% TOC availability. In total, there are 10 different scenarios (i.e., Case 1, 0.1 husk/manure ratio; Case 2, 0.5 husk manure ratio; Case 3, 1 husk/manure ratio; Case 4, psychrophilic conditions; Case 5, thermophilic conditions; Case 6, food waste as carbon source; Case 7; doubled TOC in the digester; Case 8, mixed digester; Case 9, Chinese Dome Digester (CDD); Case 10, 0.1 husk/manure ratio without RTD analysis) that are examined. These cases project the effects of carbon source/manure, temperature, different carbon source, TOC amount, digester type, and hydrodynamics of fluid. The process and equations for RTD and digester design are written detailly as follows. In ADM1, it is assumed that only biomass

which is decayed gets through the disintegration process. Also, solid residence time (SRT) and HRT are assumed to be equal because, in CSTR, this is preferable (Chuanshu , et al. 2019).

3.1. RTD Analysis

In RTD analysis, ideal models (i.e., plug flow and mixed flow) and non-ideal models (i.e., compartment model, dispersion model, tanks-in-series model, and convection model for laminar flow) are designed with the equations and plots in the literature (Levenspiel, Tracer Technology: Modelling the Flow of Fluids(Vol. 96) 2011). The equations required to analyze the models mentioned above can be checked in B1. RTD Analysis Equations.

3.2. Reactor Design

In reactor design, ordinary differential equations set of ADM1 were used. Also, default values of ADM1 were coded. Both equations and constants are available in B2. Reactor Design Equations and B3. Constants.

CHAPTER 4

RESULTS AND DISCUSSION

This chapter is divided into two sections. In the first section, hydrodynamic analysis of the liquid in the digester is analyzed and discussed. Results of RTD models are covered. In the second section, the results of methane production are shown. The discussions for effective parameters (i.e., carbon source/cattle manure ratio, temperature, type of carbon source, total solid amount, reactor type and ideal case) are made.

4.1. RTD Analysis

The concentration of tracer, fluorescein (chemical formula is $C_{20}H_{12}O_5$) versus time was taken from Jegede et al.'s study about hydrodynamics of sludge for RTD analysis with pulse method. Figure 4.1 shows the behavior of the liquid with solid matter of 24 % in the digester. Clearly, it's seen that more than a half of the tracer leaves the reactor before 20 days although the process lasts 65 days. This non-uniform behavior of the RTD curve is a sign of dead zone or short circuiting.

Mean time ($\bar{t}$) and variance (σ^2) of the curve were calculated as 22.45 days and 149.54 d^2, respectively. Normally, the researchers aimed to obtain a mean value of 30 days, so this result proves that liquid does not reach everywhere in the digester. Residence time distribution, E, was plotted as shown in Figure 4.2. θ and E_θ values which are dimensionless RTD curve is shown in Figure 4.3. Dimensionless RTD was plotted to make a comparison with different hydrodynamic behaviors to see if it matches up with any scenario so that a more accurate design can be made.

(Levenspiel, Tracer Technology: Modelling the Flow of Fluids(Vol. 96) 2011) conveyed several possible models. Those models are plug flow, mixed flow, compartment model, dispersion model, CSTRs in series and laminar flow.

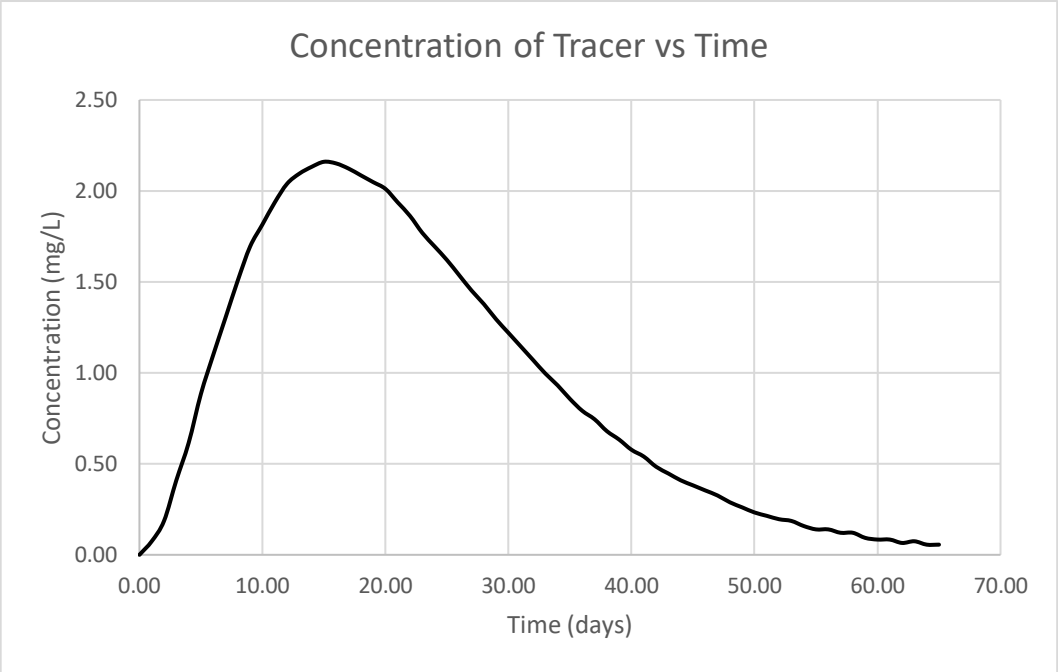

Figure 4.1. Concentration vs Time plot of the tracer

(Source: Jegede, Zeeman and Bruning 2019)

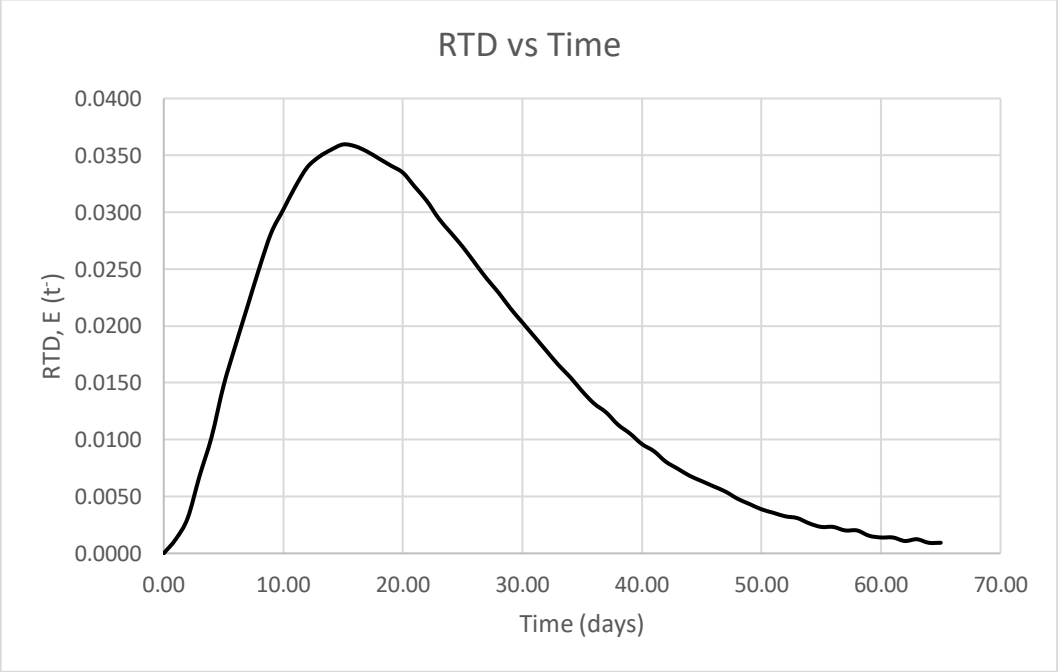

Figure 4.2. RTD vs time

(Source: Jegede, Zeeman and Bruning 2019)

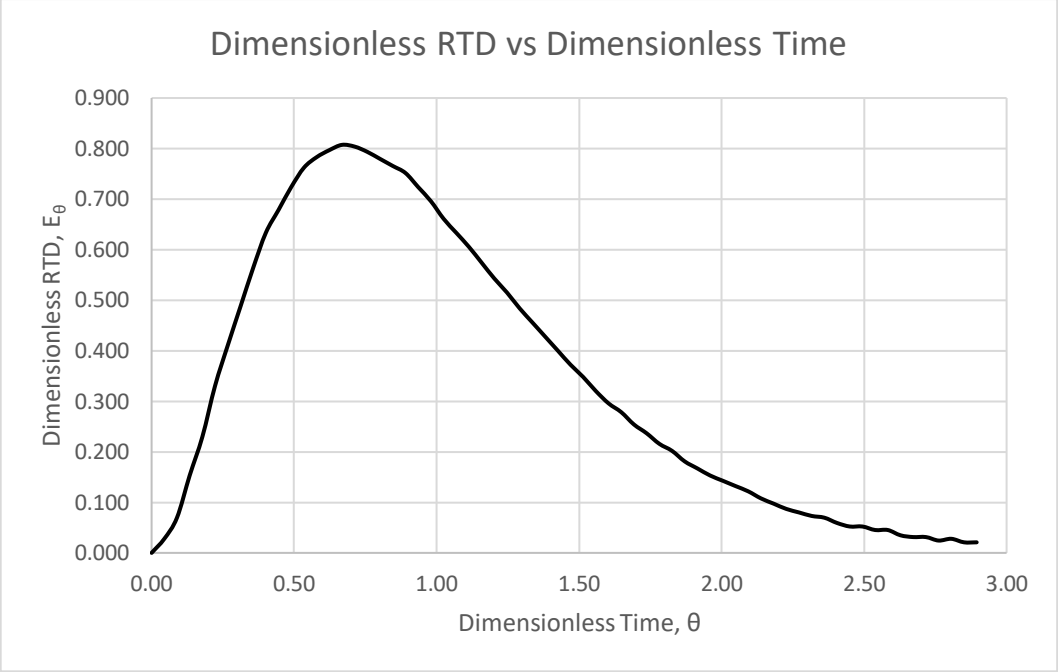

Figure 4.3. Dimensionless RTD vs dimensionless time

(Source: Jegede, Zeeman and Bruning 2019)

4.1.1. Plug Flow Model

The plug flow model is one of the two ideal cases. In this model, a spike shape is created at the mean time in the plot when the effluent's tracer concentration is measured, just like it was injected. The area is 1 while the width and height of the spike approach 0 and infinity, respectively. This is called dirac delta function, $\delta(t- \bar{t})$, which occurs in a perfect pulse injection at mean time as it is shown in Figure 4.4. Since the experimental RTD curve does not satisfy dirac delta distribution, the digester cannot be designed as PFR. To achieve a plug flow behavior, the velocity of the fluid is increased, and the diameter of the vessel is reduced. Moreover, the sludge has a high viscosity which has high adhesive force. This causes the fluid to hold the wall of the digester and prevents or hardens the plug flow behavior. Also, plug flow digesters are usually long-tunnel-shaped reactors, while these digesters do not satisfy this requirement. PFR design is not possible as expected.

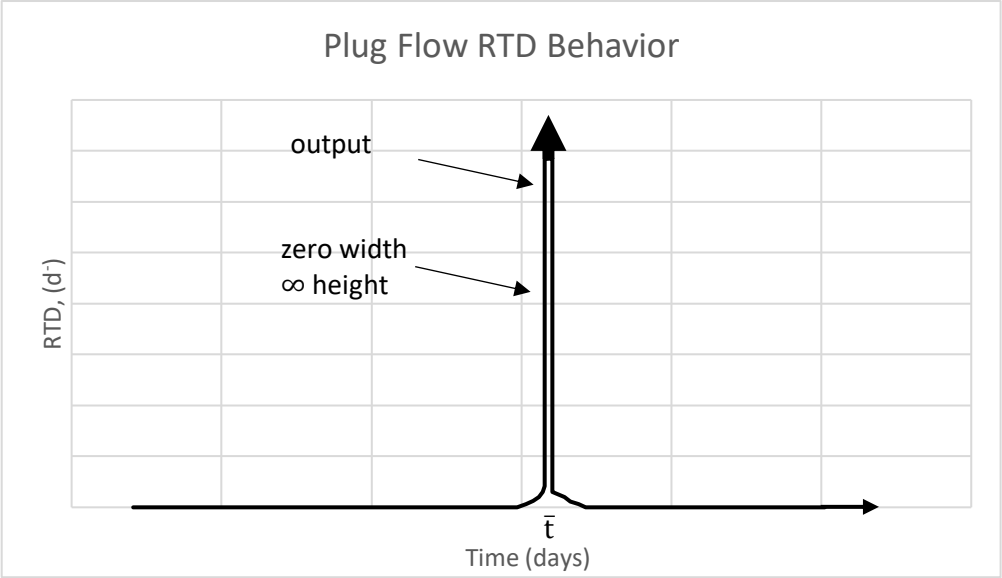

Figure 4.4. Plug flow RTD behavior

(Source: Levenspiel, Tracer Technology: Modelling the Flow of Fluids(Vol. 96) 2011)

4.1.2. Mixed Flow Model

Mixed flow is the other ideal case. In a perfectly mixed reactor with a pulse injection, the concentration is at its highest value at the beginning of the process and gradually decreases as it is shown in Figure 4.5. It is quite safe to claim that a CSTR design would be completely wrong since experimental RTD analysis does not match the hydrodynamics of a liquid in a mixed flow reactor. It was expected that the mixed flow model would fail because the tracer concentration plot belongs to an unmixed digester in (Jegede, Zeeman and Bruning 2019). It is natural to obtain a failure in a mixed flow model based on an unmixed sludge study.

4.1.3. Compartment Model

Even though there is a dead zone in the digester, the hydrodynamics of the flow is totally a CSTR behavior because the mixed flow and compartment model have the same design equations. Since there are unmixed parts, they shorten the fluid's residence

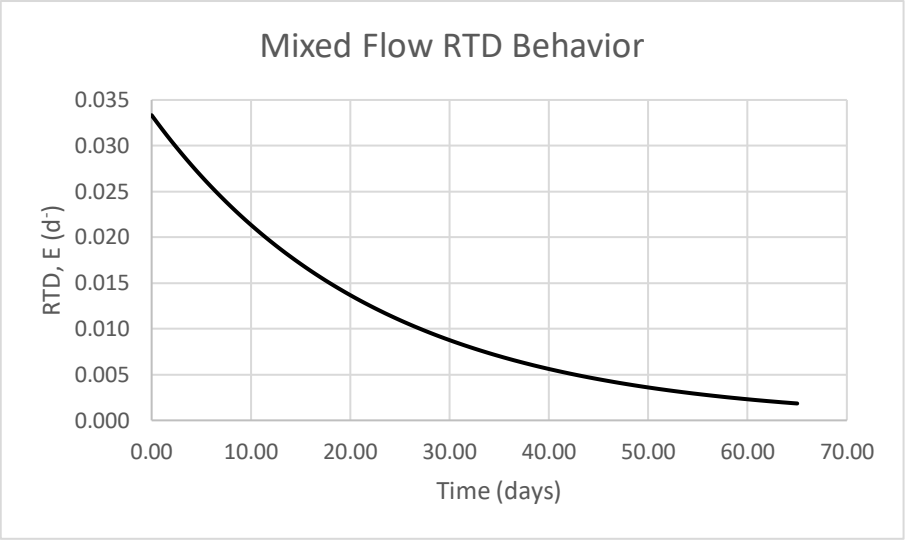

Figure 4.5. Mixed flow RTD behavior

time and prevent the flow from reaching every corner and edge in the reactor. Because an unmixed reactor's behavior is investigated in this analysis, it was expected that a compartment model could suit because it is known that there is a dead zone in the tank. However, the experimental result is completely different from the compartment model like it didn't match with the mixed flow as it is shown in Figure 4.6. This shows that the sludge is not formed from only a well-mixed and unmixed region. Thus, the design cannot be made based on a compartment model.

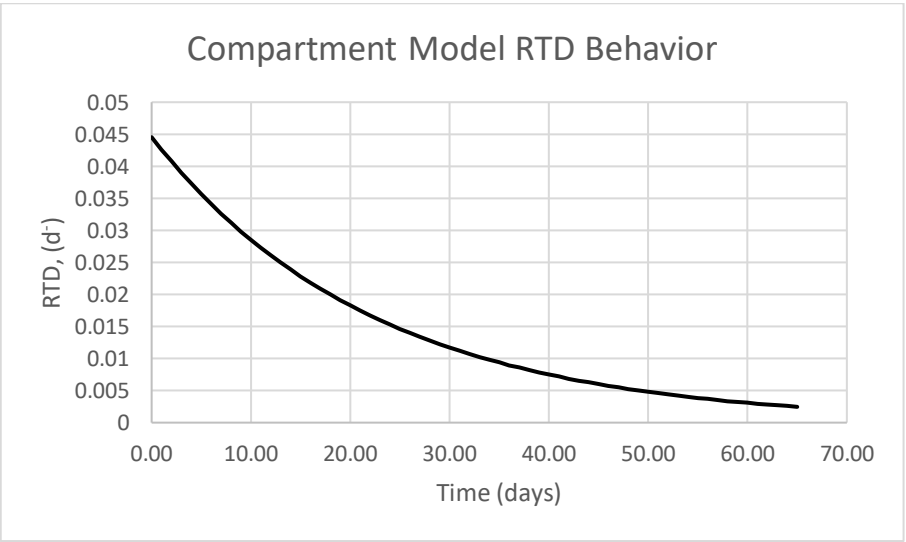

Figure 4.6. Compartment model RTD behavior

4.1.4. Dispersion Model

In the dispersion model, the Peclet Number is a significant factor that divides the models into two concepts which are a small deviation from plug flow and a large deviation from plug flow. Peclet Number tells the behavior approaches plug flow as it gets high, and mixed flow as it gets down. 0.01 is a critical value for 1/Pe, D/uL, to decide whether it is a small or large deviation. D/uL was found to be 0.148 for the small deviation model. It is large enough to claim the plug flow model fails again. Plug flow is only possible when D/uL is equal to 0 because it means there is no spreading. A large deviation from the plug flow model has 4 different concepts which are closed vessel, open – closed & closed – open vessels, and open vessel. D/uL was calculated as 0.181 for the closed-vessel. As it is seen in Figure 4.7, the curve for D/uL at 0.181, is less steep than D/uL at 0.1 and starts slightly further away from 0 than D/uL at 0.2, so the highest value of Eθ is bigger than 1 while it is 0.807 in experimental analysis. The dashed curve belongs to experimental results. It does not fit the curve for D/uL at 0.181. Thus, the closed-vessel model is not suitable. Another approach is closed – open or open – closed boundary conditions. D/uL was calculated as 0.125. The expected hydrodynamic behavior for open – closed or closed - open vessel cases can be checked in Figure 4.8. The failure reason for the closed vessel's behavior is valid in these models, too. As it is seen in the figure, experimental results almost fit the curve at D/uL is equal to 0.2 while it is calculated as 0.125. Moreover, the closed boundary condition means that the flow should have a plug flow regime until it reaches the vessel and exits from the vessel as a plug flow. The reason why the stream is unlikely to have plug flow behavior is explained before, so any model that at least one end as plug flow regime cannot completely fit the experimentally obtained hydrodynamic behavior. The last concept is open–open boundary conditions which is an open vessel. The value of D/uL is 0.1045. The comparison of dimensionless RTD analysis is shown in Figure 4.9. As it is frankly seen that experimental results and the open vessel model do not match. Therefore, it is not a suitable approach as well. Shortly, none of the dispersion models are the optimum models to design this reactor. Any of these three models can be used unless a better one shows up.

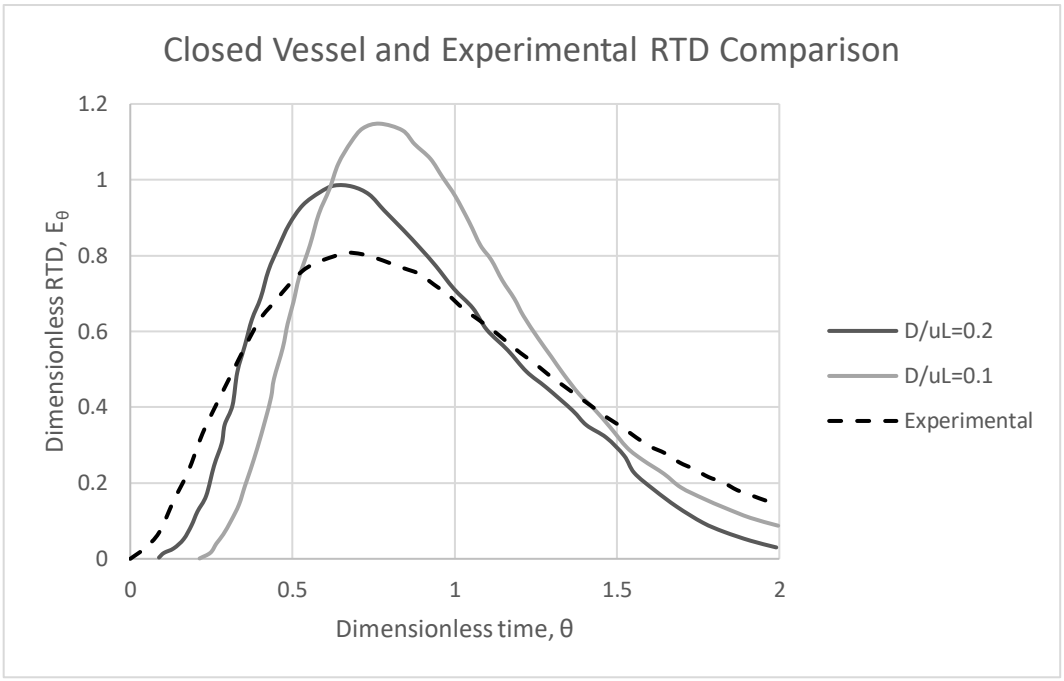

Figure 4.7. Comparison of experimental RTD and closed vessel RTD

(Source: Levenspiel, Tracer Technology: Modelling the Flow of Fluids(Vol. 96) 2011)

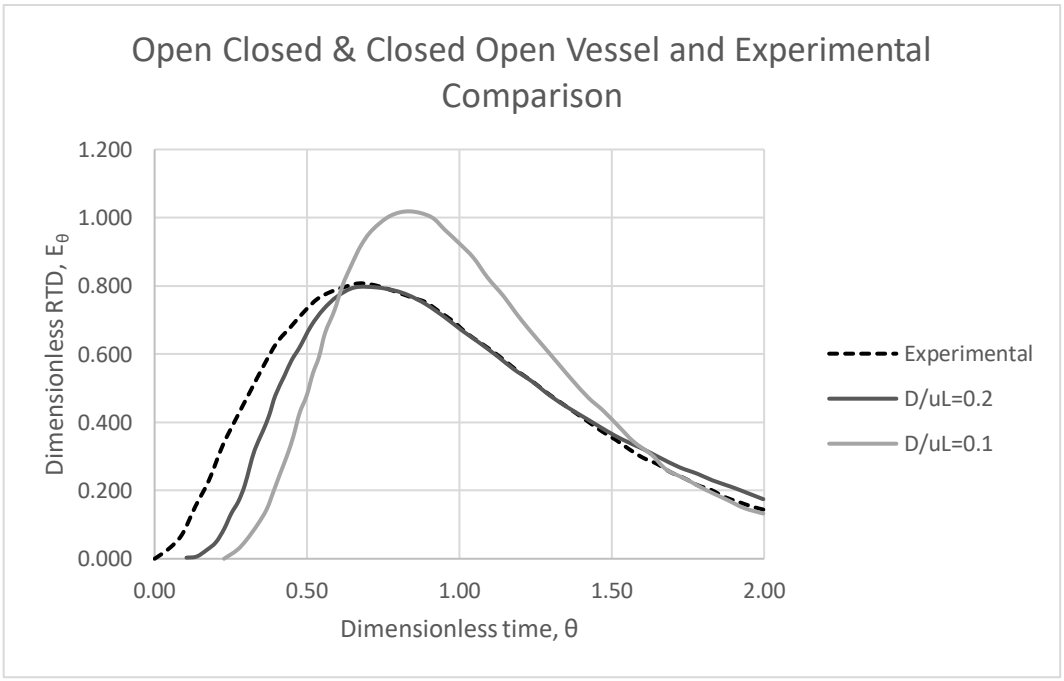

Figure 4.8. Comparison experimental and open – closed & closed – open vessel RTD

(Source: Levenspiel, Tracer Technology: Modelling the Flow of Fluids(Vol. 96) 2011)

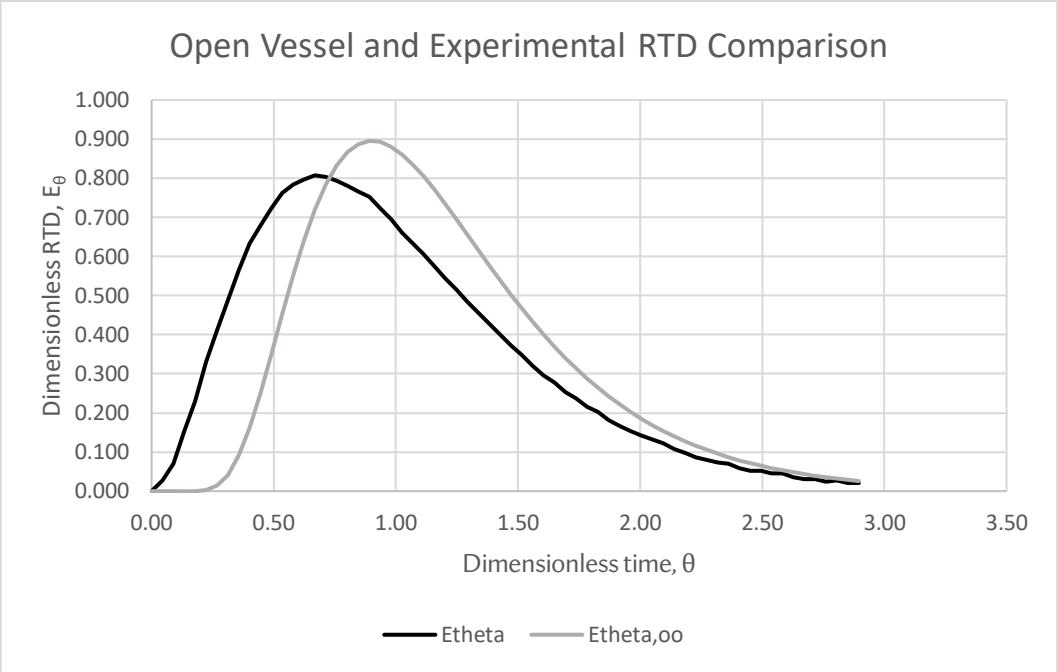

Figure 4.9. Comparison of experimental RTD and open vessel RTD

4.1.5. Tanks in Series Model

In the series CSTR model, the total volume is kept constant, and a number of equally–sized tanks are placed in series. Theoretically, an infinite number of CSTRs in series behave as a PFR. Therefore, as the number of tanks increases, the curve becomes more symmetrical, steeper, and narrower. It satisfies the rule that dirac delta function is equal to 0. Figure 4.10 shows several different scenarios and experimental analyses. As it is shown in the plot, 3 CSTRs in series totally match with experimental results, so the design can be made as 3 serial digesters. Tanks in the CSTR model were expected to work because the dispersion model or tanks in the series model have similar curves. In dispersion models, although they were not relied on for making a design, behaviors were not too far. Since the tanks in the series model are more flexible, changing the number of tanks is an advantage of this model to fit experimental results. The expectation is satisfied when 3 reactors are in series while increasing the number of reactors is slightly approaching plug flow behavior.

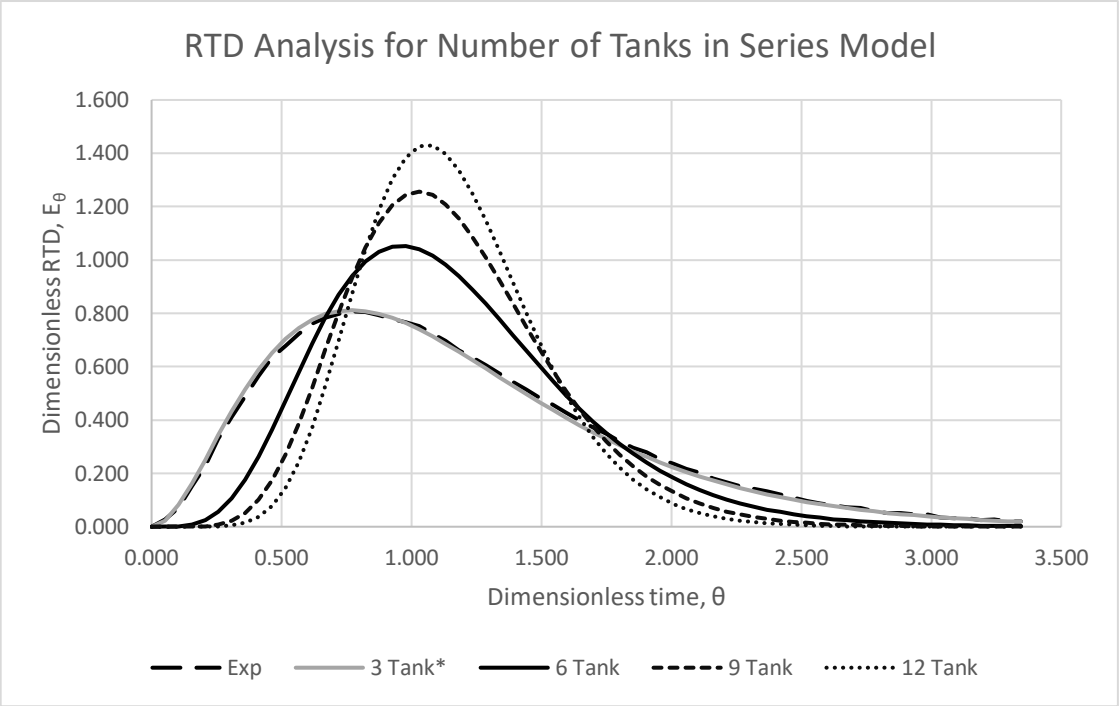

Figure 4.10. RTD Analysis for number of CSTRs in series

4.1.6. Convection Model for Laminar Flow

The laminar flow model is completely different than the experimental results as expected. If the convection model is aimed model, the reactor should be short, and the flow should be so that convective flow can be achieved. Also, this model is a pipe flow model, so the digester must have a pipe shape. The digester is not pipe-shaped, and the residence time is high. Therefore, the convection model for laminar flow is difficult to achieve under these conditions. This extreme case of laminar flow was not expected to fit experimental results. Figure 4.11 shows this discrepancy very clearly.

Different models were examined and compared with results obtained from experiments. Only one model's hydrodynamic behavior matched up with experimental RTD. It is CSTRs in series with 3 equally-sized digesters.

Different reactor types and TOC amounts are examined in this study, so the following graphs belong to their hydrodynamic behaviors. In Figure 4.12, it is clearly seen that 3 tanks-in-series have completely the same RTD with its experimental results. The reactor type is the same while the TOC ratio is twice. Figure 4.13 represents the hydrodynamic behavior of the mixed reactor. 2 digesters in series are suitable for that

digester. Since it is already a mixed reactor, it does not require dividing the reactor into 3; instead, 2 tanks are enough. Chinese Dome Digester has RTD as it is shown in Figure 4.14. It also has a similar hydrodynamic profile with 3 digesters in series.

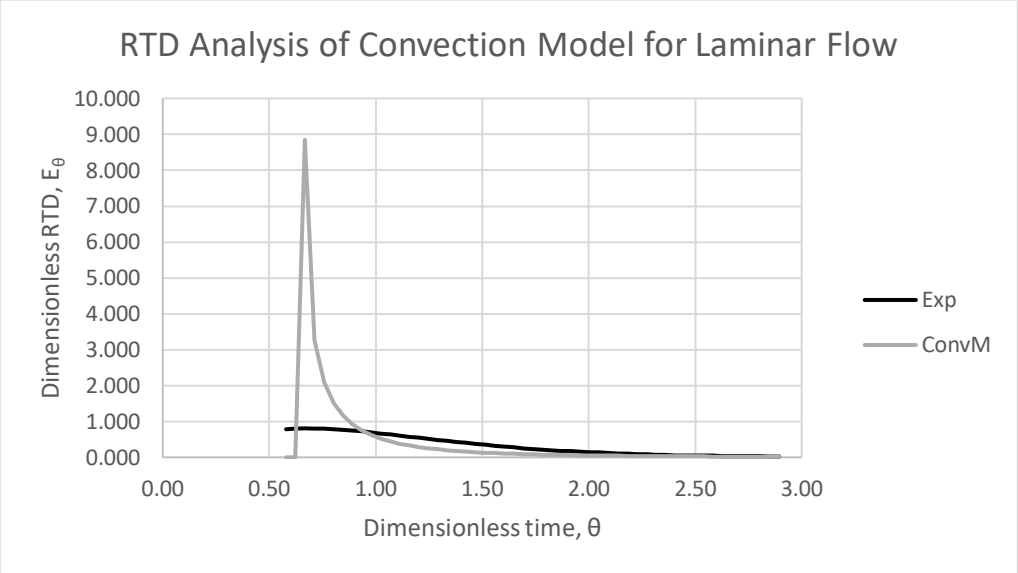

Figure 4.11. Laminar flow RTD analysis and experimental RTD comparison

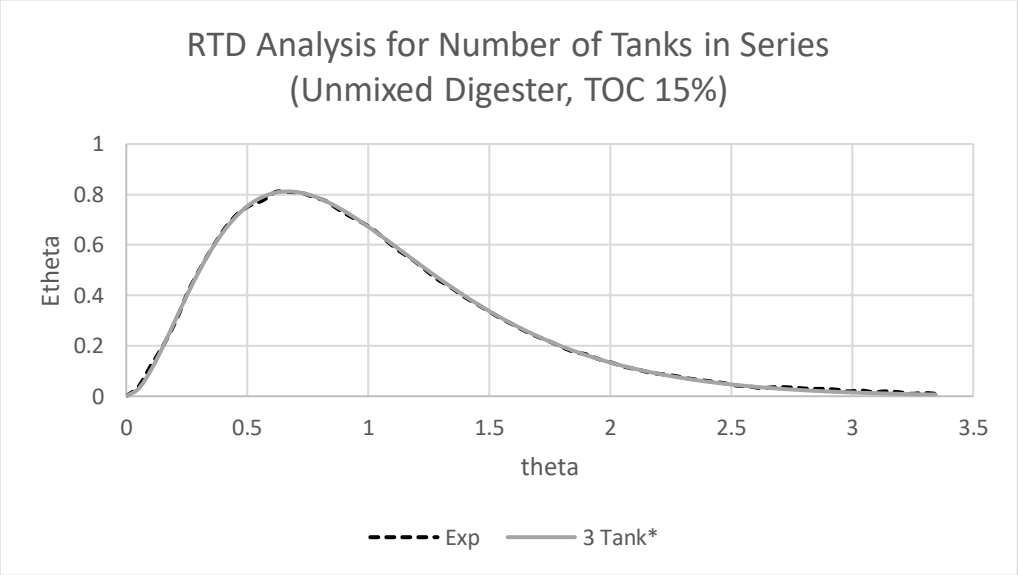

Figure 4.12. RTD Analysis for 3 CSTRs in series when the solid matter ratio is doubled

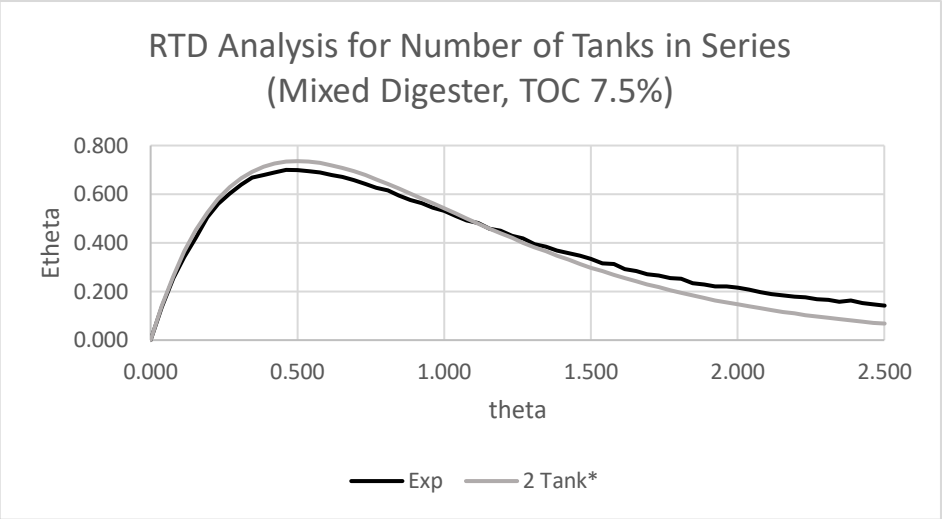

Figure 4.13. RTD Analysis for 2 of CSTRs in Series in mixed digester with same amount of TOC

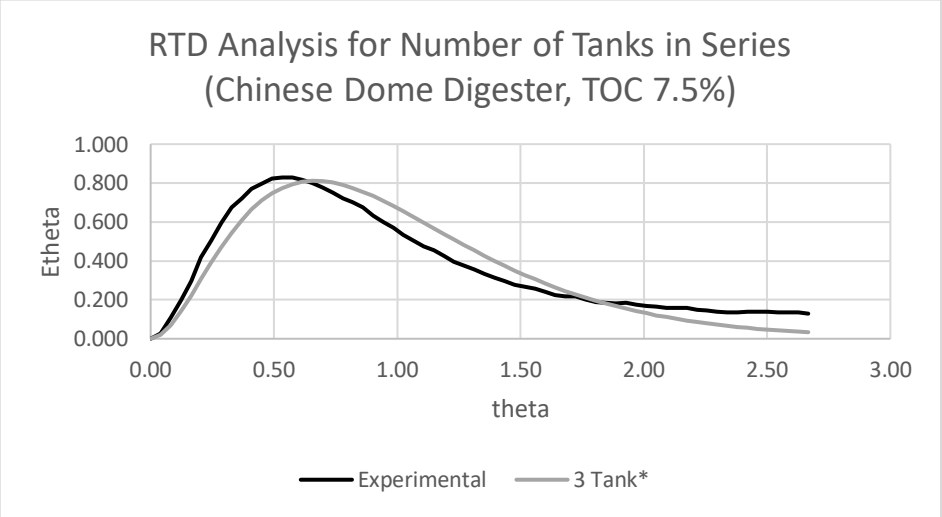

Figure 4.14. RTD Analysis for 3 CSTRs in series in CDD with the same amount of TOC

Jegede et. al. recommended a tanks-in-series model with 3 reactors for unmixed digester and CDD, and with 2 tanks for the mixed digester. In this study, different models, and different numbers of reactors for the tanks-in-series model were examined and agreed with the researchers. Therefore, the same RTD behaviors were chosen for modification of ADM1 digester modelling.

4.2. Methane Production

4.2.1. Finding Reaction Rate Constant Values

The rate constants for disintegration and hydrolysis reaction are not available in 2.3. Hazelnut Husk as Carbon Source. Therefore, they had got to be evaluated based on experimental results of an anaerobic digestion study. Since hazelnut husk is the main carbon source, (Şenol, Anaerobic digestion of hazelnut (Corylus colurna) husks after alkaline pretreatment and determination of new important points in Logistic model curves 2020) was chosen as a reference study. He operated the digester at mesophilic temperature. The active volume is 0.25L as a batch reactor with 30 days of residence time. Table 4.1 shows some of each material's physical properties.

Table 4.1. Physical Properties of manure, hazelnut husk and water (d – density, TS – total solids, VS – volatile solids, m – mass, V – volume and SM – solid matter) (Source: Wang, et al. 2019) (Şenol, Anaerobic digestion of hazelnut (Corylus colurna) husks after alkaline pretreatment and determination of new important points in Logistic model curves 2020)

	d (kg/L)	**TS (kg/kg)**	**VS (kg/kg)**	**VS/TS Ratio**	**m (kg)**	**V (L)**	**m (kg) (TS basis)**	**TS 10%**	**SM Ratio**
Manure	1.000	0.310	0.235	0.758	0.073	0.073	0.023	**10.4**	31.5
Husk	0.230	0.863	0.779	0.903	0.003	0.011	0.002		
Water	1.000	0.000	0.000		0.165	0.165	0.000		
Total					0.241	0.250	0.025		

The macromolecules that are digested by bacteria are carbohydrates, protein, and lipid. Hazelnut husk is only a carbohydrate source with approximately 30 % of lignin which is assumed as inert. Protein and lipid are available in cattle manure beside undigested carbon sources such as straw. Table 4.2 shows the COD amount and fraction of macronutrient availability in the sludge.

Table 4.2. Chemical composition in sludge

	COD (kgVS)	Ratio
Carbohydrate	0.0104	0.6618
Protein	0.0052	0.3283
Lipid	0.0002	0.0098
Total	0.0157	1.0000

Figure 4.15 shows the methane yield curve of the simulation fits the experimental results almost perfectly. The trial and error method was used for the evaluation of reaction rate constants. Table 4.3 shows their default and real values.

Table 4.3. Reaction rate constants for hydrolysis step

Rate Constants	Default	Found
$\mathbf{k_{dis}}$	0.5	0.013
$\mathbf{k_{hydch}}$	10	0.25
$\mathbf{k_{hydpr}}$	10	0.026
$\mathbf{k_{hydli}}$	10	0.11

4.2.2. Methane Production at Different Operating Conditions

The total volume of the reactor is 41.73 L with 39 L of active volume. Hydraulic retention time (HRT) is 65 days because Jegede et al. analyzed the hydrodynamic behavior of the digesters as long as 2.2 times the theoretical HRT value. The volumetric flowrate (Q) of the sludge is 0.604 L/d. Since the 3 CSTRs-in-series design was decided to be made, each reactor's total volume is 13.91 L and active volume is 13 L. HRT is 21 days. Volumetric flowrate remains the same. There are 10 different cases that are examined. Their operating conditions are shown in Table 4.4. The feed was assumed totally biodegradable.

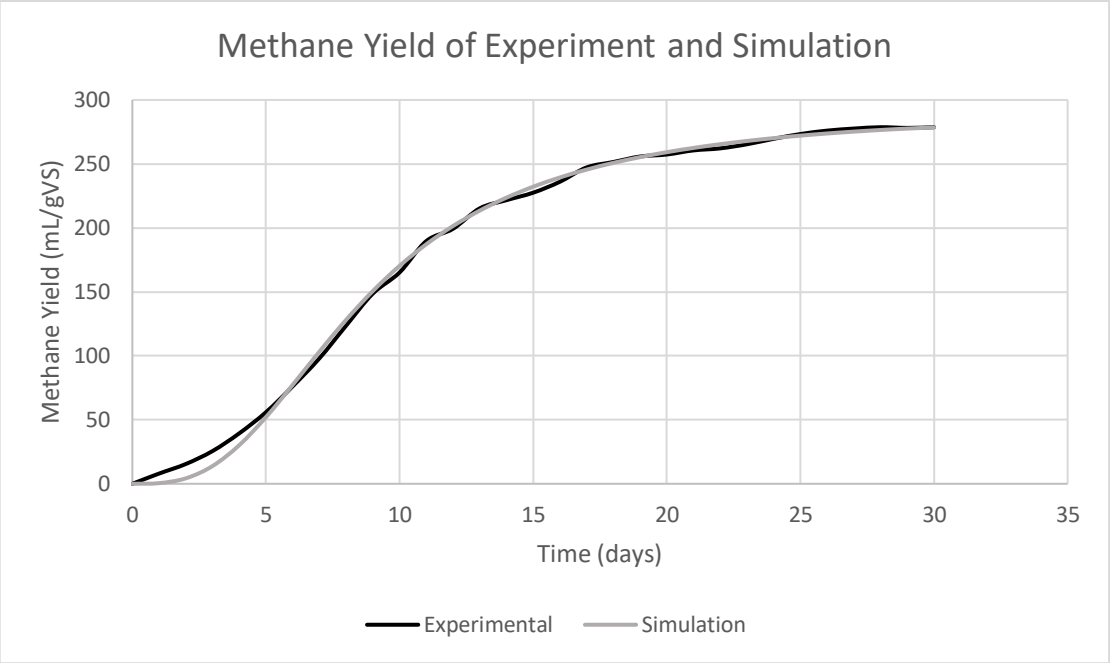

Figure 4.15. Methane yield of experiments and simulation (Source: Şenol, Anaerobic digestion of hazelnut (Corylus colurna) husks after alkaline pretreatment and determination of new important points in Logistic model curves 2020)

Table 4.4. Operating conditions of each case

	Temperature (°C)	**Waste/Manure Ratio**	**TOC (kgVS)**	**Carbohydrate (kgVS)**	**Protein (kgVS)**	**Lipid (kgVS)**	**SM Ratio (%)**
Case1	37.4	0.1	0.599	0.396	0.196	0.0059	22.8
Case2	37.4	0.5	0.603	0.464	0.135	0.0040	19.0
Case3	37.4	1	0.606	0.506	0.097	0.0029	16.5
Case4	10.0	0.1	0.599	0.396	0.196	0.0059	22.8
Case5	60.0	0.1	0.599	0.396	0.196	0.0059	22.8
Case6	37.4	0.1	0.628	0.394	0.219	0.0155	24.4
Case7	37.4	0.1	1.167	0.772	0.382	0.115	45.6
Case8	37.4	0.1	0.898	0.594	0.294	0.0885	22.8
Case9	37.4	0.1	0.725	0.479	0.237	0.0714	22.8
Case10	37.4	0.1	1.796	1.189	0.589	0.0177	22.8

The partial pressure values of gases are needed to evaluate the methane flowrate at the exit of the digester. In biogas, methane and carbon dioxide are abundant. Besides them, hydrogen, and water vapor are present in small amounts. Since methanogenic bacteria utilize carbon dioxide, the partial pressure of methane gas is close to the total pressure of biogas in the initial days. Then, acetogens create balance in population, and carbon dioxide also becomes an effluent almost as much as methane. Figure 4.16 shows the partial pressure of each element in biogas and the total gas pressure in the digester of case 1.

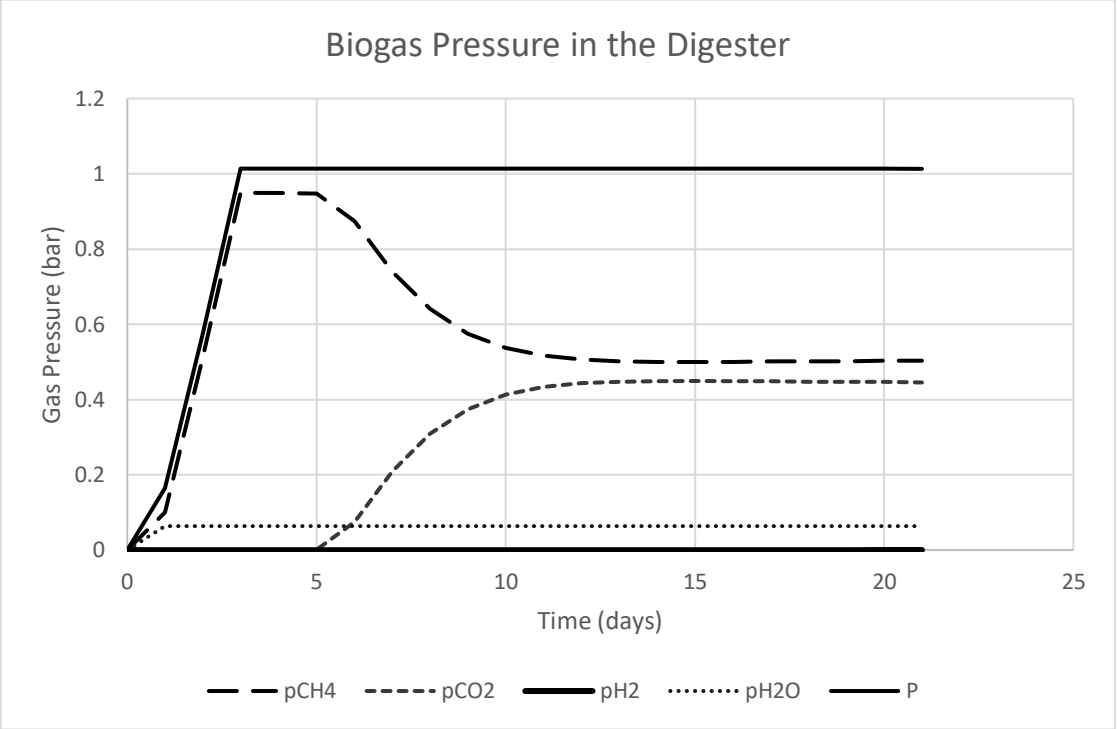

Figure 4.16. Partial pressure of each element in biogas and total pressure

4.2.2.1. Case 1 (Mesophilic, Husk/Manure Ratio of 0.1)

Methane flowrates of each reactor are 0.174, 0.119, and 0.11 L/d, respectively. The total methane produced is 0.403 L/d. At the end of the process, 66.4 % of TOC is removed. Figure 4.17 shows the methane production profile. In the first reactor, 53.6% of the carbon sources are consumed. 10.3% of TOC is removed in the second reactor. The last digester can only remove 2.5% of the carbon source.

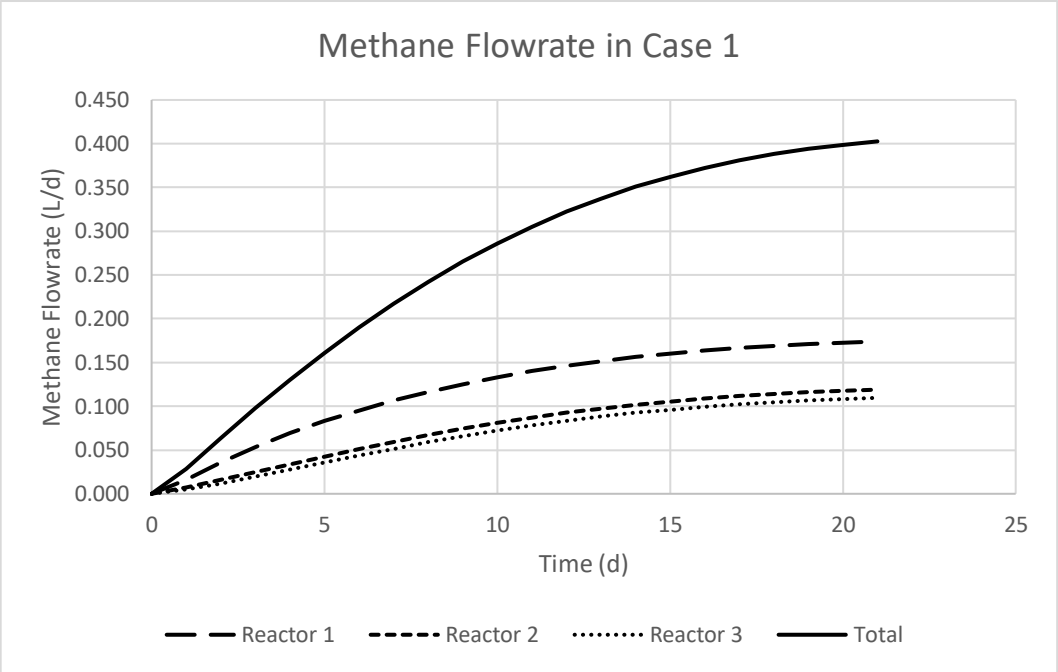

Figure 4.17. Methane flowrate in mesophilic environment with 0.1 hazelnut husk/manure ratio

4.2.2.2. Case 2 (Mesophilic, Husk/Manure Ratio of 0.5)

The overall methane production rate is 0.41 L/d. 57.2 % of TOC is removed in the first reactor with a flowrate of 0.182 L/d. In the second digester, 0.119 L/d is obtained, and the removal percentage of TOC is 9.13 %. In the final reactor, TOC removal is 1.5% with a methane flowrate of 0.109 L/d. 67.8% of carbon source is consumed in total. In Figure 4.18, the methane production rate of each digester and the total amount are shown.

4.2.2.3. Case 3 (Mesophilic, Husk/Manure Ratio of 1)

Figure 4.19 shows the production of methane on a daily basis. Flowrates of methane are 0.188, 0.118, and 0.110 for each reactor, respectively. TOC removal is highest in the first tank with 59.6 %. The second reactor removes 8.22 % of TOC. In the third reactor, only 0.723 % of the carbon source is consumed. In total, 69.22 % of raw material is used.

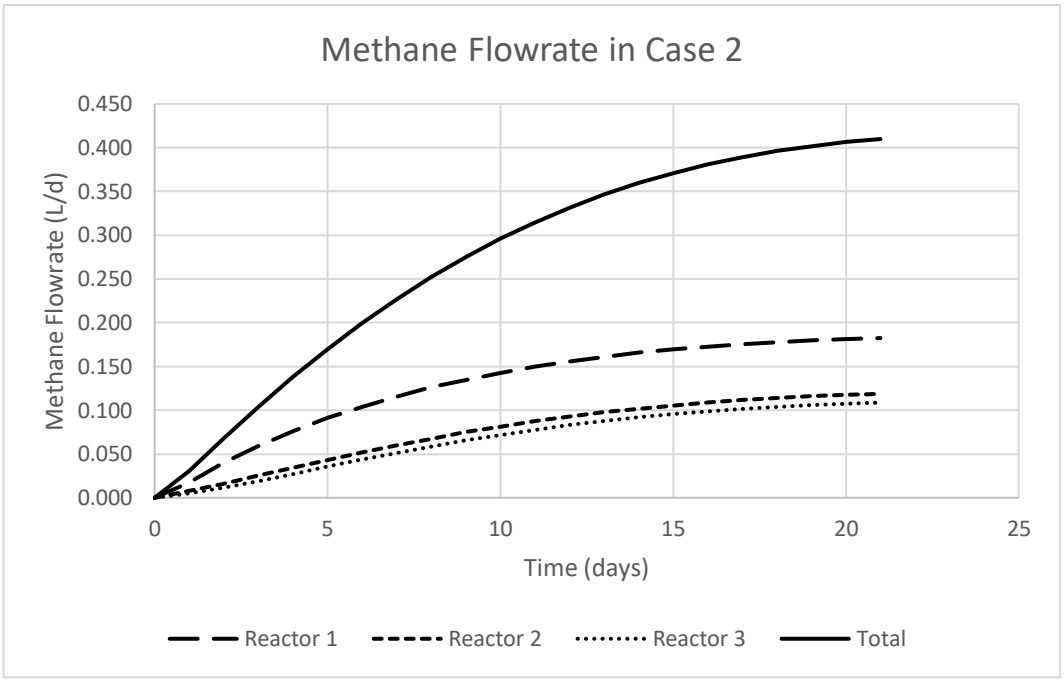

Figure 4.18. Methane flowrate in mesophilic environment with 0.5 hazelnut husk/manure ratio

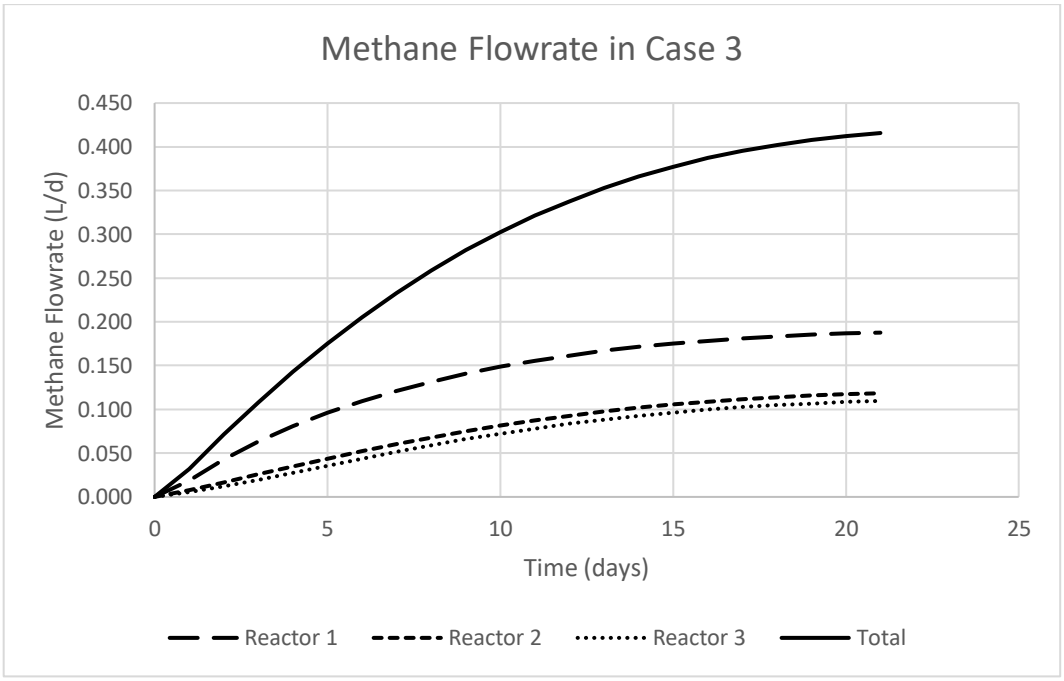

Figure 4.19. Methane flowrate in mesophilic environment with 1 hazelnut husk/manure ratio

4.2.2.4. Case 4 (Psychrophilic, Husk/Manure Ratio of 0.1)

The produced methane amount in each reactor and in total is 0.159, 0.108, 0.100, and 0.367, respectively. Percentages of TOC removal in each reactor are 48.9, 9.39, and 2.28, respectively. In total, 60.5% of the waste is consumed. Figure 4.20 shows the methane production profile of reactors and the cumulative methane production rate.

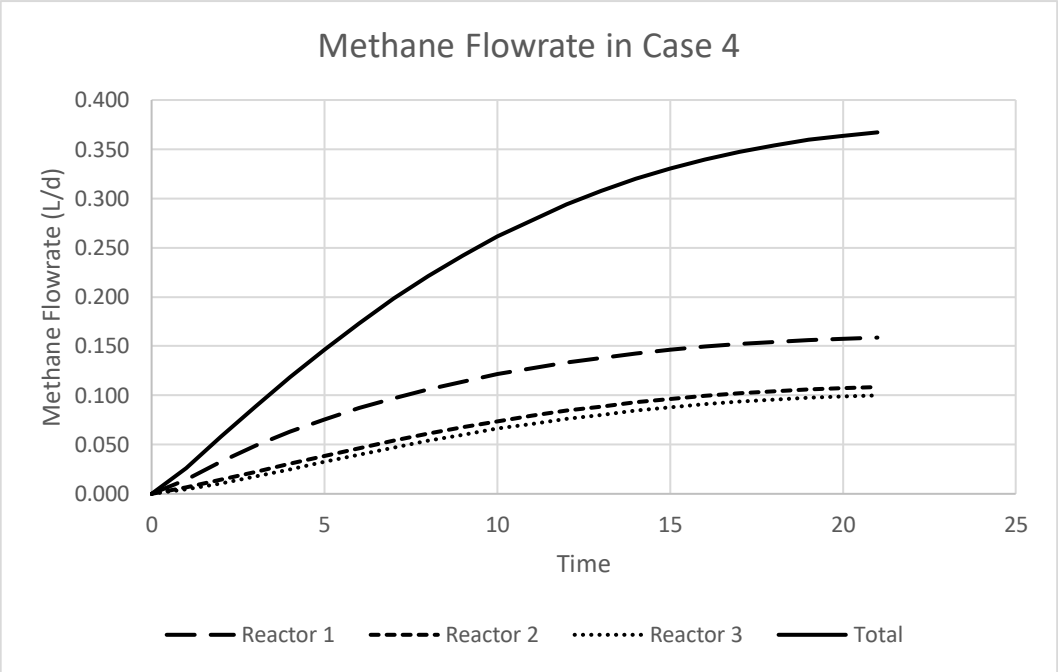

Figure 4.20. Methane flowrate in psychrophilic environment with 0.1 hazelnut husk/manure ratio

4.2.2.5. Case 5 (Thermophilic, Husk/Manure Ratio of 0.1)

In the thermophilic process, 71.2% of TOC is removed. 57.5% of carbon sources are consumed in the first reactor, and the methane flowrate is 0.187 L/d. The second reactor has a methane production rate of 0.128 with 11. % of TOC removal. The methane gas flowrate in the last reactor is 0.118 L/d and the TOC removal is 2.68%. In Figure 4.21 methane yield behaviors are shown.

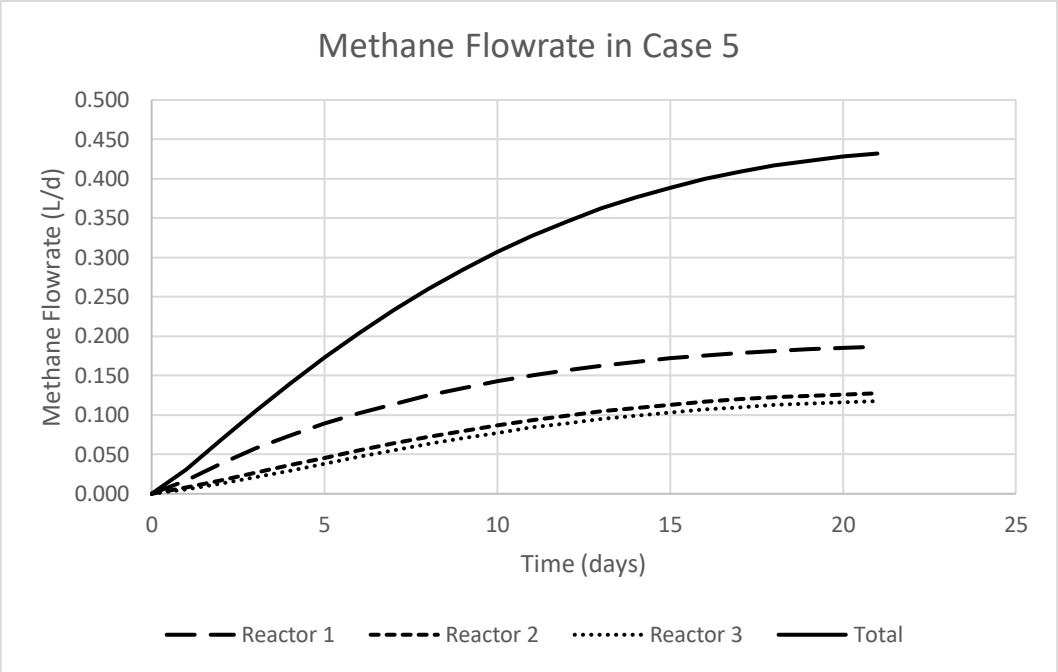

Figure 4.21. Methane flowrate in thermophilic environment with 0.1 hazelnut husk/manure ratio

4.2.2.6. Case 6 (Mesophilic, Food Waste/Manure Ratio of 0.1)

In Figure 4.22, methane production profiles of the process that food waste is a carbon source are shown. The TOC removal in total is 67.5% and the total methane production is 0.41 L/d. Flowrates of methane in each reactor are 0.179, 0.121, and 0.110 L/d. TOC removal in each reactor are 53.7%, 10.9% and 2.9%, respectively.

4.2.2.7. Case 7 (Solid Matter Ratio of 45.6%)

In case 7, the TOC ratio is 15%, unlike the other 9 reactors. The methane production rate for each reactor is 0.269, 0.139, and 0.115 L/d, respectively. In the first reactor, 66.5% of the TOC is removed while it is 10.9% in the second digester and 2.5% in the last one. In total, 79.9% of the carbon source is removed, and 0.523 L/d methane gas is produced. Figure 4.23 shows the methane production behavior in 7^{th} model.

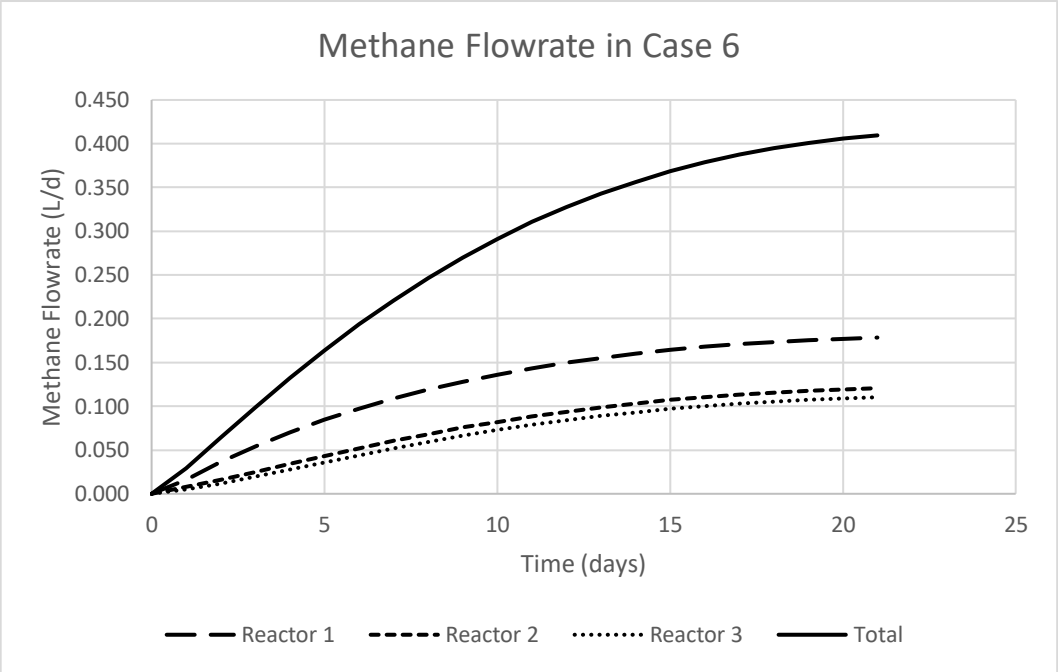

Figure 4.22. Methane flowrate in mesophilic environment with 0.1 food waste/manure ratio

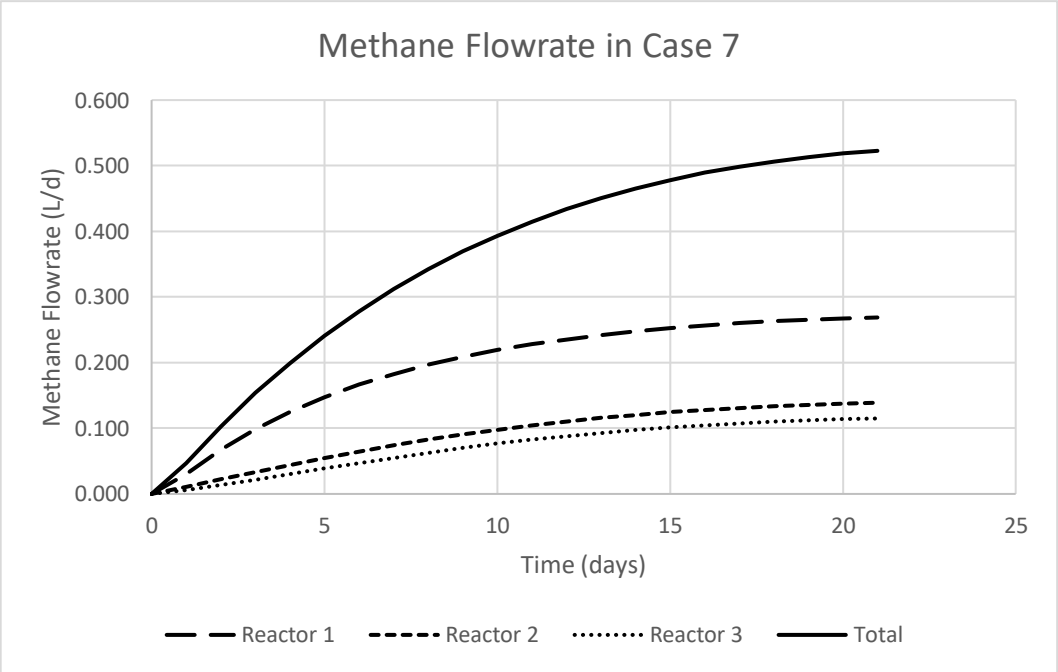

Figure 4.23. Methane flowrate in mesophilic environment with 0.1 husk/manure ratio at 15% TOC

4.2.2.8. Case 8 (Mixed Digester)

Case 8 is the only model that is designed as 2 tanks-in-series. Total methane production is 0.646 L/d with 69.6% TOC removal. The first digester produces 0.407 L/d while the second digester produces 0.239 L/d. The carbon source that is consumed 52.5% of all in the first reactor. The second digester reduces 17.1% of TOC in the process. In Figure 4.24, the methane flowrate profile in case 8 is shown.

4.2.2.9. Case 9 (Chinese Dome Digester)

Chinese Dome Digester (CDD) is the reactor type in case 9. It has an additional 10 L that doesn't violate fixed volume for RTD analysis, so again its active volume is 39 L in that aspect. However, it means an additional amount for producing methane gas. Therefore, it must be counted. Figure 4.25 shows the methane gas production profile. As it is seen, the overall gas flowrate is 0.552 L/d. For each reactor, it is 0.224, 0.168 and 0.160 L/d, respectively. TOC removal is 71.5% in total while each reactor consumes the carbon sources with percentages of 63.2, 6.9, and 1.4 %.

4.2.2.10. Case 10 (Ideal Case)

Case 10 is the imaginary scenario when the fluid behavior is an ideal case which is mixed flow. If the RTD analysis showed that it was not mandatory to split the digester, methane flowrate in the reactor would have a profile as it is seen in Figure 4.26. The methane flowrate at the end of the 21st day is 1.525 L/d which. TOC removal is 54.8 %.

In all processes, the most efficient reactors are first reactors because highest nutrient for bacteria is available.

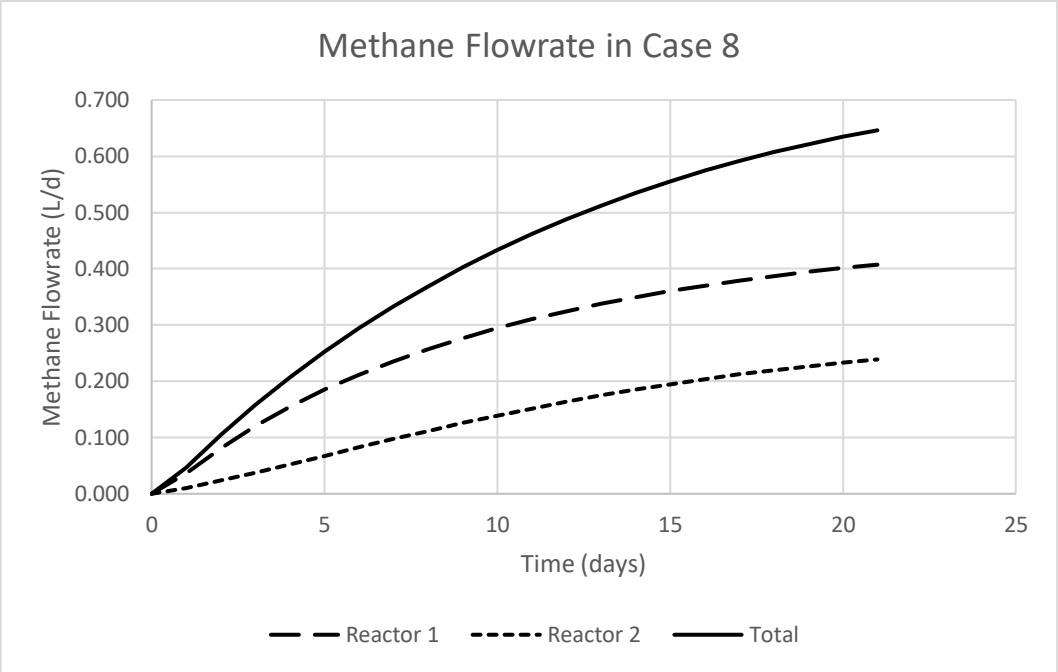

Figure 4.24. Methane flowrate in mesophilic environment with 0.1 husk/manure ratio in a mixed reactor

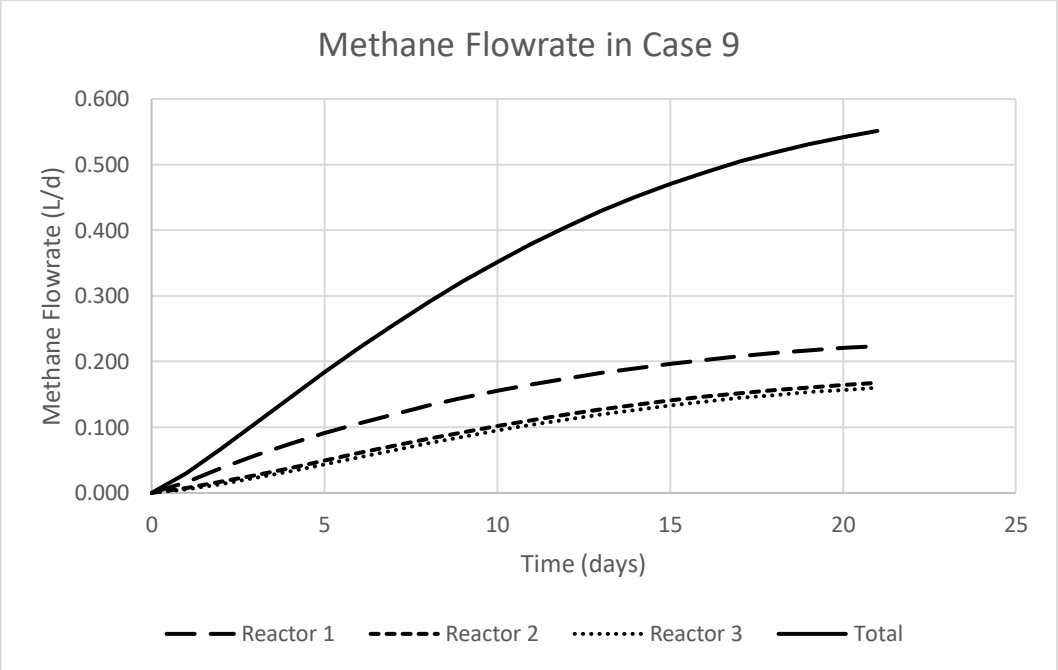

Figure 4.25. Methane flowrate in mesophilic environment with 0.1 husk/manure ratio in a CDD

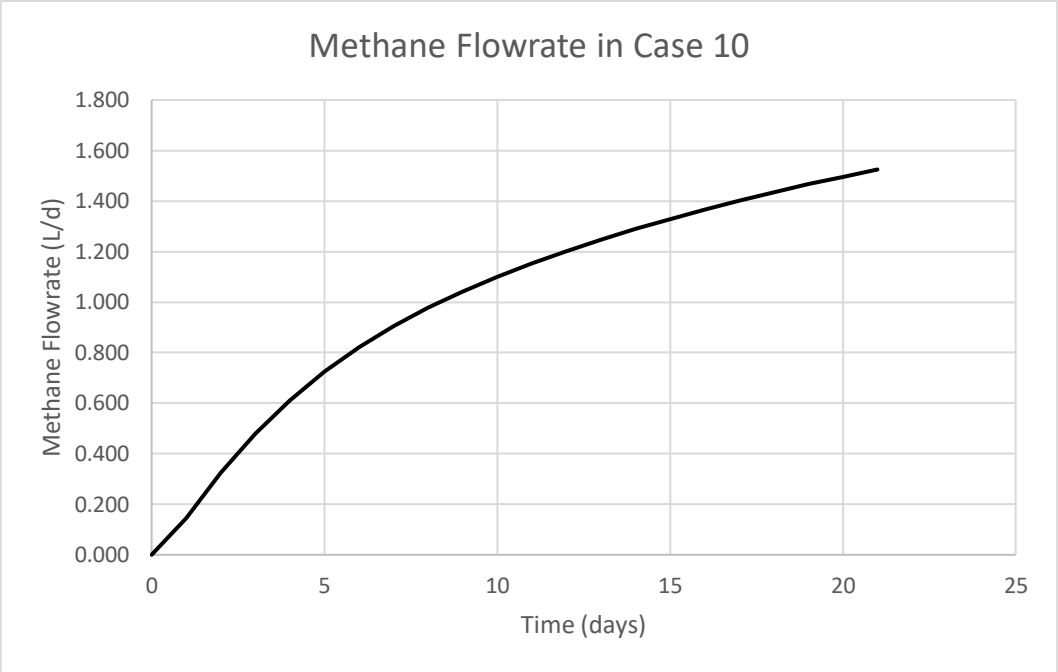

Figure 4.26. Methane flowrate if the RTD analysis proved it is mixed flow

4.2.3. Carbon Source/Manure Ratio Effect

The influence of carbon source and manure ratio is examined in the first three cases. Since the bacteria tend to consume carbohydrates because they live in the bowel of cattle, case 3 shows the best performance with the highest removal of carbon and amount of methane produced as expected. Figure 4.27 shows the methane flowrate and TOC removal in each case. However, carbon amount cannot be increased in the reactor eternally because the maximum tolerable C/N ratio is 35. An excessive amount of carbon source is inhibitive for bacteria because they populate extremely fast and nitrogen deficiency start to kill them off. The symbiotic relation between anaerobes requires the utilization of harmful contents in the environment for one another. During the degradation of complex organic matters, hydrogen gas which is an electron deposit is released. These electrons must be reduced so that the oxidation reactions in the acetogenesis step will not be inhibited. Thermodynamically, low hydrogen gas is favorable for the conversion of VFAs into acetate. Therefore, an increase in carbon sources might be harmful to the process in this aspect. Also, the solid matter ratio (i.e., 22.8 % for case 1 and 16.5 for case 2) gets decreased when hazelnut husk concentration in the sludge increases. Although too

dense and viscous sludge is undesired, too diluted sludge is another undesired case. Phase separation is a potential risk when the solid ratio reduces. Since hazelnut husk is a lignocellulosic material with a smaller density than water, it doesn't dissolve in it. Thus, in the case of phase separation where manure and hazelnut husk do not have healthy contact, microorganisms cannot utilize the substrate in the digester well.

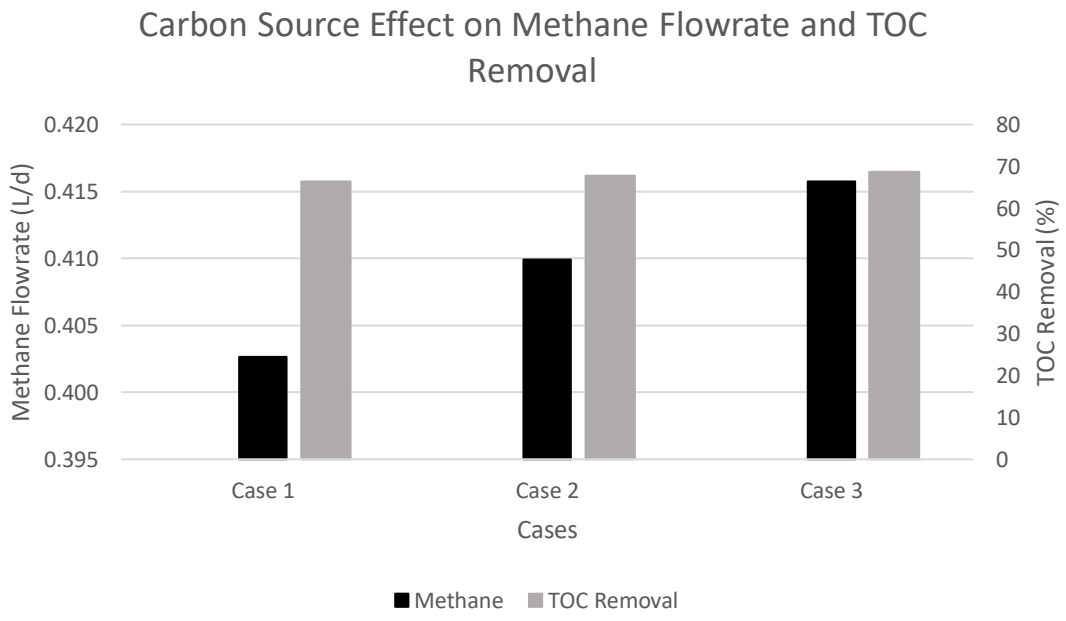

Figure 4.27. Effect of carbon source and TOC removal on the methane production

4.2.4. Temperature Effect

The effect of temperature is observed in case 1, case 4, and case 5. Although the cow's body temperature is 38.5°C which is in the mesophilic temperature range, it is not the most favorable case Arrhenius Equation is used to evaluate the reaction rate constants at different temperature values. Therefore, thermophilic conditions were expected to have higher reaction rate constants while it is vice versa for psychrophilic conditions. Besides that, it is known that acid-base reactions take place too fast, so they are considered equilibrium reactions. Thus, acid-base equations are strictly depending on temperature as Van't Hoff Equation is a function of enthalpy change. The results are not surprising. The most efficient process among all is achieved in case 5 where the thermophilic process is

held, and the least efficient one is the fourth case which is the psychrophilic process as shown in Figure 4.28. Nevertheless, there is a limit to high temperature because bacteria are living organisms which means they are protein-based organisms. Therefore, they die when the temperature increases too high since protein is permanently damaged at high-temperature values. The resilience of microorganisms against temperature depends on the species. For instance, acetogens are more durable at high temperatures than methanogens are. Even though methanogenic anaerobes can process in thermophilic conditions, a better operating approach is to run a thermophilic digester where the acetate formation process is carried out and to operate another one in mesophilic conditions for the methanation process.

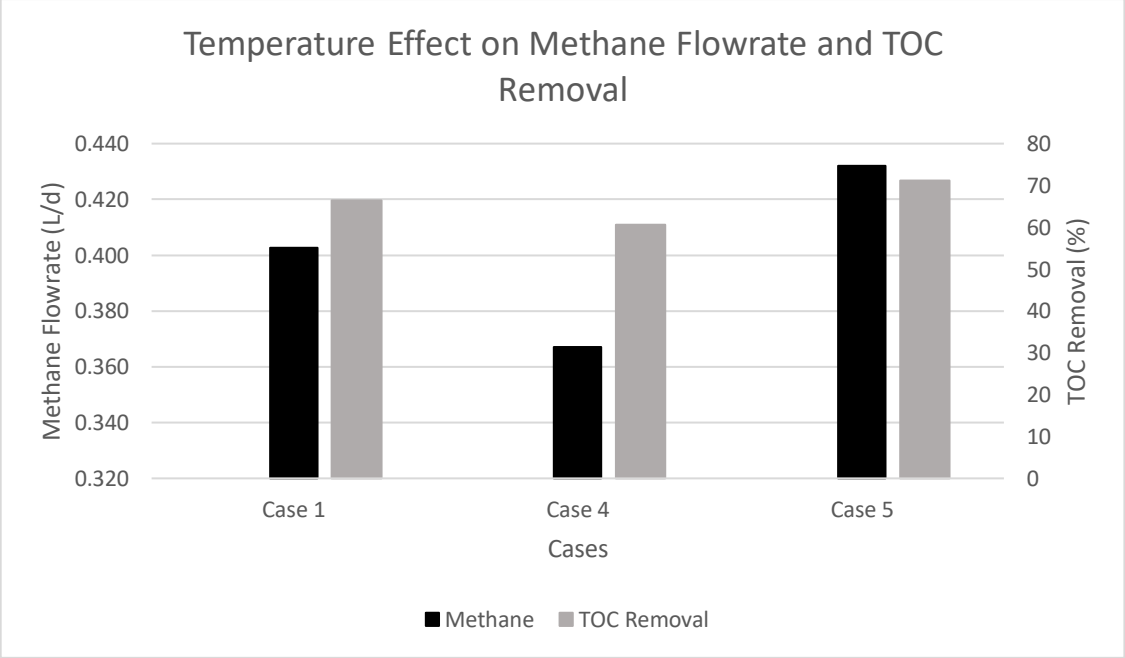

Figure 4.28. Impact of temperature on anaerobic digestion process

4.2.5. Carbon Source Effect

Different carbon source effect is examined in case 1 and case 6. In case 6, food waste is used as a carbon source whose TOC value is higher than hazelnut husk. Thus, it is a more favorable case, and the results satisfy this expectation. Figure 4.29 shows the methane production depending on the carbon source. Only if the fraction of hazelnut husk

in the sludge increases while the total solid percentage (i.e., 7.5%) is kept constant, then the performance in the food waste scenario can be reached. Case 2 with a 0.5 ratio of husk and manure has the same amount of methane production in total. Although there is more carbohydrate in case 2, the protein and lipid availability in case 6 helps the bacteria to continue producing methane. Especially, the difference between the lipid compositions favors food waste in second and third reactors. As it was said before, first reactors have more TOC, so they perform the best. The first reactor in case 2 surpasses that of case 6, but the second and third reactors are mostly where bacteria adapt themselves to the environment better where protein and lipid amounts are high and start to utilize them. Especially, lipids come in handy in latter reactors. Therefore, higher protein and lipid amounts give food waste the advantage in the last 2 reactors. Also, this case clearly shows that the primary substrate that anaerobic bacteria utilize is carbohydrate because in case 2, TOC is 0.603 kgVS while it is 0.628 kgVS for case 6. When the reactions are considered, it is thought that carbohydrate is the least efficient substrate because of the high amount of carbon dioxide produced. However, in the first reactors, carbohydrate is shown better. It is because bacteria are more familiar with carbohydrates. In the latter reactors, the situation changes. Under these conditions, both tanks produce the same amount of methane in the same period. Moreover, in case 3, the TOC amount is 0.606 kgVS and its methane flowrate at the exit is 0.416 L/d. Briefly, as the carbohydrate amount raises, the methane yield increases, too.

4.2.6. Total Solid (TS) Amount Effect

Case 1 and case 7 are the same reactors with different TS levels. In the first model, 7.5% TS is available while it is 15% in the seventh model. The solid matter ratio is 2 times of the first reactor. As was expected, it is a very inefficient process because a reactor filled with 45.6 % solid matter amount cannot be mixed well compared to the one with a 22.8% solid matter ratio. The substrate in case 7 is piled up where bacteria are not able to reach easily or at all. An excessive amount of solid matter in the digester creates a mass transfer limitation problem. Moreover, it is an unmixed reactor type. Therefore, it is an even more challenging way to produce methane. The problem of this case is not the availability of carbon sources, but the reachability of it. Even though the amount of

produced methane is more, efficiency is much less. Figure 4.30 shows the solid mater impact on methane production and yield, and removal of TOC. The methane yield of the first design is 0.224 L/kgVS while it is 0.149 L/kgVS in a reactor with doubled TS. TOC removal is highest while methane yield is lowest. It is attributed to methanogenic bacteria are not totally dominant, so rival microorganisms are also very active.

4.2.7. Reactor Type Effect

Figure 4.31 demonstrates the methane amount produced in each of the different reactor types. Case 8 has only 2 reactors. This is because, in RTD analysis, the most suitable design is found to be 2 tanks in series by researchers and proved in this study. As the mixing state of the digester goes bad, the number of reactors in the tanks-in-series model increases, too. Therefore, the mixing type of digester needed only 2 tanks in series. All conditions except for the volume of one reactor are the same as the first model's operating conditions. As it is obvious from the methane production profile in each of the models, the first reactor mostly does half of the job. Moreover, as the volume of a reactor increases, the production rate increases, too. Therefore, it is not surprising that the first reactor, having a size of 1.5 times of each reactor in case 1, produces methane even more than the total of case 1. Also, the methane yield of case 8 is 0.360 L/kgVS. The intermittently mixed reactor is the most efficient model as it is predicted. CDD type of reactor has the advantage of an additional 10L-tank which does not affect hydrodynamic behavior but clearly affects methane production. As it is said before, when the size of the digester increases, the methane production rate increases too. The efficiency of this case is 0.245 L/kgVS. It is close to case 1 in terms of efficiency, nevertheless, it is better. This shows that the bacteria population does not increase linearly. Since it is the 3D environment, the growth naturally is not linear.

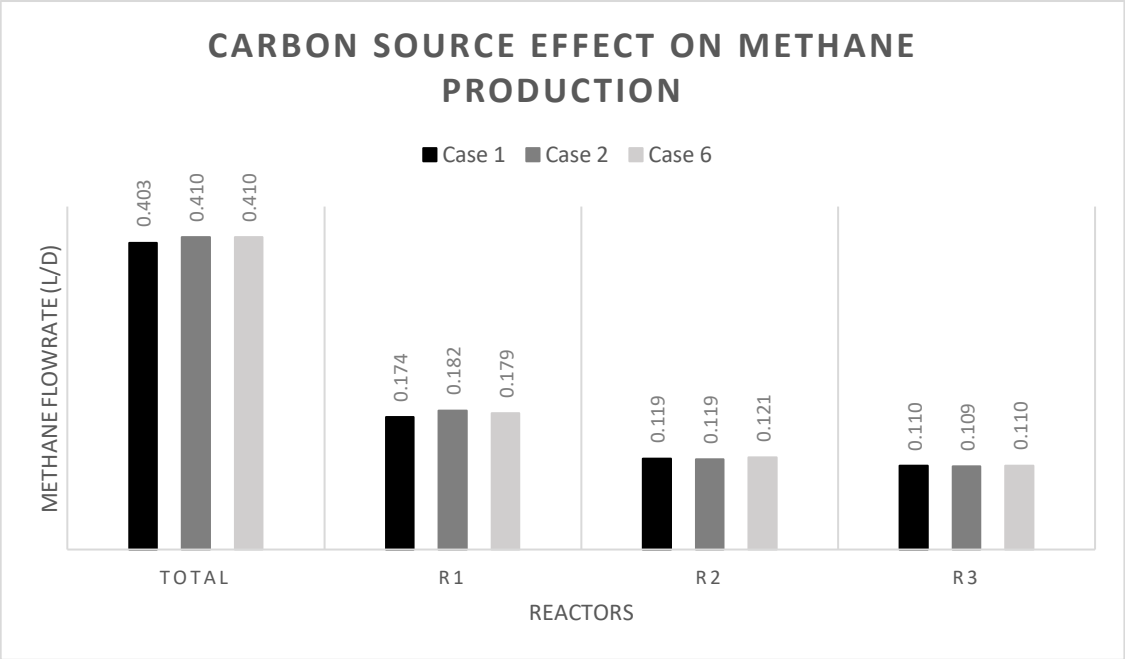

Figure 4.29. Carbon source effect on methane production

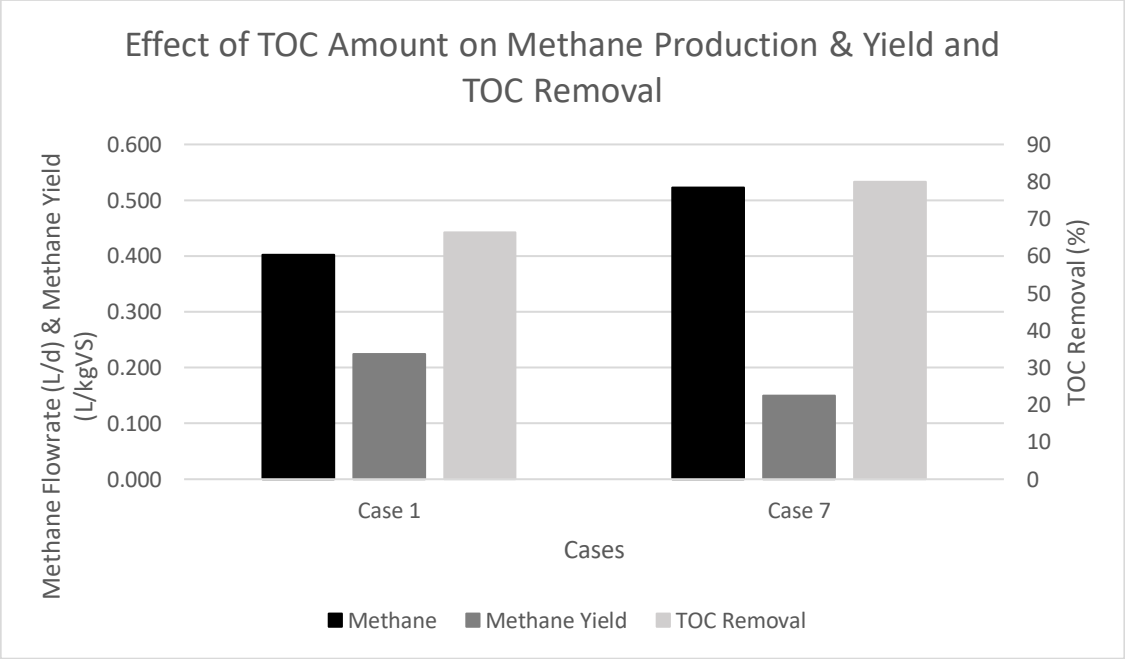

Figure 4.30. TS amount effect on anaerobic digestion process

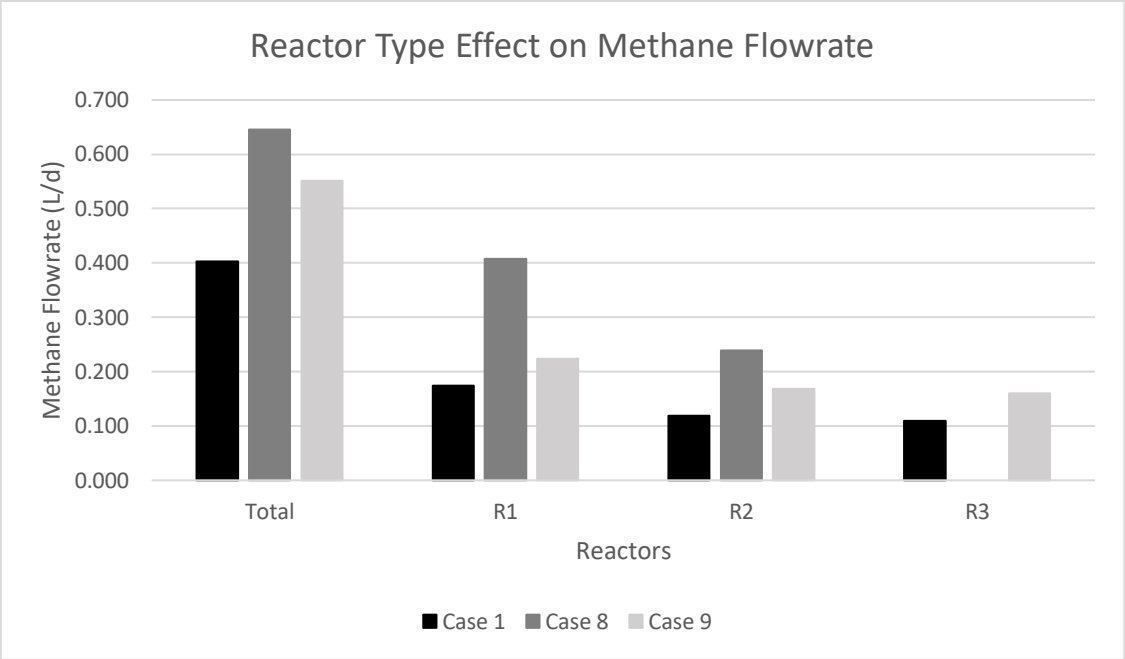

Figure 4.31. Effect of reactor type on methane flowrate

4.2.8. RTD Effect

Residence time distribution analysis is a crucially important hydrodynamic analysis for this kind of highly viscous reactor. Although the RTD effect was mentioned in the reactor type section, an imaginary case where the reactor is assumed well-mixed initially shows the remarkable difference between two digesters within the same operating conditions. The only difference is that case 1 was modified with RTD analysis result while case 10 was assumed as an ideal reactor. As is seen in Figure 4.32, methane production is more than 3 times of case 1. This shows that if RTD analysis is ignored, completely inaccurate results will be the outcome of that model. Similar to methane production, methane yield is also insanely high which indicates that the process is very efficient. However, if the reactor is modified with a piece of useful mixing equipment, process efficiency will be enormously improved as these results show.

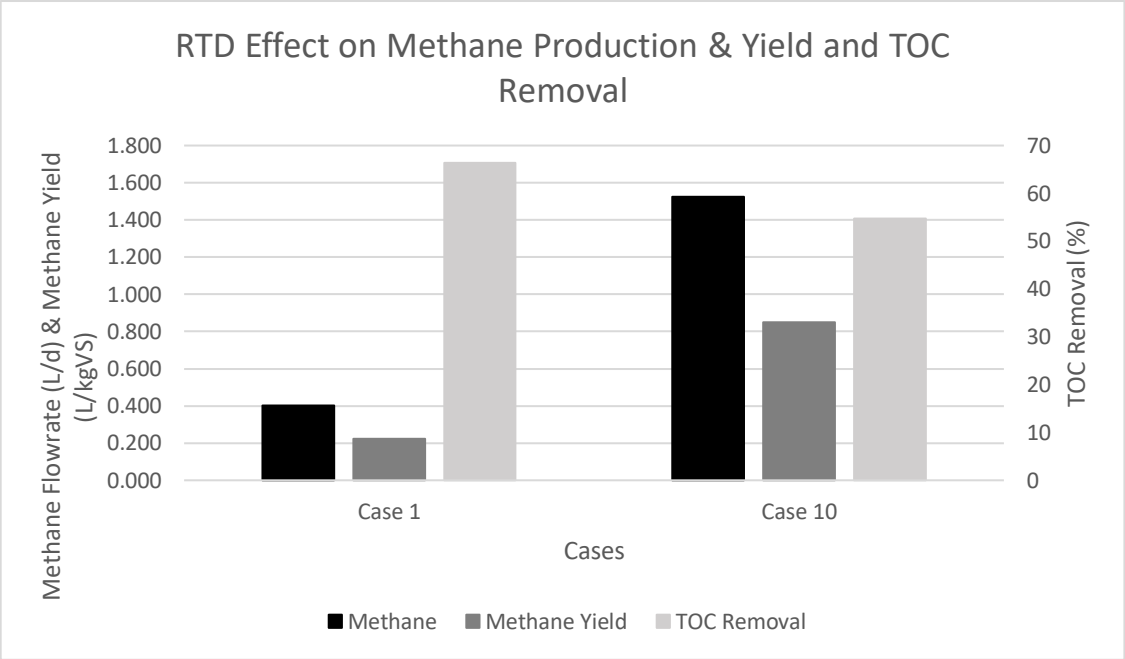

Figure 4.32. RTD effect on anaerobic digestion

When the results are compared with the outcome of the study (Jegede, Zeeman and Bruning 2019), it is shown that the models and real results match. In the research, the least efficient model is the one with an unmixed reactor and doubled TS. In this study, case 7 is the most inefficient model. A mixed reactor with 7.5% TS is the most efficient digester in their research, and this study shows that it is the most efficient process, too. CDD is a more efficient process than the unmixed process, so it is, too, modelled accurately in this study. Lastly, if the imaginary case would be the real case, it would be the best scenario for the production of biogas even though the lowest TOC removal is observed in that case.

CHAPTER 5

CONCLUSION

ADM1 is a mathematical matrix model that was applied in this study. It was developed based on a CSTR type reactor that consists of 19 biochemical, 6 acid-base, and 3 liquid-gas transfer equations. The sludge is too viscous, so achieving a well-mixed slurry is crucially important in order to collect reliable results from ADM1. Therefore, residence time distribution (RTD) analysis is made to find out the fluid's behavior in the digester and model the reactor depending on RTD results.

In this study, methane production by the anaerobic digestion method from the utilization of hazelnut husk was investigated. Residence time distribution analysis was taken into consideration for the determined operating conditions. It was aimed to investigate the performance of a household digester, therefore, a suitable RTD analysis made in the same conditions was applied. 3 tanks-in-series model gave the most accurate results in 8 cases out of 10 while one of them needed 2 tanks in series and the last one was a single digester. In 10 different cases, effects of carbon source/manure ratio, temperature, type of carbon source, TS percentage in the digester, and type of reactor were modelled as well as an imaginary case that is assumed to have an ideal hydrodynamic behavior in order to show how inaccurate results are obtained if RTD analysis is ignored.

In the first three cases, methane production is found at 0.403, 0.410, and 0.416 L/d, respectively. The population of microorganisms changes directly proportional to the amount of carbon source. Thus, when the carbon source/manure ratio increases, the population grows faster, and methane production, methane yield, and TOC removal were found to be at their highest values in the highest carbon source/manure ratio. It is suggested to feed bacteria as much waste as possible while taking the C/N ratio limitation into consideration. The reaction kinetics depends on temperature, so thermophilic conditions showed the best performance in terms of methane flowrate of 0.432 L/d, methane yield of 0.240 L/kgVS, and TOC removal of 71.2 %. As a different carbon source, kitchen waste was examined. Since its TOC content is more than hazelnut husk,

it showed a better performance in terms of methane production. In the sixth scenario in which food waste is utilized as a carbon source, total methane production was calculated at 0.410 L/d. It was 0.403 L/d for hazelnut husk digester under the same conditions. The solid matter ratio is a significantly effective factor. It was found that a higher TS ratio produces higher methane, however, methane yield is too low. The methane amount produced is 0.532 L/d while the methane yield is 0.149 L/kgVS. Therefore, it is not recommended to operate the digester at a high solid matter ratio. Mixing the sludge favors the bacteria's function because they have an opportunity to move and reach feed easily. Their mobility creates a healthier environment to thrive. Hence, the mixing reactor type had the highest methane flowrate among the 3 different reactor types. It is 0.646 L/d. Chinese Dome Digester was found to be the second-best digester type with a methane flowrate of 0.552 L/d because of additional active volume. Lastly, in the digester where RTD was ignored, methane production is 3 times of highest methane flowrate obtained among the other 9 cases. This huge difference proves that ignoring hydrodynamic analysis leads to a completely inaccurate result.

All in all, in this master thesis, an ADM1 modelling was made for the degradation of hazelnut husk in an anaerobic environment. It is expected that the best performance can be achieved if the maximum possible husk/manure ratio is adjusted in a thermophilic environment whilst the sludge is mixed as well as possible.

REFERENCES

Abbas, Syed Zaghum, and Mohd Rafatullah. 2018. "Sediment Microbial Fuel Cells in Relation to Anaerobic Digestion Technology." In *Anaerobic Digestion Processes - Application and Effluent Treatment,* by Nigel Horan, Abu Zahrim Yaser and Newati Wid, 33 - 55. Singapore: Springer.

Abdel-Shafy, Hussein I., and Mona S. M. Mansour. 2014. "Biogas production as affected by heavy metals in the anaerobic digestion of sludge." *Egyptian Journal of Petroleum, 23(4)* 409 - 417.

Age of Revolution. 2019. *Faraday's Electric Generator.* 06 20. https://ageofrevolution.org/200-object/faradays-electric-generator/.

Ahn, Johng-Hwa, Trong Hoan Do, Sang D. Kim, and Seokhwan Hwang. 2006. "The effect of calcium on the anaerobic digestion treating swine wastewater." *Biochemical Engineering Journal, 30(1)* 33 - 38.

Anwar, Naveed, Wen Wang, Jie Zhang, Yeqing Li, Chang Chen, Guangqing Liu, and Ruihong Zhang. 2016. "Effect of sodium salt on anaerobic digestion of kitchen waste." *Water Science and Technology, 73(8)* 1865 - 1871.

Argonne. 2019. *Nuclear Engineering Division.* 10 07. https://www.ne.anl.gov/About/reactors/early-reactors.shtml#:~:text=Chicago%20Pile%201%20was%20the,On%20Dec.

Barber, Nick. 2018. "1991 Gulf War Oil Spill." *Stanford University.* 11 23. http://large.stanford.edu/courses/2018/ph240/barber1/.

Batstone, D. J., J. Keller, I. Angelidaki, S. V. Kalyuzhnyi, S. G. Pavlostathis, A. Rozzi, W. T. M. Sanders, H. Siegrist, and V. A. Vavilin. 2002. *Anaerobic Digestion Model No. 1.* London: IWA Publishing.

Bellis, Mary. 2019. *The History of the Water Wheel.* 11 24. https://www.thoughtco.com/history-of-waterwheel-4077881#:~:text=The%20first%20reference%20to%20a,supply%20drinking%20water%20to%20villages.

Cabirol, N., E. J. Barragan, A. Duran, and A. Noyola. 2003. "Effect of aluminium and sulphate on anaerobic digestion of sludge from wastewater enhanced primary treatment." *Water Science and Technology, 48(6)* 235 - 240.

Chen, Shujun, Jishi Zhang, and Xikui Wang. 2015. "Effects of alkalinity sources on the stability of anaerobic digestion from food waste." *Waste Management & Research, 33(11)* 1033 - 1040.

Chen, Ye, and Jay J. Cheng. 2007. "Effect of potassium inhibition on the thermophilic anaerobic digestion of swine waste." *Water Environment Research, 79(6)* 667 - 674.

Cheng, Jay J. 2018. "Anaerobic Digestion for Biogas Production." In *Biomass to Renewable Energy Processes*, by Jay Cheng, 143 - 195. London & New York: Taylor & Francis Group.

Chuanshu , He, Mu Yang, Liu Xiaofeng, Yan Zhengying, and Yue Zhengbo. 2019. *Comprehensive Biotechnology (3rd Edition), Volume 3, Page 110-127.* Waterloo: Pergamon.

Cioabla, Adrian Eugen, Ioana Ionel, Gabriela-Alina Dumitrel, and Francisc Popescu. 2012. "Comparative study on factors affecting anaerobic digestion of agricultural vegetal residues." *Biotechnology for Biofuels, 5(1)* 1 - 9.

Clifford, Caroline Burgess. 2010. *Anaerobic Digestion.* 01 01. https://www.e-education.psu.edu/egee439/node/727.

Edison Tech Center. 2014. *The History of Electrification.* 01 01. http://edisontechcenter.org/HistElectPowTrans.html.

Ehrlich, Robert, and Harold A. Geller. 2018. "Geothermal Energy." In *Renewable Energy - A First Course*, by Robert Ehrlich and Harold A. Geller, 157 - 185. London & New York: Taylor & Francis.

Ehrlich, Robert, and Harold A. Geller. 2018. "Hydropower." In *Renewable Energy - A First Course*, by Robert Ehrlich and Harold A. Geller, 221 - 249. London & New York: Taylor & Francis Group.

Ehrlich, Robert, and Harold A. Geller. 2018. "Solar Radiation and Earth's Climate." In *Renewable Energy - A First Course*, by Robert Ehrlich and Harold A. Geller, 249 - 281. London and New York: Taylor & Francis Group.

Ehrlich, Robert, and Harold A. Geller. 2018. "Wind Power." In *Renewable Energy - A First Course*, by Robert Ehrlich and Harold A. Geller, 185 - 221. London and New York: Taylor & Francis Group.

eia. 2022. *Bioenergy.* 05 01. https://www.iea.org/fuels-and-technologies/bioenergy.

—. 2021. *Biomass.* 06 08. https://www.eia.gov/energyexplained/biomass/.

—. 2021. *Geothermal explained - Geothermal Power Plants.* 12 17. https://www.eia.gov/energyexplained/geothermal/geothermal-power-plants.php#:~:text=The%20first%20geothermal%20power%20plant,steam%20to%20drive%20generator%20turbines.

Enerdata. 2022. *Total Energy Consumption.* 01 01. https://yearbook.enerdata.net/total-energy/world-consumption-statistics.html.

—. 2022. *Total Energy Production.* 01 01. https://yearbook.enerdata.net/total-energy/world-energy-production.html.

ENERGY.GOV. 2013. *A History of Geothermal Energy in America.* 01 01. https://www.energy.gov/eere/geothermal/history-geothermal-energy-america.

—. 2013. *How Do Wind Turbines Work?* 01 01. https://www.energy.gov/eere/wind/how-do-wind-turbines-work#:~:text=Wind%20turbines%20work%20on%20a,a%20generator%2C%20which%20creates%20electricity.

Enerji. 2022. *Biyokütle.* 04 01. https://enerji.gov.tr/bilgi-merkezi-enerji-biyokutle.

—. 2022. *Güneş.* 04 01. https://enerji.gov.tr/bilgi-merkezi-enerji-gunes.

—. 2022. *Hidrolik.* 04 01. https://enerji.gov.tr/bilgi-merkezi-enerji-hidrolik.

—. 2022. *Jeotermal.* 04 01. https://enerji.gov.tr/bilgi-merkezi-enerji-jeotermal.

—. 2022. *Rüzgar.* 04 01. https://enerji.gov.tr/bilgi-merkezi-enerji-ruzgar.

EPA. 2022. *Deepwater Horizon - BP Gulf of Mexico Oil Spill.* 02 15. https://www.epa.gov/enforcement/deepwater-horizon-bp-gulf-mexico-oil-spill.

European Commission. 2015. *Paris Agreement.* 12 12. https://ec.europa.eu/clima/eu-action/international-action-climate-change/climate-negotiations/paris-agreement_en.

Feijoo, Gumersindo, Manuel Soto, Ramon Mendez, and Juan M. Lema. 1995. "Sodium inhibition in the anaerobic digestion process: Antagonism and adaptation phenomena." *Enzyme and Microbial Technology, 17(2)* 180 - 188.

Fogler, H. Scott. 2016. *Elements of Chemical Reaction Engineering, Fifth Edition.* Pearson Education.

Gagliano, Maria Cristina, Dainis Sudmalis, Hardy Temmink, and Caroline M. Plugge. 2020. "Calcium effect on microbial activity and biomass aggregation during anaerobic digestion at high salinity." *New Biotechnology, 56* 114 - 122.

García, Laura Andrea Morales, David Rodriguez, and Herbert Enrique Rojas Cubides. 2017. "Assessment of the input substrate characteristics included in the Anaerobic Digestion Model No. 1 (ADM1)." *Ingeniería, 22(2)* 269-282.

Godyn, Dorota, Piotr Herbut, and Sabina Angrecka. 2019. "Measurements of peripheral and deep body temperature in cattle – a review." *Journal of Thermal Biology (Vol. 79)* 42 - 49.

Guney, Mukrimin Sevket. 2013. "Utilization of hazelnut husk as biomass." *Sustainable Energy Technologies and Assessments, 4* 72 - 77.

Habashi, Fathi. 2000. "The First Oil Well in the World." *American Chemical Society.* 11 01. http://acshist.scs.illinois.edu/bulletin_open_access/v25-1/v25-1%20p64-66.pdf.

Herkowiak, Marcin, Mariusz Adamski, Zbigniew Dworecki, Boguslawa Waliszewska, Krzysztof Pilarski, Kamil Witaszek, Gniewko Niedbala, and Magdalena Piekutowska. 2018. "Analysis of the possibility of obtaining thermal energy from combustion of selected cereal straw species." *Journal of Research and Applications in Agricultural Engineering, 63(4).*

Ince, O. 1998. "Performance of a two-phase anaerobic digestion system when treating dairy wastewater." *Water Research, 32(9)* 2707 - 2713.

Jegede, A. O., G. Zeeman, and H. Bruning. 2019. "Evaluation of liquid and solid phase mixing in Chinese dome digesters using residence time distribution (RTD) technique." *Renewable Energy, 143* 501 - 511.

Jiang, Ying, Ewan McAdam, Yue Zhang, Sonia Heaven, Charles Banks, and Philp Longhurst. 2019. "Ammonia inhibition and toxicity in anaerobic digestion: A critical review." *Journal of Water Process Engineering, 32* 100899.

Kentucky Foundation. 2007. *Frequently Asked Questions about Coal.* 01 01. http://www.coaleducation.org/q&a/who_discovered_coal.htm#:~:text=Coal%20was%20one%20of%20man's,Richmond%2C%20Virginia%2C%20in%201748.

Kim, Jung Kon, Baek Rock Oh, Young Nam Chun, and Wouk Si Kim. 2006. "Effects of temperature and hydraulic retention time on anaerobic digestion of food waste." *Journal of Biosience and Bioengineering* 328 - 332.

Kohl, Harald, and Wolfhart Dürrschmidt. 2013. "Renewable Energy Sources - a Survey." In *Renewable Energy - Sustainable Concept for the Energy Change*, by Roland Wengenmayr and Thomas Bührke, 4 - 14. Frankfurt: WILEY - VCH.

Koster, I. W., and G. Lettinga. 1984. "The influence of ammonium-nitrogen on the specific activity of pelletized methanogenic sludge." *Agricultural Wastes, 9(3)* 205 - 216.

Kugelman, Irwin J., and Perry L. McCarty. 1965. "Cation toxicity and simulation in anaerobic waste treatment." *Journal (Water Pollution Control Federation)* 97 - 116.

Land Art Generator. 2012. *The 19th Century Solar Engines of Augustin Mouchot , Abel Pifre, and John Ericsson.* 02 29. https://landartgenerator.org/blagi/archives/2004.

Levenspiel, Octave. 1999. *Chemical Reaction Engineering, Third Edition.* John Wiley & Sons.

—. 2011. *Tracer Technology: Modelling the Flow of Fluids(Vol. 96).* Springer Science & Business Media.

Li, R., S. Chen, and X. Li. 2009. "Anaerobic co-digestion of kitchen waste and cattle manure for methane production." *Energy Sources, Part A: Recovery, Utilization, and Environmental Effects, 31(20)* 1848 - 1856.

Li, Yin, Christopher P. Alaimo, Minji Kim, Norman Y. Kado, Joshua Peppers, Jian Xue, Chao Wan, et al. 2019. "Composition and toxicity of biogas produced from different feedstocks in california." *Environmental Science & Technology* 11569 - 11579.

Manchala, Karthik R., Yewei Sun, Dian Zhang, and Zhi-Wu Wang. 2017. "Anaerobic Digestion Modelling." In *Advances in Bioenergy*, by Yebo Li and Xumeng Ge, Vol.2, 69-141. Elsevier.

McCartney, D. M., and J. A. Oleszkiwicz. 1991. "Sulfide inhibition of anaerobic degradation of lactate and acetate." *Water Research, 25(2)* 203 - 209.

McCarty, Perry L. 1964. "Anaerobic waste treatment fundamentals, Part III, toxic materials and their control." *Public Works, 95(9)* 91 - 94.

Mullen, Anne Maria, Carlos Alvarez, Milica Pojic, Tamara Dapcevic Hadnadjev, and Maria Papageorgiou. 2015. "Classificiation and Target Compounds." In *Food Waste Recovrey: Processing Technologies and Industrial Techniques*, by Charis M. Galanakis, 25 - 59. Academic Press.

National Geographic Society. 2012. *Biomass Energy.* 11 19. https://www.nationalgeographic.org/encyclopedia/biomass-energy/.

Natural Gas. 2013. *History.* 09 20. http://naturalgas.org/overview/history/.

Nghiem, L.D., F.I. Hai, W.E. Price, R. Wickham, H.H. Ngo, and W. Guo. 2017. "By-products of Anaerobic Treatment: Methane and Digestate from Manures and Cosubstrates." In *Current Developments in Biotechnology and Bioengineering - Biologica Treatment of Industrial Effluents,* by Duu-Jong Lee, Veeriah Jegatheesan, Hao Huu Ngo, Patrick C. Hallenbeck and Ashok Pandey, 469 - 484. Elsevier.

Nguyen, Luong N., Anh Q. Nguyen, and Long D. Nghiem. 2019. "Microbial Community in Anaerobic Digestion System: Progression in Microbial Ecology." In *Water and Wastewater Treatment Technologies*, by Xuan-Thanh Bui, Chart Chiemchaisri, Takahiro Fujioka and Sunita Varjani, 331 - 355. Singapore: Springer.

Noria Corporation. 2008. *The History of the Nornia.* 01 01. https://www.machinerylubrication.com/Read/1294/noria-history.

NREL. 2022. *Geothermal Electricity Production Basics.* 04 01. https://www.nrel.gov/research/re-geo-elec-production.html#:~:text=Geothermal%20power%20plants%20use%20steam,more%20below%20the%20earth's%20surface.&text=The%20steam%20rotates%20a%20turbine,a%20generator%2C%20which%20produces%20electricity.

Nunez, Christina. 2019. *Hydropower, Explained.* 05 13. https://www.nationalgeographic.com/environment/article/hydropower#:~:text=In%201882%2C%20the%20world's%20first,Fox%20River%20in%20Appleton%2C%20Wisconsin.

Office of the Historian. 2020. *Oil Embargo.* 01 01. https://history.state.gov/milestones/1969-1976/oil-embargo.

Page, D. I., K. L. Hickey, R. Narula, A. L. Main, and S. J. Grimberg. 2008. "Modeling anaerobic digestion of dairy manure using the IWA Anaerobic Digestion Model no. 1 (ADM1)." *Water Science and Technology, 58(3)* 689 - 695.

Pan, Shu-Yuan, Cheng-Yen Tsai, Chen-Wuing Liu, Sheng-Wei Wang, Hyunook Kim, and Chihhao Fan. 2021. "Anaerobic co-digestion of agricultural wastes toward circular bioeconomy." *Iscience, 24(7)* 102704.

Parkin, Gene F., Nancy A. Lynch, Wen-Chien Kuo, Edward L. Van Keuren, and Sanjoy K. Bhattacharya. 1990. "Interaction between between sulfate reducers and methanogens fed acetatre and propionate." *Research Journal of the Water Pollution Control Federation* 780 - 788.

Patel, G. B., and L. A. Roth. 1977. "Effect of sodium chloride on growth and methane production of methanogens." *Canadian Journal of Biology, 23(7)* 893 - 897.

Pimentel, David. 2008. "Renewable and Solar Energy Technologies: Energy and Environmental Issues." In *Biofuels, Solar and Winds as Renewable Energy Systems*, by David Pimentel, 1 - 19. New York: Springer.

Putri, D. A., R. R. Saputro, and Budiyono. 2012. "Biogas production from cow manure." *International Journal of Renewable Energy Development, 1(2)* 61 - 64.

Robinson, Joseph A., and James M. Tiedje. 1984. "Competition between sulfate-reducing and methanogenic bacteria for H2 under resting and growing conditions." *Archives of Microbiology, 137(1)* 26 - 32.

Romero-Güiza, M. S., J. Mata-Alvarez, J. M. Chimenos, and S. Astals. 2016. "The effect of magnesium as activator and inhibitor of anaerobic digestion." *Waste Management, 56* 137 - 142.

Rosen, Christian, and Ulf Jeppsson. 2006. "Aspects on ADM1 Implementation within the BSM2 Framework." *Department of Industrial Electrical Engineering and Automation, Lund University, Lund, Sweden* (Department of Industrial Electrical Engineering and Automation, Lund University, Lund) 1 - 35.

Rusin, Jiri, Katerina Chamradova, and Panagiotis Basinas. 2021. "Two-stage psychrophilic anaerobic digestion of food waste: comparison to conventional single-stage mesophilic process, 119." *Waste Management* 172 - 182.

Şenol, Halil. 2020. "Anaerobic digestion of hazelnut (Corylus colurna) husks after alkaline pretreatment and determination of new important points in Logistic model curves." *Bioresource technology, 300* 122660.

Şenol, Halil, Ünsal Açıkel, Serkan Demir, and Volkan Oda. 2020. "Anaerobic digestion of cattle manure, corn silage and sugar beet pulp mixtures after thermal pretreatment and kinetic modeling study." *Fuel, 263* 116651.

Shahan, Zachary. 2014. *History of Wind Turbines.* 11 22. https://www.renewableenergyworld.com/storage/history-of-wind-turbines/#gref.

Shahbaz, Muhammad, Muhammad Ammar, Rashid Mustafa Korai, Nadeem Ahmad, Awais Ali, Muhammad Sarmad Khalid, Dexun Zou, and XiuJin Li. 2020. "Impact of C/N ratios and organic loading rates of paper, cardboard and tissue wastes in batch and CSTR anaerobic digestion with food waste on their biogas production and digester stability." *SN Applied Science, 2(8)* 1 - 13.

Tharifa, Firyal, Khansa Luqyana Hapsari, Cindy Rianti Priadi, and Heri Hermansyah. 2020. "Effect of magnesium addition to volatile fatty acids and particulate chemical oxygen demand in hydrolysis phase of anaerobic waste treatment. In AIP Conference Proceedings (Vol. 2230, No. 1, p. 020005)." *AIP Publishing LLC.*

Twidell, John, and Tony Weir. 2006. "Biomass and Biofuels." In *Renewable Energy Resources,* by John Twidell and Tony Weir, 351 - 400. London & New York: Taylor & Francis Group.

Twidell, John, and Tony Weir. 2006. "Geothermal Energy." In *Renewable Energy Sources,* by John Twidell and Tony Weir, 471 - 489. London & New York: Taylor & Francis Group.

Twidell, John, and Tony Weir. 2006. "Solar Radiation." In *Renewable Energy Resources,* by John Twidell and Tony Weir, 85 - 115. Londan and New York: Taylor and Francis.

Vivas, A. Ceron, K. T. Caceres, A. Rincon, and A. A. Cajigas. 2019. "Influence of pH and the C/N ratio on the biogas production of wastewater." *Revista Facultad de Ingeniería Universidad de Antioquia, 92* 70 - 79.

Wang, Hui, Horacio A. Aguirre-Villegas, Rebecca A. Larson, and Asli Alkan-Ozkaynak. 2019. "Physical properties of dairy manure pre-and post-anaerobic digestion." *Applied Sciences, 9(13)* 2703.

Wartell, Brian A., Valdis Krumins, Jeffrey Alt, Kathleen Kang, Bryan J. Schwab, and Donna E. Fennell. 2012. "Methane production from horse manure and stall waste with softwood bedding." *Bioresource Technology, 112* 42 - 50.

Water Science School. 2018. *Hydroelectric Power: How It Works.* 06 06. https://www.usgs.gov/special-topics/water-science-school/science/hydroelectric-power-how-it-works.

White, Matthew. 2009. *The Industrial Revolution.* 10 14. https://www.bl.uk/georgian-britain/articles/the-industrial-revolution.

World Nuclear. 2022. *Chernobyl Accident 1986.* April 01. https://www.world-nuclear.org/information-library/safety-and-security/safety-of-plants/chernobyl-accident.aspx.

—. 2021. *Fukushima Daiichi Accident.* 04 01. https://www.world-nuclear.org/information-library/safety-and-security/safety-of-plants/fukushima-daiichi-accident.aspx.

—. 2022. *Heat Values of Various Fuels.* 01 01. https://world-nuclear.org/information-library/facts-and-figures/heat-values-of-various-fuels.aspx.

—. 2020. *Outline History of Nuclear Energy.* 11 01. https://www.world-nuclear.org/information-library/current-and-future-generation/outline-history-of-nuclear-energy.aspx.

Worldometer. 2022. *World Population by Year.* 04 01. https://www.worldometers.info/world-population/world-population-by-year/.

Yang, Jie, Dehan Wang, Zifeng Luo, and Weishen Zeng. 2019. "Anaerobic mono-digestion of pig manure in a leach bed coupled with a methanogenic reactor: Effects of the filter media." *Journal of Cleaner Production, 234* 1094 - 1101.

Yoda, Motoyuki, Mikio Kitagawa, and Yusho Miyaji. 1987. "Long term competition between sulfate-reducing and methane-producing bacteria for acetate in anaerobic biofilm." *Water Research, 21(12)* 1547 - 1556.

Zha, Xiao, Panagiotis Tsapekos, Merlin Alvardo-Morales, Xiwu Lu, and Irini Angelidaki. 2020. "Potassium inhibition during sludge and biopulp co-digestion; experimental and model-based approaches." *Waste Management, 113* 304 - 311.

Zhang, Cunsheng, Gang Xiao, Liyu Peng, Haijia Su, and Tianwei Tan. 2013. "The anaerobic co-digestion of food waste and cattle manure." *Bioresource Technology, 129* 170 - 176.

Zhang, Cunsheng, Haija Su, Jan Baeyens, and Tianwei Tan. 2014. "Reviewing the anaerobic digestion of food waste for biogas production." *Renewable and Sustainable Energy Reviews* 383 - 392.

Zhou, Jinghong, Xiaona Shang, Zhiwei Wang, Cancan Zhu, and Shuangfei Wang. 2019. "Effects of calcium concentration on up-flow multistage anaerobic reactor performance in treating bagasse spraying wastewater." *BioResources, 14(2)* 4254 - 4269.

APPENDICES

APPENDIX A. STOICHIOMETRIC COEFFICIENTS & RATES, AND COORDINATES

In this secion, stoichiomeric coefficients, reaction rates are shown. In MATLAB, a matrix was created. The coordinates of stoichiometric coefficients are available in Gujer matrix form.

A.1. Stoichiometric Coefficients and Rates

Stoichiometric coefficients and reaction rates for each process are tabulated by (Batstone, et al. 2002). In Table A.1, biochemical processes are shown. Table A.2 and Table A.3 show acid – base processes and gas transfer processes, respectively.

A.2. Coordinates

In MATLAB codes, matrix system is needed to solve a set of differential equations. Therefore, a matrix with size of 28x35 was created, and coordinates are determined on stoichiometric coefficients tables that are created by (Batstone, et al. 2002). Table A.4 shows the coordinates for soluble matters' biochemical process. Table A.5 shows particulate matters' biochemical process. In Table A.6 and Table A.7, coordinates for acid – base process and gas transfer process, respectively are shown.

Table A.1. Stoichiometric coefficients and rates of biochemical processes in ADM1

Component i		1	2	3	4	5	6	7	8	Rate($kgCODm^{-3}d^{-1}$)
j	Process	S_{su}	S_{aa}	S_{fa}	S_{va}	S_{bu}	S_{pro}	S_{ac}	S_{h2}	
1	Disintegration									$k_{dis}X_c$
2	Hydrolysis of Carbohydrates	1								$k_{hyd,ch}X_{ch}$
3	Hydrolysis of Protein		1							$k_{hyd,pr}X_{pr}$
4	Hydrolysis of Lipids	1 - $f_{fa,li}$		$f_{fa,li}$						$k_{hyd,li}X_{li}$
5	Uptake of Sugars	-1				(1 - Y_{su})$f_{bu,su}$	(1 - Y_{su})$f_{pro,su}$	(1 - Y_{su})$f_{ac,su}$	(1 - Y_{su})$f_{h2,su}$	$k_{m,su}\frac{S_{su}}{K_{S,su}+S_{su}}X_{su}I_5$
6	Uptake of Amino Acids		-1		(1 - Y_{aa})$f_{va,aa}$	(1 - Y_{aa})$f_{bu,aa}$	(1 - Y_{aa})$f_{pro,aa}$	(1 - Y_{aa})$f_{ac,aa}$	(1 - Y_{aa})$f_{h2,aa}$	$k_{m,aa}\frac{S_{aa}}{K_{S,aa}+S_{aa}}X_{aa}I_6$
7	Uptake of LCFA			-1				(1 - Y_{fa})0.7	(1 - Y_{aa})0.3	$k_{m,fa}\frac{S_{fa}}{K_{S,fa}+S_{fa}}X_{fa}I_7$
8	Uptake of Valerate				-1		(1 - Y_{c4})0.54	(1 - Y_{c4})0.31	(1 - Y_{c4})0.15	$k_{m,c4}\frac{S_{va}}{K_{S,c4}+S_{va}}X_{c4}\frac{S_{va}}{S_{va}+S_{bu}}I_8$
9	Uptake of Butyrate					-1		(1 - Y_{c4})0.8	(1 - Y_{c4})0.2	$k_{m,c4}\frac{S_{bu}}{K_{S,c4}+S_{bu}}X_{c4}\frac{S_{bu}}{S_{bu}+S_{va}}I_9$
10	Uptake of Propionate						-1	(1 - Y_{pro})0.57	(1 - Y_{pro})0.43	$k_{m,pro}\frac{S_{pro}}{K_{S,pro}+S_{pro}}X_{pro}I_{10}$
11	Uptake of Acetate							-1		$k_{m,ac}\frac{S_{ac}}{K_{S,ac}+S_{ac}}X_{ac}I_{11}$
12	Uptake of Hydrogen								-1	$k_{m,h2}\frac{S_{h2}}{K_{S,h2}+S_{h2}}X_{h2}I_{12}$
13	Decay of X_{su}									$k_{dec,Xsu}X_{su}$
14	Decay of X_{aa}									$k_{dec,Xaa}X_{aa}$
15	Decay of X_{fa}									$k_{dec,Xfa}X_{fa}$
16	Decay of X_{c4}									$k_{dec,Xc4}X_{c4}$
17	Decay of X_{pro}									$k_{dec,Xpro}X_{pro}$
18	Decay of X_{ac}									$k_{dec,Xac}X_{ac}$
19	Decay of X_{h2}									$k_{dec,Xh2}X_{h2}$

(cont. on next page)

Table A.1(cont.). Stoichiometric coefficients and rates of biochemical processes in ADM1

Component i		9	10	11	12	13	14	15	16	Rate($kgCODm^{-3}d^{-1}$)
j	Process	S_{ch4}	S_{IC}	S_{IN}	S_I	X_c	X_{ch}	X_{pr}	X_{li}	
1	Disintegration		$=-\Sigma C_i \nu_{i,1}$		$f_{sI,xc}$	-1	$f_{ch,xc}$	$f_{pr,xc}$	$f_{li,xc}$	$k_{dis}X_c$
2	Hydrolysis of Carbohydrates		$=-\Sigma C_i \nu_{i,2}$				-1			$k_{hyd,ch}X_{ch}$
3	Hydrolysis of Protein		$=-\Sigma C_i \nu_{i,3}$					-1		$k_{hyd,pr}X_{pr}$
4	Hydrolysis of Lipids		$=-\Sigma C_i \nu_{i,4}$						-1	$k_{hyd,li}X_{li}$
5	Uptake of Sugars		$=-\Sigma C_i \nu_{i,5}$	$-(Y_{su})N_{bac}$						$k_{m,su}\frac{S_{su}}{K_{S,su}+S_{su}}X_{su}I_5$
6	Uptake of Amino Acids		$=-\Sigma C_i \nu_{i,6}$	$N_{aa}-(Y_{aa})N_{bac}$						$k_{m,aa}\frac{S_{aa}}{K_{S,aa}+S_{aa}}X_{aa}I_6$
7	Uptake of LCFA		$=-\Sigma C_i \nu_{i,7}$	$-(Y_{fa})N_{bac}$						$k_{m,fa}\frac{S_{fa}}{K_{S,fa}+S_{fa}}X_{fa}I_7$
8	Uptake of Valerate		$=-\Sigma C_i \nu_{i,8}$	$-(Y_{c4})N_{bac}$						$k_{m,c4}\frac{S_{va}}{K_{S,c4}+S_{va}}X_{c4}\frac{S_{va}}{S_{va}+S_{bu}}I_8$
9	Uptake of Butyrate		$=-\Sigma C_i \nu_{i,9}$	$-(Y_{c4})N_{bac}$						$k_{m,c4}\frac{S_{bu}}{K_{S,c4}+S_{bu}}X_{c4}\frac{S_{bu}}{S_{bu}+S_{va}}I_9$
10	Uptake of Propionate		$=-\Sigma C_i \nu_{i,10}$	$-(Y_{pro})N_{bac}$						$k_{m,pro}\frac{S_{pro}}{K_{S,pro}+S_{pro}}X_{pro}I_{10}$
11	Uptake of Acetate	$(1-Y_{ac})$	$=-\Sigma C_i \nu_{i,11}$	$-(Y_{ac})N_{bac}$						$k_{m,ac}\frac{S_{ac}}{K_{S,ac}+S_{ac}}X_{ac}I_{11}$
12	Uptake of Hydrogen	$(1-Y_{h2})$	$=-\Sigma C_i \nu_{i,12}$	$-(Y_{h2})N_{bac}$						$k_{m,h2}\frac{S_{h2}}{K_{S,h2}+S_{h2}}X_{h2}I_{12}$
13	Decay of X_{su}		$=-\Sigma C_i \nu_{i,13}$	$N_{bac}-N_{xc}$		1				$k_{dec,Xsu}X_{su}$
14	Decay of X_{aa}		$=-\Sigma C_i \nu_{i,14}$	$N_{bac}-N_{xc}$		1				$k_{dec,Xaa}X_{aa}$
15	Decay of X_{fa}		$=-\Sigma C_i \nu_{i,15}$	$N_{bac}-N_{xc}$		1				$k_{dec,Xfa}X_{fa}$
16	Decay of X_{c4}		$=-\Sigma C_i \nu_{i,16}$	$N_{bac}-N_{xc}$		1				$k_{dec,Xc4}X_{c4}$
17	Decay of X_{pro}		$=-\Sigma C_i \nu_{i,17}$	$N_{bac}-N_{xc}$		1				$k_{dec,Xpro}X_{pro}$
18	Decay of X_{ac}		$=-\Sigma C_i \nu_{i,18}$	$N_{bac}-N_{xc}$		1				$k_{dec,Xac}X_{ac}$
19	Decay of X_{h2}		$=-\Sigma C_i \nu_{i,19}$	$N_{bac}-N_{xc}$		1				$k_{dec,Xh2}X_{h2}$

(cont. on next page)

Table A.1(cont.). Stoichiometric coefficients and rates of biochemical processes in ADM1

Component i		17	18	19	20	21	22	23	24	Rate ($kgCODm^{-3}d^{-1}$)
j	Process	X_{su}	X_{aa}	X_{fa}	X_{c4}	X_{pro}	X_{ac}	X_{h2}	X_I	
1	Disintegration								$f_{xI,xc}$	$k_{dis}X_c$
2	Hydrolysis of Carbohydrates									$k_{hyd,ch}X_{ch}$
3	Hydrolysis of Protein									$k_{hyd,pr}X_{pr}$
4	Hydrolysis of Lipids									$k_{hyd,li}X_{li}$
5	Uptake of Sugars	Y_{su}								$k_{m,su}\frac{S_{su}}{K_{S,su}+S_{su}}X_{su}I_5$
6	Uptake of Amino Acids		Y_{aa}							$k_{m,aa}\frac{S_{aa}}{K_{S,aa}+S_{aa}}X_{aa}I_6$
7	Uptake of LCFA			Y_{fa}						$k_{m,fa}\frac{S_{fa}}{K_{S,fa}+S_{fa}}X_{fa}I_7$
8	Uptake of Valerate				Y_{c4}					$k_{m,c4}\frac{S_{va}}{K_{S,c4}+S_{va}}X_{c4}\frac{S_{va}}{S_{va}+S_{bu}}I_8$
9	Uptake of Butyrate				Y_{c4}					$k_{m,c4}\frac{S_{bu}}{K_{S,c4}+S_{bu}}X_{c4}\frac{S_{bu}}{S_{bu}+S_{va}}I_9$
10	Uptake of Propionate					Y_{pro}				$k_{m,pro}\frac{S_{pro}}{K_{S,pro}+S_{pro}}X_{pro}I_{10}$
11	Uptake of Acetate						Y_{ac}			$k_{m,ac}\frac{S_{ac}}{K_{S,ac}+S_{ac}}X_{ac}I_{11}$
12	Uptake of Hydrogen							Y_{h2}		$k_{m,h2}\frac{S_{h2}}{K_{S,h2}+S_{h2}}X_{h2}I_{12}$
13	Decay of X_{su}	-1								$k_{dec,Xsu}X_{su}$
14	Decay of X_{aa}		-1							$k_{dec,Xaa}X_{aa}$
15	Decay of X_{fa}			-1						$k_{dec,Xfa}X_{fa}$
16	Decay of X_{c4}				-1					$k_{dec,Xc4}X_{c4}$
17	Decay of X_{pro}					-1				$k_{dec,Xpro}X_{pro}$
18	Decay of X_{ac}						-1			$k_{dec,Xac}X_{ac}$
19	Decay of X_{h2}							-1		$k_{dec,Xh2}X_{h2}$

Table A.2. Stoichiometric coefficients and rates of acid – base processes in ADM1

Component i		27	28	29	30	31	32	Rate ($kgCODm^{-3}d^{-1}$)
j	**Process**	S_{va-}	S_{bu-}	S_{pro-}	S_{ac-}	S_{hco3-}	S_{nh3}	
A4	**Valerate acid-base**	-1						$K_{A/Bva}(S_{va,ac}(K_{a,va}+S_h)-K_{a,va}S_{va})$
A5	**Butyrate acid-base**		-1					$K_{A/Bbu}(S_{bu,ac}(K_{a,bu}+S_h)-K_{a,bu}S_{bu})$
A6	**Propionate acid-base**			-1				$K_{A/Bpro}(S_{pro,ac}(K_{a,pro}+S_h)-K_{a,pro}S_{pro})$
A7	**Acetate acid-base**				-1			$K_{A/Bac}(S_{ac,ac}(K_{a,ac}+S_h)-K_{a,ac}S_{ac})$
A10	**Inorganic carbon acid-base**					-1		$K_{A/BCO2}(S_{IC,ac}(K_{a,IC}+S_h)-K_{a,IC}S_{IC})$
A11	**Inorganic nitrogen acid-base**						-1	$K_{A/BIN}(S_{IN,,ac}(K_{a,IN}+S_h)-K_{a,IN}S_{IN})$

Table A.3. Stoichiometric coefficients and rates of gas transfer processes in ADM1

		Liquid Phase Yield Coefficients			Gas Reaction Coefficients			
Component i		33	34	35	33	34	35	Rate ($kgCODm^{-3}d^{-1}$)
j	**Process**	S_{h2}	S_{ch4}	S_{IC}	S_{h2}	S_{ch4}	S_{IC}	
T8	**H_2**	-1			V_{liq}/V_{gas}			$k_La(S_{liq,H2}-16K_{H,H2}P_{gas,H2})$
T9	**CH_4**		-1			V_{liq}/V_{gas}		$k_La(S_{liq,CH4}-64K_{H,CH4}P_{gas,CH4})$
T10	**CO_2**			-1			V_{liq}/V_{gas}	$k_La(S_{liq,CO2}-K_{H,CO2}P_{gas,CO2})$

Table A.4. Coordinates used in MATLAB codes for biochemical processes of soluble matters

Component	i	1	2	3	4	5	6	7	8	9	10	11	12
j	Process	S_{su}	S_{aa}	S_{fa}	S_{va}	S_{bu}	S_{pro}	S_{ac}	S_{h2}	S_{ch4}	S_{IC}	S_{IN}	S_{I}
1	Disintegration										1,10	1,11	1,12
2	Hydrolysis of Carbohydrates	2,1									2,10		
3	Hydrolysis of Protein		3,2								3,10		
4	Hydrolysis of Lipids	4,1		4,3							4,10		
5	Uptake of Sugars	5,1				5,5	5,6	5,7	5,8		5,10	5,11	
6	Uptake of Amino Acids		6,2		6,4	6,5	6,6	6,7	6,8		6,10	6,11	
7	Uptake of LCFA			7,3				7,7	7,8		7,10	7,11	
8	Uptake of Valerate				8,4		8,6	8,7	8,8		8,10	8,11	
9	Uptake of Butyrate					9,5		9,7	9,8		9,10	9,11	
10	Uptake of Propionate						10,6	10,7	10,8		10,10	10,11	
11	Uptake of Acetate							11,7		11,9	11,10	11,11	
12	Uptake of Hydrogen								12,8	12,9	12,10	12,11	
13	Decay of X_{su}										13,10	13,11	
14	Decay of X_{aa}										14,10	14,11	
15	Decay of X_{fa}										15,10	15,11	
16	Decay of X_{c4}										16,10	16,11	
17	Decay of X_{pro}										17,10	17,11	
18	Decay of X_{ac}										18,10	18,11	
19	Decay of X_{h2}										19,10	19,11	

Table A.5. Coordinates used in MATLAB codes for biochemical processes of particulate matters

Component	i	13	14	15	16	17	18	19	20	21	22	23	24
j	Process	X_c	X_{ch}	X_{pr}	X_{li}	X_{su}	X_{aa}	X_{fa}	X_{c4}	X_{pro}	X_{ac}	X_{h2}	X_I
1	Disintegration	1,13	1,14	1,15	1,16								1,24
2	Hydrolysis of Carbohydrates		2,14										
3	Hydrolysis of Protein			3,15									
4	Hydrolysis of Lipids				4,16								
5	Uptake of Sugars					5,17							
6	Uptake of Amino Acids						6,18						
7	Uptake of LCFA							7,19					
8	Uptake of Valerate								8,20				
9	Uptake of Butyrate								9,20				
10	Uptake of Propionate									10,21			
11	Uptake of Acetate										11,22		
12	Uptake of Hydrogen											12,23	
13	Decay of X_{su}	13,13				13,17							
14	Decay of X_{aa}	14,13					14,18						
15	Decay of X_{fa}	15,13						15,19					
16	Decay of X_{c4}	16,13							16,20				
17	Decay of X_{pro}	17,13								17,21			
18	Decay of X_{ac}	18,13									18,22		
19	Decay of X_{h2}	19,13										19,23	

Table A.6. Coordinates used in MATLAB codes for acid – base processes

Component	i	27	28	29	30	31	32
j	**Process**	**S_{va-}**	**S_{bu-}**	**S_{pro-}**	**S_{ac-}**	**S_{hco3-}**	**S_{nh3}**
A4	**Valerate acid-base**	20,27					
A5	**Butyrate acid-base**		21,28				
A6	**Propionate acid-base**			22,29			
A7	**Acetate acid-base**				23,30		
A10	**Inorganic carbon acid-base**					24,31	
A11	**Inorganic nitrogen acid-base**						25,32

Table A.7. Coordinates used in MATLAB codes for gas transfer processes

		Liquid Phase Yield Coefficients			Gas Reaction Coefficients		
Component	**i**	**33**	**34**	**35**	**33**	**34**	**35**
j	**Process**	**S_{h2}**	**S_{ch4}**	**S_{IC}**	**S_{h2}**	**S_{ch4}**	**S_{IC}**
T8	**H_2**	26,8			26,33		
T9	**CH_4**		27,9			27,34	
T10	**CO_2**			28,10			28,35

APPENDIX B. ADDITIONAL INFORMATION

B1. RTD Analysis Equations

Space time of the fluid in the vessel is shown with the Greek letter τ, and it is a theoretical measurement of residence time. The unit is day.

$$\tau = \frac{V}{v} \ (where\ V\ is\ volume, v\ is\ volumetric\ flowrate)$$

The mean and the variance are calculated by using the experimental pulse-response data which are the concentration of the tracer measured in the effluent. The mean that locates at the center of gravity in time is shown with $\bar{t}$, and its unit is d. It indicates the time concentration of the trace curve passes a measuring point. The variance is a variable that shows how the tracer spreads out in time. Its unit is d^2.

$$\bar{t} = \frac{\int_0^\infty tCdt}{\int_0^\infty Cdt} \ (where\ C\ is\ concentration\ of\ tracer, t\ is\ time)$$

$$\sigma^2 = \frac{\int_0^\infty t^2 Cdt}{\int_0^\infty Cdt} - \bar{t}^2$$

If the data are taken closely spaced and time interval is equal:

$$\bar{t} = \frac{\sum t_i C_i \Delta t_i}{\sum C_i \Delta t_i} = \frac{\sum t_i C_i}{\sum C_i}$$

$$\sigma^2 = \frac{\sum {t_i}^2 C_i \Delta t_i}{\sum C_i \Delta t_i} - \bar{t}^2 = \frac{\sum {t_i}^2 C_i}{\sum C_i} - \bar{t}^2$$

B1.1. E Curve

E curve is derived from experimental data in order to make the concentration scale having unity in area under the curve so that it is possible to make a comparison with different models. The unit is d^{-1}. The unit of area is $kg.s/m^3$.

$$A = \int_0^\infty C dt \cong \sum_i \bar{C}_i \Delta t_i = \frac{M}{v} \ (where\ M\ is\ instantaneous\ pulse)$$

$$E = \frac{C}{M/v} = \frac{C}{A}$$

Mostly dimensionless E curve is plotted by dimensionless time. Dimensionless time is shown with a Greek letter, θ, and dimensionless E is shown with E_θ.

$$\theta = \frac{t}{\bar{t}}$$

$$E_\theta = \bar{t}\frac{C}{A} = \bar{t}E$$

Dimensionless E curve is already available in Jegede et. al.'s research. Therefore, their results were used to create E curves for different models and compared with their experimental results. The following models were examined to decide whether they are suitable to design the reactor based on their hydrodynamic behavior or not.

First of all, ideal models which are plug flow and mixed flow were checked.

B1.2. Plug Flow

If the behavior is plug flow, E curve has the shape of a spike if the injection is pulse injection. Dirac delta function, $\delta(t - \bar{t})$, is a function that has 0 width and ∞ height. It is equal to 0. Since the injection is a pulse, only pulse output represents plug flow behavior.

B1.3. Mixed Flow

In pulse injection, mixed flow starts at its highest value and gradually reduces. Since it is one of the two ideal behaviors with plug flow, it has only one pattern.
Modelling equation for mixed flow:

$$E = \frac{1}{\bar{t}} e^{-\theta}$$

$$E_\theta = e^{-t}$$

After ideal models were investigated, their derivations in compartment model were analyzed.

B1.4. Compartment Model

Compartment model is a combination of different possible zones in a vessel such as mixed region, plug flow region, semi-dead or dead regions, recycling etc. There are too many different combinations of these regions. Since in this study, it was expected a CSTR with dead zone to be observed, its behavior was compared to the experimental results.

$$E = \frac{v}{V_m} e^{\left[-\frac{v}{V_m}t\right]} \ (where\ v\ is\ the\ volumetric\ flowrate, V_m\ is\ volume\ of\ the\ mixing\ tank)$$

Since $\frac{v}{V_m} = \frac{1}{t}$, therefore, the regime is same as mixed flow regime.

Then, dispersion model that has a basis of plug flow principles was studied.

B1.5. Dispersion Model

In dispersion model, Peclet Number (Pe) that tells if the flow is plug flow or mixed flow, or it is approaching one of them. Therefore, the deviation from plug flow is a key point at the beginning of this analysis. If Pe is a too big number, it is plug flow while it is mixed flow in the opposite direction.

$$Pe = \frac{uL}{D} \ (where\ u\ is\ velocity, L\ is\ the\ length\ and\ D\ is\ dispersion\ coefficient)$$

When D = 0, it means there is not any spreading, so it is plug flow.

The critical point to decide if deviation is small or big is 1/Pe = 0.01.

Mean and variance are already calculated. Thus, $\frac{D}{uL}$ can easily be calculated from variance equations for each model by trial-and-error method.

B1.5.1. Small Deviation

Mean:

$$\bar{t}_E = \frac{V}{v} = \frac{L}{u}$$

Variance:

$$\sigma_t^2 = 2\left(\frac{DL}{u^3}\right)$$

Response Data:

$$E = \sqrt{\frac{u^3}{4\pi DL}} \exp\left[-\frac{(L-ut)^2}{4\left(DL/u\right)}\right]$$

Dimensionless Response Data:

$$E_\theta = \bar{t}.E$$

B1.5.2. Large Deviation

There are 4 large deviation models with different boundary conditions. They are closed vessel, open – close & close – open boundary conditions and open vessel.

B1.5.2.1. Closed Vessel

Mean:

$$\bar{t}_E = \bar{t}$$

Variance:

$$\sigma_t^2 = \bar{t}^2 \left\{ 2\left(\frac{D}{uL}\right) - 2\left(\frac{D}{uL}\right)^2 \left[1 - e^{-\frac{uL}{D}}\right] \right\}$$

Dimensionless Variance:

$$\sigma_\theta^2 = \frac{\sigma_t^2}{\bar{t}^2}$$

B1.5.2.2. Open – Closed & Closed – Open Vessels

Mean:

$$\bar{t}_{E_{oc}} = \bar{t}_{E_{co}} = \frac{V}{v}\left(1 + \frac{D}{uL}\right)$$

Dimensionless Mean:

$$\bar{\theta}_{E_{oc}} = \bar{\theta}_{E_{co}} = 1 + \frac{D}{uL}$$

Variance:

$$\sigma_{t_{oc}}^2 = \sigma_{t_{co}}^2 = \bar{t}^2 \left[2\left(\frac{D}{uL}\right) + 3\left(\frac{D}{uL}\right)^2 \right]$$

Dimensionless Variance:

$$\sigma_{\theta_{oc}}^2 = \sigma_{\theta_{co}}^2 = \frac{\sigma_{t_{oc}}^2}{\bar{t}^2} = \frac{\sigma_{t_{co}}^2}{\bar{t}^2}$$

B1.5.2.3. Open Vessel

Mean:

$$\bar{t}_{E_{oo}} = \bar{t}\left(1 + 2\frac{D}{uL}\right)$$

Dimensionless Mean:

$$\bar{\theta}_{E_{oo}} = \frac{\bar{t}_{E_{oo}}}{\bar{t}}$$

Response Data:

$$E_{oo} = \frac{u}{\sqrt{4\pi Dt}} e^{\left[-\frac{(L-ut)^2}{4Dt}\right]}$$

Dimensionless Response Data:

$$E_{\theta_{oo}} = \frac{1}{\sqrt{4\pi\left(\frac{D}{uL}\right)\theta}} e^{\left[-\frac{(1-\theta)^2}{4\theta\left(\frac{D}{uL}\right)}\right]}$$

B1.6. The Tanks in Series Model

In series tank model, the total capacity is kept constant, and the number of tanks increases. If the number is more than 50, it is considered as plug flow. If N is the number of tanks, general equation for E data is as shown below:

$$E_\theta = \bar{t}_i E = \frac{1}{(N-1)!}\left(\frac{t}{\bar{t}_i}\right)^{N-1} e^{-t/\bar{t}_i}$$

Mean:

$$\bar{t}_i = \frac{\bar{t}}{N}$$

Variance:

$$\sigma^2 = N\bar{t}_i{}^2 = \frac{\bar{t}^2}{N}$$

B1.7. Laminar Flow

Power law fluids are non-Newtonian fluids. Slurry in this study behaves as a power law fluid. Dimensionless response data is calculated with the following equation:

$$E_\theta = \frac{2n}{3n+1}\frac{1}{\theta^3}\left[1-\frac{n+1}{3n+1}\frac{1}{\theta}\right]^{\frac{n-1}{n+1}} \quad for\ \theta \geq \frac{n+1}{3n+1}\ (where\ n\ is\ behavior\ index)$$

After RTD analysis was made, reactor was designed with the differential algebraic equations in ADM1.

B2. Reactor Design Equations

The differential equation set of ADM1 needs to be solved with a software. The differential equations are are shown in this section.

B2.1. Differential Equations

There are 35 state variables in total. 26 variables are for biochemical reactions including 2 more cation and anion variables. 6 variables belong to acid-base reactions. 3 remaining variables represent the gas concentration. Following differential equation is a general differential equation form applied in this modelling study (Batstone, et al. 2002).

$$\frac{dS_{liq,i}}{dt} = q_{liq}\left(\frac{S_{i,in}}{V_{liq}} - \frac{S_{liq,i}}{V_{liq}}\right) + \sum_{j=1-19}\rho_j v_{i,j}$$

$$\frac{dX_{liq,i}}{dt} = q_{liq}\left(\frac{X_{i,in}}{V_{liq}} - \frac{X_{liq,i}}{V_{liq}}\right) + \sum_{j=1-19}\rho_j v_{i,j}$$

where j represents the process, i represents the species and $\sum_{j=1-19}\rho_j v_{i,j}$ is the sum of specific kinetic rates for the process j (ρ_j) multiplied by stoichiometric coefficients ($v_{i,j}$) shown in A.1. Stoichiometric Coefficients and Rates.

B2.1.1 Soluble Matter

$$\frac{dS_{su}}{dt} = \frac{q_{in}}{V_{liq}}\left(S_{su,in} - S_{su}\right) + rate_2 + \left(1 - f_{fa,li}\right) * rate_4 - rate_5$$

$$\frac{dS_{aa}}{dt} = \frac{q_{in}}{V_{liq}}\left(S_{aa,in} - S_{aa}\right) + rate_3 - rate_6$$

$$\frac{dS_{fa}}{dt} = \frac{q_{in}}{V_{liq}}\left(S_{fa,in} - S_{fa}\right) + f_{fa,li} * rate_4 - rate_7$$

$$\frac{dS_{va}}{dt} = \frac{q_{in}}{V_{liq}}\left(S_{va,in} - S_{va}\right) + (1 - Y_{aa}) * f_{va,aa} * rate_6 - rate_8$$

$$\frac{dS_{bu}}{dt} = \frac{q_{in}}{V_{liq}}\left(S_{bu,in} - S_{bu}\right) + (1 - Y_{su)} * f_{bu,su} * rate_5 + (1 - Y_{aa}) * f_{bu,aa} * rate_6 - rate_9$$

$$\frac{dS_{pro}}{dt} = \frac{q_{in}}{V_{liq}}\left(S_{pro,in} - S_{pro}\right) + (1 - Y_{su}) * f_{pro,su} * rate_5 + (1 - Y_{aa}) * f_{pro,aa} * rate_6 + (1 - Y_{c4}) * 0.54 * rate_8 - rate_{10}$$

$$\frac{dS_{ac}}{dt} = \frac{q_{in}}{V_{liq}}\left(S_{ac,in} - S_{ac}\right) + (1 - Y_{su}) * f_{ac,su} * rate_5 + (1 - Y_{aa}) * f_{ac,aa} * rate_6 + \left(1 - Y_{fa}\right) * 0.7 * rate_7 + (1 - Y_{c4}) * 0.31 * rate_8 + (1 - Y_{c4}) * 0.8 * rate_9 + \left(1 - Y_{pro}\right) * 0.57 * rate_{10} - rate_{11}$$

$$\frac{dS_{H2}}{dt} = \frac{q_{in}}{V_{liq}}\left(S_{H2,in} - S_{H2}\right) + (1 - Y_{su}) * f_{H2,su} * rate_5 + (1 - Y_{aa}) * f_{H2,aa} * rate_6 + \left(1 - Y_{fa}\right) * 0.3 * rate_7 + (1 - Y_{c4}) * 0.15 * rate_8 + (1 - Y_{c4}) * 0.2 * rate_9 + \left(1 - Y_{pro}\right) * 0.43 * rate_{10} - rate_{12} - rate_{T8}$$

$$\frac{dS_{CH4}}{dt} = \frac{q_{in}}{V_{liq}}\left(S_{CH4,in} - S_{CH4}\right) + (1 + Y_{ac}) * rate_{11} + (1 - Y_{H2}) * rate_{12} - rate_{T9}$$

$$\frac{dS_{IC}}{dt} = \frac{q_{in}}{V_{liq}}\left(S_{IC,in} - S_{IC}\right) + \sum_{j=1}^{19}\sum_{i=1}^{24} C_i * v_{i,j} * rate_j$$

$$\frac{dS_{IN}}{dt} = \frac{q_{in}}{V_{liq}}\left(S_{IN,in} - S_{IN}\right) - Y_{su} * N_{bac} * rate_5 + (N_{aa} - Y_{aa} * N_{bac}) * rate_6 - Y_{fa} * N_{bac} * rate_7 - Y_{c4} * N_{bac} * rate_8 - Y_{c4} * N_{bac} * rate_9 - Y_{pro} * N_{bac} * rate_{10} - Y_{ac} * N_{bac} * rate_{11} - Y_{H2} * N_{bac} * rate_{12} + (N_{bac} - N_{xc}) * \sum_{i=13}^{19} rate_i + \left(N_{xc} - f_{xI,xc} * N_I - f_{sI,xc} * N_I - f_{pr,xc} * N_{aa}\right) * rate_1$$

$$\frac{dS_I}{dt} = \frac{q_{in}}{V_{liq}}\left(S_{I,in} - S_I\right) + f_{sI,xc} * rate_1$$

B2.1.2. Carbon Balance (Rosen and Jeppsson 2006)

$$\sum_{j=1}^{19}\sum_{i=1}^{24} C_i * v_{i,j} * rate_j = \sum_{k=1-12} v_k * rate_k + v_{13} * (rate_{13} + rate_{14} + rate_{15} + rate_{16} + rate_{17} + rate_{18} + rate_{19})$$

$$v_1 = -C_{xc} + f_{sI,xc} * C_{sI} + f_{ch,xc} * C_{ch} + f_{pr,xc} * C_{pr} + f_{li,xc} * C_{li} + f_{xI,xc} * C_{xI}$$

$$v_2 = -C_{ch} + C_{su}$$

$$v_3 = -C_{aa}$$

$$v_4 = -C_{li} + \left(1 - f_{fa,li}\right) * C_{su} + f_{fa,li} * C_{fa}$$

$$v_5 = -C_{su} + (1 - Y_{su}) * \left(f_{bu,su} * C_{bu} + f_{pro,su} * C_{pro} + f_{ac,su} * C_{ac}\right) + Y_{su} * C_{bac}$$

$$v_6 = -C_{aa} + (1 - Y_{aa}) * \left(f_{va,aa} * C_{va} + f_{bu,aa} * C_{bu} + f_{pro,aa} * C_{pro} + f_{ac,aa} * C_{ac}\right) + Y_{aa} * C_{bac}$$

$$v_7 = -C_{fa} + \left(1 - Y_{fa}\right) * 0.7 * C_{ac} + Y_{c4} * C_{bac}$$

$$v_8 = -C_{va} + (1 - Y_{c4}) * 0.54 * C_{pro} + (1 - Y_{c4}) * 0.31 * C_{ac} + Y_{c4} * C_{bac}$$

$$v_9 = -C_{bu} + (1 - Y_{c4}) * 0.8 * C_{ac} + Y_{c4} * C_{bac}$$

$$v_{10} = -C_{pro} + (1 - Y_{pro}) * 0.57 * C_{ac} + Y_{pro} * C_{bac}$$

$$v_{11} = -C_{ac} + (1 - Y_{ac}) * C_{CH4} + Y_{ac} * C_{bac}$$

$$v_{12} = -C_{H2} + (1 - Y_{H2}) * C_{Ch4} + Y_{H2} * C_{bac}$$

$$v_{13} = -C_{bac} + C_{xc}$$

B2.1.3. Particulate Matter

$$\frac{dX_c}{dt} = \frac{q_{in}}{V_{liq}}(X_{c,in} - X_c) - rate_1 + \sum_{i=13}^{19} rate_i$$

$$\frac{dX_{ch}}{dt} = \frac{q_{in}}{V_{liq}}(X_{ch,in} - X_{ch}) + f_{ch,xc} * rate_1 - rate_2$$

$$\frac{dX_{pr}}{dt} = \frac{q_{in}}{V_{liq}}(X_{pr,in} - X_{pr}) + f_{pr,xc} * rate_1 - rate_3$$

$$\frac{dX_{li}}{dt} = \frac{q_{in}}{V_{liq}}(X_{li,in} - X_{li}) + f_{li,xc} * rate_1 - rate_4$$

$$\frac{dX_{su}}{dt} = \frac{q_{in}}{V_{liq}}(X_{su,in} - X_{su}) + Y_{su} * rate_5 - rate_{13}$$

$$\frac{dX_{aa}}{dt} = \frac{q_{in}}{V_{liq}}(X_{aa,in} - X_{aa}) + Y_{aa} * rate_6 - rate_{14}$$

$$\frac{dX_{fa}}{dt} = \frac{q_{in}}{V_{liq}}(X_{fa,in} - X_{fa}) + Y_{fa} * rate_7 - rate_{15}$$

$$\frac{dX_{c4}}{dt} = \frac{q_{in}}{V_{liq}}(X_{c4,in} - X_{c4}) + Y_{c4} * rate_8 + Y_{c4} * rate_9 - rate_{16}$$

$$\frac{dX_{pro}}{dt} = \frac{q_{in}}{V_{liq}}(X_{pro,in} - X_{pro}) + Y_{pro} * rate_{10} - rate_{17}$$

$$\frac{dX_{ac}}{dt} = \frac{q_{in}}{V_{liq}}(X_{ac,in} - X_{ac}) + Y_{ac} * rate_{11} - rate_{18}$$

$$\frac{dX_{H2}}{dt} = \frac{q_{in}}{V_{liq}}\left(X_{H2,in} - X_{H2}\right) + Y_{H2} * rate_{12} - rate_{19}$$

$$\frac{dX_I}{dt} = \frac{q_{in}}{V_{liq}}\left(X_{I,in} - X_I\right) + f_{xI,xc} * rate_1$$

B2.1.4. Cation and Anion

$$\frac{dS_{cat}}{dt} = \frac{q_{in}}{V_{liq}}\left(S_{cat,in} - S_{cat}\right)$$

$$\frac{dS_{an}}{dt} = \frac{q_{in}}{V_{liq}}\left(S_{an,in} - S_{an}\right)$$

B2.1.5. Acid – Base

General differential equation for acid equations is shown below.

$$\frac{dS_{acid^-,i}}{dt} = -1 * \rho_{A,i}$$

where $\rho_{A,i} = -k_{A/B_{acid}}\left(S_{acid,i^-} * \left(K_{a_{acid,i}} + S_{H+}\right) - K_{a_{acid,i}} * S_{acid,i}\right)$

$$\frac{dS_{va-}}{dt} = -rate_{A4}$$

$$\frac{dS_{bu-}}{dt} = -rate_{A5}$$

$$\frac{dS_{pro-}}{dt} = -rate_{A6}$$

$$\frac{dS_{ac-}}{dt} = -rate_{A7}$$

$$\frac{dS_{hco3-}}{dt} = -rate_{A10}$$

$$\frac{dS_{nh3}}{dt} = -rate_{A11}$$

B2.1.6. Gas Transfer

Following equation shows the general equation of gas transfer reactions.

$$\frac{dS_{gas,i}}{dt} = -\frac{S_{gas,i} * q_{gas}}{V_{gas}} + \rho_{T,i} * \frac{V_{liq}}{V_{gas}}$$

where $\rho_{T,i} = k_L a\left(S_{liq,i} - c * K_{H,i} * p_{gas,i}\right)$

where c is conversion factor.

$$\frac{dS_{gas,H2}}{dt} = -\frac{S_{gas,H2} * q_{gas}}{V_{gas}} + rate_{T8} * \frac{V_{liq}}{V_{gas}}$$

$$\frac{dS_{gas,CH4}}{dt} = -\frac{S_{gas,CH4} * q_{gas}}{V_{gas}} + rate_{T9} * \frac{V_{liq}}{V_{gas}}$$

$$\frac{dS_{gas,CO2}}{dt} = -\frac{S_{gas,CO2} * q_{gas}}{V_{gas}} + rate_{T10} * \frac{V_{liq}}{V_{gas}}$$

B2.2. Rates

B2.2.1. Biochemical Rates

First Order Reaction Rate

$$rate_1 = k_{dis} * X_c$$

$$rate_2 = k_{hyd,ch} * X_{ch}$$

$$rate_3 = k_{hyd,pr} * X_{pr}$$

$$rate_4 = k_{hyd,li} * X_{li}$$

Monod Maximum Specific Uptake Rate

$$rate_5 = k_{m,su} * \frac{S_{su}}{K_{S,su} + S_{su}} * X_{su} * I_5$$

$$rate_6 = k_{m,aa} * \frac{S_{aa}}{K_{S,aa} + S_{aa}} * X_{aa} * I_6$$

$$rate_7 = k_{m,fa} * \frac{S_{fa}}{K_{S,fa} + S_{fa}} * X_{fa} * I_7$$

$$rate_8 = k_{m,c4} * \frac{S_{va}}{K_{S,c4} + S_{va}} * X_{c4} * \frac{S_{va}}{S_{va} + S_{bu}} * I_8$$

$$rate_9 = k_{m,c4} * \frac{S_{bu}}{K_{S,c4} + S_{bu}} * X_{c4} * \frac{S_{bu}}{S_{bu} + S_{va}} * I_9$$

$$rate_{10} = k_{m,pro} * \frac{S_{pro}}{K_{S,pro} + S_{pro}} * X_{pro} * I_{10}$$

$$rate_{11} = k_{m,ac} * \frac{S_{ac}}{K_{S,ac} + S_{ac}} * X_{ac} * I_{11}$$

$$rate_{12} = k_{m,h2} * \frac{S_{h2}}{K_{S,h2} + S_{h2}} * X_{h2} * I_{12}$$

First Order Decay Rate

$$rate_{13} = k_{dec,Xsu} * X_{su}$$

$$rate_{14} = k_{dec,Xaa} * X_{aa}$$

$$rate_{15} = k_{dec,Xfa} * X_{fa}$$

$$rate_{16} = k_{dec,Xc4} * X_{c4}$$

$$rate_{17} = k_{dec,Xpro} * X_{pro}$$

$$rate_{18} = k_{dec,Xac} * X_{ac}$$

$$rate_{19} = k_{dec,Xh2} * X_{h2}$$

B2.2.2 Acid Base Rates

$$rate_{A4} = K_{A_{/Bva}} * (S_{va,ac} * (K_{a,va} + S_{H+}) - K_{a,va} * S_{va})$$

$$rate_{A5} = K_{A_{/Bbu}} * (S_{bu,ac} * (K_{a,bu} + S_{H+}) - K_{a,bu} * S_{bu})$$

$$rate_{A6} = K_{A_{/Bpro}} * (S_{pro,ac} * (K_{a,pro} + S_{H+}) - K_{a,pro} * S_{pro})$$

$$rate_{A7} = K_{A_{/Bac}} * (S_{ac,ac} * (K_{a,ac} + S_{H+}) - K_{a,ac} * S_{ac})$$

$$rate_{A10} = K_{A_{/BCO2}} * (S_{IC,ac} * (K_{a,IC} + S_{H+}) - K_{a,IC} * S_{IC})$$

$$rate_{A11} = K_{A_{/BIN}} * (S_{IN,,ac} * (K_{a,IN} + S_{H+}) - K_{a,IN} * S_{IN})$$

B2.2.3. Gas Transfer Rates

$$rate_{T8} = k_L a * (S_{liq,H2} - 16 * K_{H,H2} * P_{gas,H2})$$

$$rate_{T9} = k_L a * (S_{liq,CH4} - 64 * K_{H,CH4} * P_{gas,CH4})$$

$$rate_{T10} = k_L a * (S_{liq,CO2} - K_{H,CO2} * P_{gas,CO2})$$

Amount of Hydronium (Batstone, et al. 2002) (Rosen and Jeppsson 2006)

$$S_{cat+} + S_{nh4+} + S_{H+} - S_{HCO3-} - \frac{S_{ac-}}{64} - \frac{S_{pro-}}{112} - \frac{S_{bu-}}{160} - \frac{S_{va-}}{208} - S_{an-} = 0$$

$$S_{H+} = -\frac{\theta}{2} + \frac{1}{2} * \sqrt{\theta^2 + 4 * K_w}$$

$$\theta = S_{cat+} + S_{nh4+} - S_{hco3-} - \frac{S_{ac-}}{64} - \frac{S_{pro-}}{112} - \frac{S_{bu-}}{160} - \frac{S_{va-}}{208} - S_{an-}$$

$$S_{nh4+} = S_{IN} - S_{nh3}$$

$$S_{co2} = S_{IC} - S_{hco3-}$$

B2.3. pH Calculation

$$pH = -\log 10(S_{H+})$$

B2.4. Inhibition Functions

$$I_5 = I_{pH,aa} * I_{lim}$$

$$I_6 = I_{pH,aa} * I_{lim}$$

$$I_7 = I_{pH,aa} * I_{lim} * I_{H2,fa}$$

$$I_8 = I_{pH,aa} * I_{lim} * I_{H2,c4}$$

$$I_9 = I_{pH,aa} * I_{lim} * I_{H2,c4}$$

$$I_{10} = I_{pH,aa} * I_{lim} * I_{H2,pro}$$

$$I_{11} = I_{pH,ac} * I_{lim} * I_{NH3}$$

$$I_{12} = I_{pH,H2} * I_{lim}$$

B2.4.1. pH Inhibition

Hill inhibition function is used as (Rosen and Jeppsson 2006) suggest in order to eliminate the risk of numerical instabilities instead of using switch functions for evaluating pH inhibitions as suggested by (Batstone, et al. 2002).

$$I_{pH,aa} = \frac{\left(K_{pH,aa}{}^{24}\right)}{S_H{}^{24}} + K_{pH,aa}{}^{24}$$

$$I_{pH,ac} = \frac{\left(K_{pH,ac}{}^{45}\right)}{S_H{}^{45}} + K_{pH,ac}{}^{45}$$

$$I_{pH,H2} = \frac{\left(K_{pH,H2}{}^{3}\right)}{S_H{}^{3}} + K_{pH,H2}{}^{3}$$

$$K_{pH,aa} = \frac{1}{\sqrt{10^{pH_{LL,aa}+pH_{UL,aa}}}}$$

$$K_{pH,ac} = \frac{1}{\sqrt{10^{pH_{LL,ac}+pH_{UL,ac}}}}$$

$$K_{pH,H2} = \frac{1}{\sqrt{10^{pH_{LL,H2}+pH_{UL,H2}}}}$$

where pH_{LL} and pH_{UL} represent lower limit for pH and upper limit for pH.

B2.4.2. Lack of Nitrogen Inhibition

$$I_{lim} = \frac{1}{1 + \frac{K_{s,IN}}{S_{IN}}}$$

B2.4.3. Hydrogen Inhibition

$$I_{H2,fa} = \frac{1}{1 + \frac{S_{H2}}{Ki_{H2,fa}}}$$

$$I_{H2,c4} = \frac{1}{1 + \frac{S_{H2}}{Ki_{H2,c4}}}$$

$$I_{H2,pro} = \frac{1}{1 + \frac{S_{H2}}{Ki_{H2,pro}}}$$

B2.4.4. Ammonia Inhibition

$$I_{NH3} = \frac{1}{1 + \frac{S_{IN,ac}}{Ki_{NH3}}}$$

B2.5. Gas Pressure and Flowrate

$$p_{gas,H2} = S_{gas,H2} * \frac{R * T_{op}}{16}$$

$$p_{gas,CH4} = S_{gas,CH4} * \frac{R * T_{op}}{64}$$

$$p_{gas,CO2} = S_{gas,CO2} * R * T_{op}$$

$$P_{gas} = p_{gas,H2} + p_{gas,CH4} + p_{gas,CO2} + p_{gas,H2O}$$

Biogas Flowrate at the Exit (Rosen and Jeppsson 2006)

$$q_{gas} = k_p * \left(P_{gas} - P_{atm}\right) * \frac{P_{gas}}{P_{atm}}$$

B3. Constants

In this section, the required input data of ADM1 are shown.

B3.1. State Variables

The state variables which are needed to design an ADM1 digester are shown in Table B.1.

Table B.1. State variables in ADM1

State Variable	i	Description
S_{su}	1	Monosaccharides
S_{aa}	2	Amino Acids
S_{fa}	3	Total Long Chain Fatty Acids
S_{va}	4	Total Valerate
S_{bu}	5	Total Butyrate
S_{pro}	6	Total Propionate
S_{ac}	7	Total Acetate
S_{h2}	8	Hydrogen
S_{ch4}	9	Methane
S_{IC}	10	Inorganic Nitrogen
S_{IN}	11	Inorganic Carbon
S_{I}	12	Soluble Inerts
X_{c}	13	Composite
X_{ch}	14	Carbohydrates
X_{pr}	15	Proteins
X_{li}	16	Lipids
X_{su}	17	Particulate Monosaccharides
X_{aa}	18	Particulate Amino Acids
X_{fa}	19	Particulate Fatty Acids
X_{c4}	20	Particulate Valerate & Butyrate
X_{pro}	21	Particulate Propionate
X_{ac}	22	Particulate Acetate
X_{h2}	23	Particulate Hydrogen
X_{I}	24	Particulate Inerts
S_{cat}	25	Cation
S_{an}	26	Anion
S_{va-}	27	Valerate Ion
S_{bu-}	28	Butyrate Ion
S_{pro-}	29	Propionate Ion
S_{ac-}	30	Acetate Ion
S_{hco3-}	31	Bicarbonate
S_{nh3}	32	Ammonia
S_{gasH2}	33	Hydrogen Gas
S_{gasCH4}	34	Methane Gas
S_{gasCO2}	35	Carbon Dioxide Gas

B3.2. Stoichiometric Coefficients (Rosen and Jeppsson 2006)

The stoichiometric coefficients for degradation reactions are shown in Table B.2.

Table B.2. Stoichiometric coefficients in ADM1

Parameter	Description	Value
$f_{sI,xc}$	Soluble inerts from composites	0.10
$f_{xI,xc}$	Particulate inerts from composites	0.20
$f_{ch,xc}$	Carbohydrates from composites	0.20
$f_{pr,xc}$	Protein from composites	0.20
$f_{li,xc}$	Lipids from composites	0.30
N_{xc}	Nitrogen contents of composites	0.0376/14
N_I	Nitrogen contents of inerts	0.06/14
$f_{fa,li}$	Fatty acids from lipids	0.95
$f_{h2,su}$	Hydrogen from sugars	0.19
$f_{bu,su}$	Butyrate from sugars	0.13
$f_{pro,su}$	Propionate from sugars	0.27
$f_{ac,su}$	Acetate from sugars	0.41
$f_{h2,aa}$	Hydrogen from amino acids	0.06
N_{aa}	Nitrogen in amino acids and proteins	0.007
$f_{va,aa}$	Valerate from amino acids	0.23
$f_{bu,aa}$	Butyrate from amino acids	0.26
$f_{pro,aa}$	Propionate from amino acids	0.05
$f_{ac,aa}$	Acetate from amino acids	0.40
N_{bac}	Nitrogen content in bacteria cell	0.08/14

where $f_{product,substrate}$ (kgCOD/kgCOD) is yield (catabolism only) of product on substrate, N_i nitrogen content of component i.

B3.3. Kinetic Parameters and Rates (Batstone, et al. 2002) (Rosen and Jeppsson 2006)

Table B.3 shows the kinetic parameters needed in ADM1 design.

Table B.3. Kinetic parameters and rates in ADM1

Parameter	Description	Value
Y_{su}	Yield of biomass on sugar	0.10
Y_{aa}	Yield of biomass on amino acids	0.08
Y_{fa}	Yield of biomass on fatty acids	0.06
Y_{c4}	Yield of biomass on methane	0.06
Y_{pro}	Yield of biomass on propionate	0.04
Y_{ac}	Yield of biomass on acetate	0.05
Y_{h2}	Yield of biomass on hydrogen	0.06
k_{dis}	First order parameter for disintegration	0.013
$k_{hyd,ch}$	First order parameter for carbohydrate hydrolysis	0.25
$k_{hyd,pr}$	First order parameter for protein hydrolysis	0.026
$k_{hyd,li}$	First order parameter for lipid hydrolysis	0.11
$k_{m,su}$	Monod maximum specific uptake rate of sugar	30
$k_{m,aa}$	Monod maximum specific uptake rate of amino acids	50
$k_{m,fa}$	Monod maximum specific uptake rate of fatty acids	6
$k_{m,c4}$	Monod maximum specific uptake rate of methane	20
$k_{m,pro}$	Monod maximum specific uptake rate of propionate	13
$k_{m,ac}$	Monod maximum specific uptake rate of acetate	8
$k_{m,h2}$	Monod maximum specific uptake rate of hydrogen	35
k_{dec}	First order decay rate	0.02
$K_{s,su}$	Half saturation value of sugar	0.5
$K_{s,aa}$	Half saturation value of amino acids	0.3
$K_{s,fa}$	Half saturation value of fatty acids	0.4
$K_{s,c4}$	Half saturation value of methane	0.2
$K_{s,pro}$	Half saturation value of propionate	0.1
$K_{s,ac}$	Half saturation value of acetate	0.15
$K_{s,h2}$	Half saturation value of hydrogen	$7*10^{-6}$
$K_{s,IN}$	Half saturation value of inorganic nitrogen	$1*10^{-4}$
$K_{i,h2\_fa}$	50 % inhibitory concentration of fatty acids	$5*10^{-6}$
$K_{i,h2\_c4}$	50 % inhibitory concentration of methane	$1*10^{-5}$
$K_{i,h2\_pro}$	50 % inhibitory concentration of propionate	$3.5*10^{-6}$
$K_{i,nh3}$	50 % inhibitory concentration of ammonia	$1.8*10^{-3}$
$k_{A/Bva}$	Acid base kinetic parameter for valerate	$1*10^{10}$
$k_{A/Bbu}$	Acid base kinetic parameter for butyrate	$1*10^{10}$
$k_{A/Bpro}$	Acid base kinetic parameter for propionate	$1*10^{10}$
$k_{A/Bac}$	Acid base kinetic parameter for acetate	$1*10^{10}$
$k_{A/BCO2}$	Acid base kinetic parameter for inorganic carbon	$1*10^{10}$
$k_{A/BIN}$	Acid base kinetic parameter for inorganic nitrogen	$1*10^{10}$
$K_{a,va}$	Acid base equilibrium coefficient of valerate	$1*10^{-4.86}$
$K_{a,bu}$	Acid base equilibrium coefficient of butyrate	$1*10^{-4.82}$
$K_{a,pro}$	Acid base equilibrium coefficient of propionate	$1*10^{-4.88}$
$K_{a,ac}$	Acid base equilibrium coefficient of acetate	$1*10^{-4.76}$
$K_{a,IC}$	Acid base equilibrium coefficient of inorganic carbon	$1*10^{-6.35}$
$K_{a,IN}$	Acid base equilibrium coefficient of inorganic nitrogen	$1*10^{-9.25}$
$K_{h,h2}$	Henry's Law coefficient of hydrogen	$7.38*10^{-4}$
$K_{h,ch4}$	Henry's Law coefficient of methane	$1.16*10^{-3}$
$K_{h,co2}$	Henry's Law coefficient of carbon dioxide	$2.71*10^{-2}$
k_La	Gas – liquid transfer coefficient	200
K_w		$1*10^{-14}$
kp	Constant for gas supply	$5*10^{7}$

where the unit of $Y_{substrate}$ is $kgCOD_X/kgCOD_S$, the unit of $k_{process}$ is d^{-1}, the unit of $k_{m,process}$ is $kgCOD_S/kgCOD_X*d$, the unit of k_{dec} is d^{-1}, the unit of $K_{s,process}$ is $kgCOD_S/m^3$, the unit of $K_{i,inhibit,substrate}$ is $kgCOD/m^3$, the unit of $k_{A/Bi}$ is $M^{-1}d^{-1}$, the unit of $K_{a,acid}$ is M(kmole m^{-3}), the unit of Henry's constant is M/bar (kmole/m^3*bar), the unit of k_La is d^{-1} and the unit of kp is L/d*bar.

B3.4. Carbon Content (Rosen and Jeppsson 2006)

Carbon content of each species are show in Table B.4.

Table B.4. Carbon content of each species

Parameter	Description	Value
C_{biom}	Carbon content in bacteria cell	0.0313
C_{su}	Carbon content in sugar	0.0313
C_{aa}	Carbon content in amino acids	0.03
C_{fa}	Carbon content in fatty acids	0.0217
C_{va}	Carbon content in valerate	0.024
C_{bu}	Carbon content in butyrate	0.025
C_{pro}	Carbon content in propionate	0.0268
C_{ac}	Carbon content in acetate	0.0313
C_{h2}	Carbon content in hydrogen	0
C_{ch4}	Carbon content in methane	0.0156
C_{IC}	Carbon content in inorganic carbon	1
C_{IN}	Carbon content in inorganic nitrogen	0
C_{I}	Carbon content in inert	0.03
C_{c}	Carbon content in composite	0.02786
C_{ch}	Carbon content in carbohydrates	0.0313
C_{pr}	Carbon content in proteins	0.03
C_{li}	Carbon content in lipids	0.022
C_{x} = (particulate su, aa, fa,c4, pro, ac, h2)	Carbon content in particulate matters	0.0313

where the unit of Ci is C/COD.

B3.5. pH Lower and Upper Limits (Batstone, et al. 2002)

pH limits for pH inhibition equations are shown in Table B.5.

Table B.5. Lower and upper limits of pH

Parameter	Value
pH_{LL_aa}	4
pH_{UL_aa}	5.5
pH_{LL_h2}	5
ph_{UL_h2}	6
pH_{LL_ac}	6
pH_{UL_ac}	7

APPENDIX C. MATLAB CODES

This section is divided into three parts. They are MATLAB packages (i.e., AMD1 variables, ADM1 function and ADM1 digester).

C.1. ADM1 Variables

```
%%This MATLAB function conveys the variables (i.e., stoichiometric
%%coefficeints, kinetic parameters, carbon content and upper and lower
%%limits for pH).

%VARIABLES

function  Variables()
%STOICHIOMETRIC COEFFICIENTS
%Composite Utilizing
global f_sIxc          %Soluble_inerts_from_composites
global f_xIxc          %Particulate_inerts_from_composites
global f_chxc          %Carbohydrates_from_composites
global f_prxc          %Proteins_from_composites
global f_lixc          %Lipids_from_composites
global N_xc            %Nitrogen_contents_of_composites

%Inert
global N_I             %Nitrogen_contents_of_inerts

%Lipid Utilizing
global f_fali          %Fatty_acids_from_lipids

%Sugar Utilizing
global f_h2su          %Hydrogen_from_sugars
```

```
global f_busu          %Butyrate_from_sugars
global f_prosu         %Propionate_from_sugars
global f_acsu          %Acetate_from_sugars

%Amino Acid Utilizing
global f_h2aa          %Hydrogen_from_amino_acids
global N_aa            %Nitrogen_in_amino_acids_and_proteins
global f_vaaa          %Valerate_from_amino_acids
global f_buaa          %Butyrate_from_amino_acids
global f_proaa         %Propionate_from_amino_acids
global f_acaa          %Acetate_from_amino_acids

%Bacteria Cell
global N_bac           %Nitrogen_contents_in_bacteria_cell

%KINETIC PARAMETERS
%Yield of Biomass
global Y_su            %Yield_of_biomass_on_sugar
global Y_aa            %Yield_of_biomass_on_amino_acids
global Y_fa            %Yield_of_biomass_on_fatty_acids
global Y_c4            %Yield_of_biomass_on_methane
global Y_pro           %Yield_of_biomass_on_propionate
global Y_ac            %Yield_of_biomass_on_acetate
global Y_h2            %Yield_of_biomass_on_hydrogen

%First order parameter
global k_dis           %First_order_parameter_for_disintegration
global khyd_ch         %First_order_parameter_for_carbohydrate_hydrolysis
global khyd_pr         %First_order_parameter_for_protein_hydrolysis
global khyd_li         %First_order_parameter_for_lipid_hydrolysis

%Monod Maximum Specific Uptake Rate
global km_su           %Monod_maximum_specific_uptake_rate_of_sugar
```

```
global km_aa          %Monod_maximum_specific_uptake_rate_of_amino_acids
global km_fa          %Monod_maximum_specific_uptake_rate_of_fatty_acids
global km_c4          %Monod_maximum_specific_uptake_rate_of_methane
global km_pro         %Monod_maximum_specific_uptake_rate_of_propionate
global km_ac          %Monod_maximum_specific_uptake_rate_of_acetate
global km_h2          %Monod_maximum_specific_uptake_rate_of_hydrogen

%First Order Decay Rate
global k_dec          %First_order_decay_rate

%Half Saturation Value
global Ks_su          %Half_saturation_value_of_sugar
global Ks_aa          %Half_saturation_value_of_amino_acids
global Ks_fa          %Half_saturation_value_of_fatty_acids
global Ks_c4          %Half_saturation_value_of_methane
global Ks_pro         %Half_saturation_value_of_propionate
global Ks_ac          %Half_saturation_value_of_acetate
global Ks_h2          %Half_saturation_value_of_hydrogen
global Ks_IN          %Half_saturation_value_of_inorganic_nitrogen

%Inhibitory Concentrations
global Ki_h2_fa       %50%_inhibitory_concentration_of_fatty_acids
global Ki_h2_c4       %50%_inhibitory_concentration_of_methane
global Ki_h2_pro      %50%_inhibitory_concentration_of_propionate
global Ki_NH3         %50%_inhibitory_concentration_of_ammonia

%Acid – Base Kinetic Parameters
global kab_va         %Acid_base_kinetic_parameter_for_valerate
global kab_bu         %Acid_base_kinetic_parameter_for_butyrate
global kab_pro        %Acid_base_kinetic_parameter_for_propionate
global kab_ac         %Acid_base_kinetic_parameter_for_acetate
global kab_CO2        %Acid_base_kinetic_parameter_for_inorganic_carbon
global kab_IN         %Acid_base_kinetic_parameter_for_inorganic_nitrogen
```

```
%Acid – Base Equilibrium Coefficients
global Ka_va        %Acid_base_equilibrium_coefficient_of_valerate
global Ka_bu        %Acid_base_equilibrium_coefficient_of_butyrate
global Ka_pro       %Acid_base_equilibrium_coefficient_of_propionate
global Ka_ac        %Acid_base_equilibrium_coefficient_of_acetate
global Ka_IC        %Acid_base_equilibrium_coefficient_of_inorganic_carbon
global Ka_IN        %Acid_base_equilibrium_coefficient_of_inorganic_nitrogen

%Henry's Law Coefficients
global Kh_h2        %Henry's_Law_coefficient_of_hydrogen
global Kh_ch4       %Henry's_Law_coefficient_of_methane
global Kh_co2       %Henry's_Law_coefficient_of_carbon_dioxide

%Gas – Liquid Transfer Coefficient
global kla          %Gas_liquid_transfer_coefficient

%Constant for Gas Supply
global kp           %Constant_for_gas_supply

%Carbon Content
global C_biom       %Carbon_content_in_bacteria_cell
global C_1          %Carbon_content_in_sugar
global C_2          %Carbon_content_in_amino_acids
global C_3          %Carbon_content_in_fatty_acids
global C_4          %Carbon_content_in_valerate
global C_5          %Carbon_content_in_butyrate
global C_6          %Carbon_content_in_propionate
global C_7          %Carbon_content_in_acetate
%golabal C_8        %Carbon_content_in_hydrogen
global C_9          %Carbon_content_in_methane
%golabal C_10       %Carbon_content_in_inorganic carbon
%golabal C_11       %Carbon_content_in_inorganic_nitrogen
global C_12         %Carbon_content_in_inert
```

```
global C_13          %Carbon_content_in_composite
global C_14          %Carbon_content_in_carbohydrates
global C_15          %Carbon_content_in_proteins
global C_16          %Carbon_content_in_lipids
%golabal C_17        %Carbon_content_in_particulate_sugar
%golabal C_18        %Carbon_content_in_particulate_amino_acid
%golabal C_19        %Carbon_content_in_particulate_fatty_acid
%golabal C_20        %Carbon_content_in_particulate_methane
%golabal C_21        %Carbon_content_in_particulate_propionate
%golabal C_22        %Carbon_content_in_particulate_acetate
%golabal C_23        %Carbon_content_in_particulate_hydrogen
global C_24          %Carbon_content_in_particulate_inert

%pH Lower and Upper Limits
global pH_LL_aa       %Lower_limit_pH_of_amino_acids
global pH_UL_aa       %Upper_limit_pH_of_amino_acids
global pH_LL_H2       %Lower_limit_pH_of_hydrogen
global pH_UL_H2       %Upper_limit_pH_of_hydrogen
global pH_LL_ac       %Lower_limit_pH_of_acetate
global pH_UL_ac       %Upper_limit_pH_of_acetate

%Other Parameters
global P_atm          %Atmospheric_pressure
global R              %Ideal_gas_constant
global K_w


%VALUES
%Composite Utilizing
f_sIxc = 0.1;
f_xIxc = 0.2;
f_chxc = 0.20;
f_prxc = 0.20;
```

```
f_lixc = 0.3;
N_xc = 0.0376/14;

%Inert
N_I = 0.06/14;

%Lipid Utilizing
f_fali = 0.95;

%Sugar Utilizing
f_h2su = 0.19;
f_busu = 0.13;
f_prosu = 0.27;
f_acsu = 0.41;

%Amino Acid Utilizing
f_h2aa = 0.06;
N_aa = 0.007;
f_vaaa = 0.23;
f_buaa = 0.26;
f_proaa = 0.05;
f_acaa = 0.4;

%Bacteria Cell
N_bac = 0.08/14;

%Yield of Biomass
Y_su = 0.1;
Y_aa = 0.08;
Y_fa = 0.06;
Y_c4 = 0.06;
Y_pro = 0.04;
Y_ac = 0.05;
```

```
Y_h2 = 0.06;

%First Order Parameter
k_dis = 0.013;
khyd_ch = 0.25;
khyd_pr = 0.026;
khyd_li = 0.11;

%Monod Maximum Specific Uptake Rate
km_su = 30;
km_aa = 50;
km_fa = 6;
km_c4 = 20;
km_pro = 13;
km_ac = 8;
km_h2 = 35;

%First Order Decay Rate
k_dec = 0.02;

%Half Saturation Value
Ks_su = 0.5;
Ks_aa = 0.3;
Ks_fa = 0.4;
Ks_c4 = 0.2;
Ks_pro = 0.1;
Ks_ac = 0.15;
Ks_h2 = 7e-06;
Ks_IN = 1E-4;

%Inhibitory Concentrations
Ki_h2_fa = 5E-6;
Ki_h2_c4 = 1E-5;
```

```
Ki_h2_pro = 3.5E-6;
Ki_NH3 = 0.0018;

%Acid – Base Kinetic Parameters
kab_va = 1E10;
kab_bu = 1E10;
kab_pro = 1E10;
kab_ac = 1E10;
kab_CO2 = 1E10;
kab_IN = 1E10;
 %Acid – Base Equilibrium Coefficients
Ka_va = 10^(-4.72);
Ka_bu = 10^(-4.82);
Ka_pro = 10^(-4.88);
Ka_ac = 10^(-4.76);
Ka_IC = 10^(-6.35);
Ka_IN = 10^(-9.25);

%Henry's Law Coefficients
Kh_h2 = 7.38E-4;
Kh_ch4 = 0.00116;
Kh_co2 = 0.0271;

%Gas – Liquid Transfer Coefficient
kla = 200;

%Constant for Gas Supply
kp = 5*10^7;

%Carbon Content
C_biom = 0.0313;
C_1 = 0.0313;
C_2 = 0.03;
```

```
C_3 = 0.0217;
C_4 = 0.024;
C_5 = 0.025;
C_6 = 0.0268;
C_7 = 0.0313;
%C_8 = 0;
C_9 = 0.0156;
%C_10=1;
%C_11=0;
C_12 = 0.03;
C_13 = 0.02786;
C_14 = 0.0313;
C_15 = 0.03;
C_16 = 0.022;
%C_17 = C_biom;
%C_18 = C_biom;
%C_19 = C_biom;
%C_20 = C_biom;
%C_21 = C_biom;
%C_22 = C_biom;
%C_23 = C_biom;
C_24 = 0.03;

%pH Lower and Upper Limits
pH_LL_aa = 4;
pH_UL_aa = 5.5;
pH_LL_H2 = 5;
pH_UL_H2 = 6;
pH_LL_ac = 6;
pH_UL_ac = 7;
```

```
%Other Parameters
P_atm = 1.013;
R = 0.083145;
K_w = 1*10^-14;

end
```

C.2. ADM1 Function

```
%%In this MATLAB codes, ADM1 functions are processed. Differential
%%equations and algebraic equations are functions of parameters in variable
%%function. The equations of sets are taken from Batstone, 2002 ADM1 study,
%%and written in the same order with modifications as Rosen suggested.


function
dS=ADM1_Digester_3CSTRS_in_Series_fun(t,C,Carbohydrates,Proteins,Lipids,Sugars
,Cations,Anions,~)

%Constant Variables
d_tank = 3.6;                    %Diameter_of_tank_(dm)
h_tank = 4.1;                    %Height_of_tank_(dm)
V_tank = (pi()*((d_tank/2)^2)*h_tank)/3;    %Volume_of_tank_(L)
q_in = 0.604;                    %Volumetric_inflow_(L/d)
V_liq = 39/3;                    %Liquid_volume_(L)
V_gas = V_tank - V_liq;          %Gas_volume_(m^3)
T = (310.55);                    %Temperature_(K)

%Global Variables
global f_sIxc
global f_xIxc
global f_chxc
```

```
global f_prxc
global f_lixc
global N_xc
global N_I
global f_fali
global f_h2su
global f_busu
global f_prosu
global f_acsu
global f_h2aa
global N_aa
global f_vaaa
global f_buaa
global f_proaa
global f_acaa
global N_bac
global Y_su
global Y_aa
global Y_fa
global Y_c4
global Y_pro
global Y_ac
global Y_h2
global k_dis
global khyd_ch
global khyd_pr
global khyd_li
global km_su
global km_aa
global km_fa
global km_c4
global km_pro
global km_ac
```

```
global km_h2
global k_dec
global Ks_su
global Ks_aa
global Ks_fa
global Ks_c4
global Ks_pro
global Ks_ac
global Ks_h2
global Ks_IN
global Ki_h2_fa
global Ki_h2_c4
global Ki_h2_pro
global Ki_NH3
global kab_va
global kab_bu
global kab_pro
global kab_ac
global kab_CO2
global kab_IN
global Ka_va
global Ka_bu
global Ka_pro
global Ka_ac
global Ka_IC
global Ka_IN
global Kh_h2
global Kh_ch4
global Kh_co2
global kla
global kp
global C_biom
global C_1
```

```
global C_2
global C_3
global C_4
global C_5
global C_6
global C_7
%global C_8
global C_9
%global C_10
%global C_11
global C_12
global C_13
global C_14
global C_15
global C_16
%global C_17
%global C_18
%global C_19
%global C_20
%global C_21
%global C_22
%global C_23
global C_24
global pH_LL_aa
global pH_UL_aa
global pH_LL_H2
global pH_UL_H2
global pH_LL_ac
global pH_UL_ac
global P_atm
global R
global K_w
```

```
%Arrhenius Equation
kT = ((1/298.15) - (1/T));

%Concentration in CSTR Anaerobic Digester
S_su = C(1);        %Sugar
S_aa = C(2);        %Amino_Acid
S_fa = C(3);        %LCFA
S_va = C(4);        %Valerate
S_bu = C(5);        %Butyrate
S_pro = C(6);       %Propinate
S_ac = C(7);        %Acetate
S_h2 = C(8);        %Hydrogen
S_ch4 = C(9);       %Methane
S_IC = C(10);       %Inoragnic_Carbon
S_IN = C(11);       %Inorganic_Nitrogen
S_I = C(12);        %Dissolved_Inerts
X_c = C(13);        %Composites
X_ch = C(14);       %Carbohydrates
X_pr = C(15);       %Proteins
X_li = C(16);       %Lipids
X_su = C(17);       %Sugar_Degraders_(Particulate)
X_aa = C(18);       %Amino_Acid_Degraders_(Particulate)
X_fa = C(19);       %LCFA_Degrades_(Particulate)
X_c4 = C(20);       %Valerate_and_Butyrate_Degraders_(Particulate)
X_pro = C(21);      %Propionate_Degraders_(Particulate)
X_ac = C(22);       %Acetate_Degraders_(Particulate)
X_h2 = C(23);       %Hydrogen_Degraders_(Particulate)
x_I = C(24);        %Inerts_(Particulate)
S_cat = C(25);      %Cation
S_an = C(26);       %Anion
S_va_ac = C(27);    %Valeric_Acid
S_bu_ac = C(28);    %Butyric_Acid
S_pro_ac = C(29);   %Propionic_Acid
```

```
S_ac_ac = C(30);    %Acetic_Acid
S_IC_ac = C(31);    %HCO3-
S_IN_ac = C(32);    %Ammonia
S_h2_gas = C(33);   %Hydrogen_Gas
S_ch4_gas = C(34);  %Methane_Gas
S_co2_gas = C(35);  %Carbon_Dioxide_Gas

%Initial Concentration
%%Only variables are sugar, carbohydrate, protein, lipid, cations and
%%anions. Therefore, they will be entered by hand when the program is
%%executed.

S_su_in = Sugars;
S_aa_in = 0;
S_fa_in = 0;
S_va_in = 0;
S_bu_in = 0;
S_pro_in = 0;
S_ac_in = 0;
S_h2_in = 0;
S_ch4_in = 0;
S_IC_in = 0;
S_IN_in = 0;
S_I_in = 0;
X_c_in = 0;
X_ch_in = Carbohydrates;
X_pr_in = Proteins;
X_li_in = Lipids;
X_su_in = 0;
X_aa_in = 0;
X_fa_in = 0;
X_c4_in = 0;
X_pro_in = 0;
```

```
X_ac_in = 0;
X_h2_in = 0;
X_I_in = 0;
S_cat_in = Cations;
S_an_in = Anions;
S_va_ac_in = 0;
S_bu_ac_in = 0;
S_pro_ac_in = 0;
S_ac_ac_in = 0;
S_IC_ac_in = 0;
S_IN_ac_in = 0;
S_h2_gas_in = 0;
S_ch4_gas_in = 0;
S_co2_gas_in = 0;

%%INORGANIC CARBON STOICHIOMETRIC COEFFICIENTS
%%Inorganic carbon stoichiometric coefficient is the sum of all carbon
%%contents in a process. The following calculations belong to each process.
%%v_i_j is the general form of coefficient where i represents species and j
%%represents process.

v_10_1 = -(f_sIxc * C_12 - C_13 + f_chxc * C_14 + f_prxc * C_15 + f_lixc * C_16 +
f_xIxc * C_24); %Inorganic_carbon_coefficient_for_disintegration
v_10_2 = -(C_1 - C_14);
%Inorganic_carbon_coefficient_for_hydrolysis_of_carbohydrates
v_10_3 = -(C_2 - C_15); %Inorganic_carbon_coefficient_for_hydrolysis_of_proteins
v_10_4 = -((1 - f_fali) * C_1 + f_fali * C_3 - C_16);
%Inorganic_carbon_coefficient_for_hydrolysis_of_lipids
v_10_5 = -(-C_1 + (1 - Y_su) * f_busu * C_5 + (1 - Y_su) * f_prosu * C_6 + (1 - Y_su)
* f_acsu * C_7 + Y_su * C_biom);
%Inorganic_carbon_coefficient_for_fermentation_of_sugars
```

```
v_10_6 = -(-C_2 + (1 - Y_aa) * f_vaaa * C_4 + (1 - Y_aa) * f_buaa * C_5 + (1 - Y_aa)
* f_proaa * C_6 + (1 - Y_aa) * f_acaa * C_7 + Y_aa * C_biom);
%Inorganic_carbon_coefficient_for_fermentation_of_amino_acids
v_10_7 = -(-C_3 + (1 - Y_fa) * 0.7 * C_7 + Y_fa * C_biom);
%Inorganic_carbon_coefficient_for_fermentation_of_LCFA
v_10_8 = -(-C_4 + (1 - Y_c4) * 0.54 * C_6 + (1 - Y_c4) * 0.31 * C_7 + Y_c4 *
C_biom); %Inorganic_carbon_coefficient_for_fermentation_of_valerate
v_10_9 = -(-C_5 + (1 - Y_c4) * 0.8 * C_7 + Y_c4 * C_biom);
%Inorganic_carbon_coefficient_for_fermentation_of_butyrate
v_10_10 = -(-C_6 + (1 - Y_pro) * 0.57 * C_7 + Y_pro * C_biom);
%Inorganic_carbon_coefficient_for_fermentation_of_propionate
v_10_11 = -(-C_7 + (1 - Y_ac) * C_9 + Y_ac * C_biom);
%Inorganic_carbon_coefficient_for_fermentation_of_acetate
v_10_12 = -((1 - Y_h2) * C_9 + Y_h2 * C_biom);
%Inorganic_carbon_coefficient_for_fermentation_of_hydrogen
v_10_13 = -(C_13 - C_biom);
%Inorganic_carbon_coefficient_for_decay_of_particulate_sugars
v_10_14 = -(C_13 - C_biom);
%Inorganic_carbon_coefficient_for_decay_of_particulate_amino_acids
v_10_15 = -(C_13 - C_biom);
%Inorganic_carbon_coefficient_for_decay_of_particulate_fatty_acids
v_10_16 = -(C_13 - C_biom);
%Inorganic_carbon_coefficient_for_decay_of_particulate_methane
v_10_17 = -(C_13 - C_biom);
%Inorganic_carbon_coefficient_for_decay_of_particulate_propionate
v_10_18 = -(C_13 - C_biom);
%Inorganic_carbon_coefficient_for_decay_of_particulate_acetate
v_10_19 = -(C_13 - C_biom);
%Inorganic_carbon_coefficient_for_decay_of_particulate_hydrogen

%%STOICHIOMETRIC COEFFICENT MATRIX
%%Since ADM1 is developed as a matrix model, and MATLAB is a matrix based
%%software, it is wise to create a matrix that evaluates all the
```

```
%%stoichiometric coefficients. St_C is the name of the matrix that is
%%short for stoichiometric coefficient. There are 3 different equation sets.
%%These are biochemical process, acid - base equations and gas transfer
%%equations. They are combined and one matrix system is built with size of
%%[28X35]. Biochemical process equation set occupies between (0,0) and
%%(19,26). Acid - base equations occupy between (20,27) and (25,32), and
%%gas transfer equations occupy (26,33) and (28,35).

St_C = zeros(28,35);
%Biochemical Process
St_C(1,10) = v_10_1;
St_C(1,11) = (N_xc - f_xIxc * N_I - f_sIxc * N_I - f_prxc * N_aa);
St_C(1,12) = f_sIxc;
St_C(1,13) = -1;
St_C(1,14) = f_chxc;
St_C(1,15) = f_prxc;
St_C(1,16) = f_lixc;
St_C(1,24) = f_xIxc;
St_C(2,1) = 1;
St_C(2,10) = v_10_2;
St_C(2,14) = -1;
St_C(3,2) = 1;
St_C(3,10) = v_10_3;
St_C(3,15) = -1;
St_C(4,1) = (1 - f_fali);
St_C(4,3) = (f_fali);
St_C(4,10) = v_10_4;
St_C(4,16) = -1;
St_C(5,1) = -1;
St_C(5,5) = ((1 - Y_su) * f_busu);
St_C(5,6) = ((1 - Y_su) * f_prosu);
St_C(5,7) = ((1 - Y_su) * f_acsu);
St_C(5,8) = ((1 - Y_su) * f_h2su);
```

```
St_C(5,10) = v_10_5;
St_C(5,11) = -(Y_su * N_bac);
St_C(5,17) = Y_su;
St_C(6,2) = -1;
St_C(6,4) = ((1 - Y_aa) * f_vaaa);
St_C(6,5) = ((1 - Y_aa) * f_buaa);
St_C(6,6) = ((1 - Y_aa) * f_proaa);
St_C(6,7) = ((1 - Y_aa) * f_acaa);
St_C(6,8) = ((1 - Y_aa) * f_h2aa);
St_C(6,10) = v_10_6;
St_C(6,11) = N_aa - (Y_aa * N_bac);
St_C(6,18) = Y_aa;
St_C(7,3) = -1;
St_C(7,7) = (1 - Y_fa) * 0.7;
St_C(7,8) = (1 - Y_fa) * 0.3;
St_C(7,10) = v_10_7;
St_C(7,11) = -Y_fa * N_bac;
St_C(7,19) = Y_fa;
St_C(8,4) = -1;
St_C(8,6) = ((1 - Y_c4) * 0.54);
St_C(8,7) = ((1 - Y_c4) * 0.31);
St_C(8,8) = ((1 - Y_c4) * 0.15);
St_C(8,10) = v_10_8;
St_C(8,11) = (-Y_c4 * N_bac);
St_C(8,20) = Y_c4;
St_C(9,5) = -1;
St_C(9,7) = ((1 - Y_c4) * 0.8);
St_C(9,8) = ((1 - Y_c4) * 0.2);
St_C(9,10) = v_10_9;
St_C(9,11) = (-Y_c4 * N_bac);
St_C(9,20) = Y_c4;
St_C(10,6) = -1;
St_C(10,7) = ((1 - Y_pro) * 0.57);
```

```
St_C(10,8) = ((1 - Y_pro) * 0.43);
St_C(10,10) = v_10_10;
St_C(10,11) = (-Y_pro * N_bac);
St_C(10,21) = Y_pro;
St_C(11,7) = -1;
St_C(11,9) = (1 - Y_ac);
St_C(11,10) = v_10_11;
St_C(11,11) = (-Y_ac * N_bac);
St_C(11,22) = Y_ac;
St_C(12,8) = -1;
St_C(12,9) = (1 - Y_h2);
St_C(12,10) = v_10_12;
St_C(12,11) = (-Y_h2 * N_bac);
St_C(12,23) = Y_h2;
St_C(13,10) = v_10_13;
St_C(13,11) = N_bac - N_xc;
St_C(13,13) = 1;
St_C(13,17) = -1;
St_C(14,10) = v_10_14;
St_C(14,11) = (N_bac - N_xc);
St_C(14,13) = 1;
St_C(14,18) = -1;
St_C(15,10) = v_10_15;
St_C(15,11) = (N_bac - N_xc);
St_C(15,13) = 1;
St_C(15,19) = -1;
St_C(16,10) = v_10_16;
St_C(16,11) = (N_bac - N_xc);
St_C(16,13) = 1;
St_C(16,20) = -1;
St_C(17,10) = v_10_17;
St_C(17,11) = (N_bac - N_xc);
St_C(17,13) = 1;
```

```
St_C(17,21) = -1;
St_C(18,10) = v_10_18;
St_C(18,11) = (N_bac - N_xc);
St_C(18,13) = 1;
St_C(18,22) = -1;
St_C(19,10) = v_10_19;
St_C(19,11) = (N_bac - N_xc);
St_C(19,23) = -1;

%Acid - Base Equations
St_C(20,27) = -1;
St_C(21,28) = -1;
St_C(22,29) = -1;
St_C(23,30) = -1;
St_C(24,31) = -1;
St_C(25,32) = -1;

%Gas Transfer Equations
St_C(26,8) = -1;
St_C(27,9) = -1;
St_C(28,10) = -1;
St_C(26,33) = (V_liq/V_gas);
St_C(27,34) = (V_liq/V_gas);
St_C(28,35) = (V_liq/V_gas);

%%pH Calculation
%In order to calculate pH, concentration of hydrogen should be calculated.
%The charge balance in implemented ADM1 has the term Sh and SOH which is a
%function of Sh. Therefore, Terms with Sh are taken out of the equation and
%rest is called theta. Sum of theta and Sh terms is equal to 0.
%Calculation of Theta
Theta = S_cat - S_an + (S_IN - S_IN_ac) - S_IC_ac - (S_ac_ac/64) - (S_pro_ac/112) -
(S_bu_ac/160) - (S_va_ac/208);
```

```
 %Calculation of Sh
Sh = -Theta * 0.5 + 0.5 * sqrt((Theta^2) + 4 * K_w);

%%Process Inhibition
%K_pH values, function of lower and upper pH limit are calculated with the
%following formula for amino acids, hydrogen and acetate. Then, Hill
%(Inhibition) Functions are calculated. After that, inhibition terms that
%belong to pH, nitrogen, hydrogen (depending on fatty acid, valerate and
%butyrate, propionate) and ammonia are calculated. Lastly, inhibition
%equations are solved.

%K_pH Equations
K_pH_aa = 10^(-(0.5 * (pH_LL_aa + pH_UL_aa)));       %Amino_Acids
K_pH_h2 = 10^(-(0.5 * (pH_LL_H2 + pH_UL_H2)));       %Hydrogen
K_pH_ac = 10^(-(0.5 * (pH_LL_ac + pH_UL_ac)));       %Acetate

%Hill Inhibition Function Calculations
I_pH_aa = (((K_pH_aa^24)/(Sh^(24) + K_pH_aa^(24))));  %Amino_Acids
I_pH_h2 = (((K_pH_h2^3)/(Sh^(3) + K_pH_h2^(3))));     %Hydrogen
I_pH_ac = (((K_pH_ac^45)/(Sh^(45) + K_pH_ac^(45))));  %Acetate

%Inhibition Terms Calculations
I_lim = 1/(1 + (Ks_IN/S_IN));                  %Nitrogen_Inhibition
I_h2_fa = 1/(1 + (S_h2/Ki_h2_fa));             %Hydrogen_Inhibition on Fatty Acid
I_h2_c4 = 1/(1 + (S_h2/Ki_h2_c4));             %Hydrogen_Inhibition on Valerate and
Butyrate
I_h2_pro = 1/(1 + (S_h2/Ki_h2_pro));           %Hydrogen_Inhibition on Propinate
I_NH3 = 1/(1 + (S_IN_ac/Ki_NH3));              %Ammonia_Inhibition

%Inhibition Equations
I_5 = I_pH_aa * I_lim;
I_6 = I_pH_aa * I_lim;
I_7 = I_pH_aa * I_lim * I_h2_fa;
```

```
I_8 = I_pH_aa * I_lim * I_h2_c4;
I_9 = I_pH_aa * I_lim * I_h2_c4;
I_10 = I_pH_aa * I_lim * I_h2_pro;
I_11 = I_pH_ac * I_lim * I_NH3;
I_12 = I_pH_h2 * I_lim;

%%Gas Pressure
%Gas pressure of each element in biogas is calculated as following
%formulas. Partial pressure of gases are necessary to calculate for
%evaluation of their concentration.

%Calculation of Water Vapor Pressure in Biogas
P_gas_H2O = 0.0313 * exp(5290 * kT);

%Calculation of Partial Pressure of Hydrogen, Methane and Carbon Dioxide
P_gas_h2 = ((S_h2_gas * R * T)/16);
P_gas_ch4 = (S_ch4_gas * R * T/64);
P_gas_co2 = S_co2_gas * R * T;

%Calculation of Partial Pressure of Nitrogen
pn2 = P_atm - P_gas_H2O;

%Total Pressure
P_gas = pn2 + P_gas_h2 + P_gas_ch4 + P_gas_co2 + P_gas_H2O;

%Gas Flowrate Calculation
q_gas = kp * (P_gas - P_atm) * (P_gas/P_atm);
if q_gas<0
q_gas = 0;
else
q_gas = kp * (P_gas - P_atm) * (P_gas/P_atm);
end
```

```
%%Rates Equations
%Biochemical Rate Equations
Rate1 = k_dis * X_c;
Rate2 = khyd_ch * X_ch;
Rate3 = khyd_pr * X_pr;
Rate4 = khyd_li * X_li;
Rate5 = km_su * (S_su/(Ks_su + S_su)) * X_su * I_5;
Rate6 = km_aa * (S_aa/(Ks_aa + S_aa)) * X_aa * I_6;
Rate7 = km_fa * (S_fa/(Ks_fa + S_fa)) * X_fa * I_7;
Rate8 = km_c4 * (S_va/(Ks_c4 + S_va)) * X_c4 * (S_va/(S_va + S_bu + 1E-6)) * I_8;
Rate9 = km_c4 * (S_bu/(Ks_c4 + S_bu)) * X_c4 * (S_bu/(S_va + S_bu + 1E-6)) * I_9;
Rate10 = km_pro * (S_pro/(Ks_pro + S_pro)) * X_pro * I_10;
Rate11 = km_ac * X_ac * S_ac/(Ks_ac + S_ac) * I_11;
Rate12 = km_h2 * (S_h2/(S_h2 + Ks_h2)) * X_h2 * I_12;
Rate13 = k_dec * X_su;
Rate14 = k_dec * X_aa;
Rate15 = k_dec * X_fa;
Rate16 = k_dec * X_c4;
Rate17 = k_dec * X_pro;
Rate18 = k_dec * X_ac;
Rate19 = k_dec * X_h2;

%Acid - Base Rate Equations
RateA4 = kab_va * (S_va_ac * (Ka_va + Sh) - Ka_va * S_va);
RateA5 = kab_bu * (S_bu_ac * (Ka_bu + Sh)- Ka_bu * S_bu);
RateA6 = kab_pro * (S_pro_ac * (Ka_pro + Sh) - Ka_pro * S_pro);
RateA7 = kab_ac * (S_ac_ac * (Ka_ac + Sh) - Ka_ac * S_ac);
RateA10 = kab_CO2 * (S_IC_ac * (Ka_IC + Sh) - Ka_IC * S_IC);
RateA11 = kab_IN * (S_IN_ac * (Ka_IN + Sh) - Ka_IN * S_IN);

%Gas Transfer Rate Equations
RateT8 = kla * (S_h2 - 16 * Kh_h2 * P_gas_h2);
RateT9 = kla * (S_ch4 - 64 * Kh_ch4 * P_gas_ch4);
```

```
RateT10 = kla * ((S_IC - S_IC_ac) - Kh_co2 * P_gas_co2);

%In order to solve differential equations, firstly, matrix with size of
%[1 x 28] for rates is created. Then, it is multiplied with the
%stoichiometric coefficient matrix, St_C, with size of [28 x 35] created
%before. This multiplication gives generation & consumption term in a
%general material balance equation which is shown as Gen_Con below. Then, 2
%matrix with size of [1 x 35] for state input variables are
%created. Differential equations are solved as output of this MATLAB
%function.

%Rate Matrix
Rate = [Rate1 Rate2 Rate3 Rate4 Rate5 Rate6 Rate7 Rate8 Rate9 Rate10 Rate11
Rate12 Rate13 Rate14 Rate15 Rate16 Rate17 Rate18 Rate19 RateA4 RateA5 RateA6
RateA7 RateA10 RateA11 RateT8 RateT9 RateT10];

Gen_Con = Rate * St_C;
Gen_Con = Gen_Con';
SRT = (q_in/V_liq);
SRT_gas = (q_gas/V_gas);

%State Input Variable Matrix
S_out = [S_su S_aa S_fa S_va S_bu S_pro S_ac S_h2 S_ch4 S_IC S_IN S_I X_c X_ch
X_pr X_li X_su X_aa X_fa X_c4 X_pro X_ac X_h2 x_I S_cat S_an 0 0 0 0 0 0
(SRT_gas*S_h2_gas/SRT) (SRT_gas*S_ch4_gas/SRT)
((SRT_gas*S_co2_gas)/SRT)].';
S_in = [S_su_in S_aa_in S_fa_in S_va_in S_bu_in S_pro_in S_ac_in S_h2_in S_ch4_in
S_IC_in S_IN_in S_I_in X_c_in X_ch_in X_pr_in X_li_in X_su_in X_aa_in X_fa_in
X_c4_in X_pro_in X_ac_in X_h2_in X_I_in S_cat_in S_an_in S_va_ac_in S_bu_ac_in
S_pro_ac_in S_ac_ac_in S_IC_ac_in S_IN_ac_in S_h2_gas_in S_ch4_gas_in
S_co2_gas_in].';

%Differential Equation
```

```
dS = (SRT * S_in - SRT * S_out + Gen_Con);
end
```

C.3. ADM1 Digester

```
%%This MATLAB codes are developed for solving differential equations that
%%were created as another MATLAB code function,
%%ADM1_Digester_3CSTRS_in_Series_fun. Input values that are needed in that
%%function are inserted in this pack of codes. As an output, methane
%%concentration is obtained, and its plot versus time is drawn.

clear all
clc
Variables();
options = odeset('NonNegative', 1:35, 'Reltol', 1E-7, 'AbsTol', 1E-6);

%initial values
%C(1)   Sugar
%C(2)   Amino_Acid
%C(3)   Long_Chain_Fatty_Acids_(LCFA)
%C(4)   Valerate
%C(5)   Butyrate
%C(6)   Propionate
%C(7)   Acetate
%C(8)   Dissolved_Hydrogen
%C(9)   Dissolved_Methane
%C(10)  Inorganic_Carbon
%C(11)  Inorganic_Nitrogen
%C(12)  Dissolved_Inerts
%C(13)  Composites_(Dead_Cells)
%C(14)  Particulate_Carbohydrates
%C(15)  Particulate_Proteins
```

```
%C(16)  Particulate_Lipids
%C(17)  Sugars_(Biomass)
%C(18)  Amino_Acids_(Biomass)
%C(19)  Fatty_Acids_(Biomass)
%C(20)  Butyrate_and_Valerate_(Biomass)
%C(21)  Propinate_(Biomass)
%C(22)  Acetate_(Biomass)
%C(23)  Hydrogen_(Biomass)
%C(24)  Particulate_Inerts
%C(25)  Cations
%C(26)  Anions
%C(27)  Valeric_Acid
%C(28)  Butyrica_Acid
%C(29)  Propionic_Acid
%C(30)  Acetic_Acid
%C(31)  Bicarbonate
%C(32)  Ammonia
%C(33)  Hydrogen_Gas
%C(34)  Methane_Gas
%C(35)  Carbon_Dioxide_Gas

%Input Matrix
ss = [0 0 0 0 0 0 0 0 0 0 0 0 0 0 0 0 0 0 0.05 0.05 0.05 4 4 25 0.5 0 0.04 0.02 0 0 0 0 0 0 0 0
0];

T = 310.55;                         %Temperature_(K)
kp = 5E4*1000;                      %Constant_for_Gas_Supply (L/d*atm)
R = 0.083145;                       %Ideal_Gas_Constant (L*bar/K*mol)
P_atm = 1.013;                      %Atmospheric_Pressure_(atm)
V_liq = 39/3;                       %Liquid_Volume_(L)
SRT = 64.61/3;                      %Solid_Residence_Time_(days)

%OLR For Husk
```

```
OLR_C = (2.137078271/21)/3;
%Organic_Loading_Rate_for_Carbohydrates_(kgCOD/L*d)_(Total_in_39L)
OLR_P = (2.550127012/21)/3;
%Organic_Loading_Rate_for_Proteins_(kgCOD/L*d)_(Total_in_39L)
OLR_L = (5.20800587/21)/3;
%Organic_Loading_Rate_for_Lipids_(kgCOD/L*d)_(Total_in_39L)
OLR_S = (2.047285066/21)/3;
%Organic_Loading_Rate_for_Sugars_(kgCOD/L*d)_(Total_in_39L)
OLR_Ca = (0.004256198/21)/3;
%Organic_Loading_Rate_for_Cations_(kgCOD/L*d)_(Total_in_39L)
OLR_A = (1.07752E-05/21)/3;
%Organic_Loading_Rate_for_Anions_(kgCOD/L*d)_(Total_in_39L)

% %OLR For Food Waste
% OLR_C = (2.241801742/21)/3;
%Organic_Loading_Rate_for_Carbohydrates_(kgCOD/L*d)_(Total_in_39L)
% OLR_P = (2.675091154/21)/3;
%Organic_Loading_Rate_for_Proteins_(kgCOD/L*d)_(Total_in_39L)
% OLR_L = (5.463214329/21)/3;
%Organic_Loading_Rate_for_Lipids_(kgCOD/L*d)_(Total_in_39L)
% OLR_S = (2.147608391/21)/3;
%Organic_Loading_Rate_for_Sugars_(kgCOD/L*d)_(Total_in_39L)
% OLR_Ca = (0.004464765/21)/3;
%Organic_Loading_Rate_for_Cations_(kgCOD/L*d)_(Total_in_39L)
% OLR_A = (1.13032E-05/21)/3;
%Organic_Loading_Rate_for_Anions_(kgCOD/L*d)_(Total_in_39L)

tic

%For Husk
OLR = (1.79586409302326/21)/3;
%Organic_Loading_Rate_for_Husk_(kgVS/L*d)
Carbohydrates = OLR_C*SRT*0.66196;          %Carbohydrates_Input_(kgCOD/L)
```

```
Proteins = OLR_P*SRT*0.328187418;          %Proteins_Input_(kgCOD/L)
Lipids = OLR_L*SRT*0.009845623;            %Lipids_Input_(kgCOD/L)
Sugars = OLR_S*SRT*0;                      %Sugars_Input_(kgCOD/L)
Cations = OLR_Ca*SRT*0;                    %Cations_(kgCOD/L)
Anions = OLR_A*SRT*0;                      %Aninons_(kgCOD/L)

% %For food waste
% OLR = (1.88386701/21)/3;                 %Organic_Loading_Rate_for_Food_Waste
% Carbohydrates = OLR*SRT*0.626991321;     %Carbohydrates_Input
% Proteins = OLR*SRT*0.348319699;          %Proteins_Input
% Lipids = OLR*SRT*0.02468898;             %Lipids_Input
% Sugars = OLR*SRT*0;                      %Sugars_Input
% Cations = OLR*SRT*0;                     %Cations
% Anions = OLR*SRT*0;                      %Anions

%Time
to = 0;                                    %Initial_Time
tf = 21;                                   %Final_Time

for j = 1:1:1

tspan = to:1:tf;

[t C] =
ode15s(@ADM1_Digester_3CSTRS_in_Series_fun,tspan,ss,options,Carbohydrates,Pro
teins,Lipids,Sugars,Cations,Anions,SRT);

S_su_in = C(21,1);
S_aa_in = C(21,2);
S_fa_in = C(21,3);
S_va_in = C(21,4);
S_bu_in = C(21,5);
S_pro_in = C(21,6);
```

```
S_ac_in = C(21,7);
S_h2_in = C(21,8);
S_ch4_in = C(21,9);
S_IC_in = C(21,10);
S_IN_in = C(21,11);
S_I_in = C(21,12);
X_c_in = C(21,13);
X_ch_in = C(21,14);
X_pr_in = C(21,15);
X_li_in = C(21,16);
X_su_in = C(21,17);
X_aa_in = C(21,18);
X_fa_in = C(21,19);
X_c4_in = C(21,20);
X_pro_in = C(21,21);
X_ac_in = C(21,22);
X_h2_in = C(21,23);
X_I_in = C(21,24);
S_cat_in = C(21,25);
S_an_in = C(21,26);
S_va_ac_in = C(21,27);
S_bu_ac_in = C(21,28);
S_pro_ac_in = C(21,29);
S_ac_ac_in = C(21,30);
S_IC_ac_in = C(21,31);
S_IN_ac_in = C(21,32);
S_h2_gas_in = C(21,33);
S_ch4_gas_in = C(21,34);
S_co2_gas_in = C(21,35);

ss = [0 0 0 0 0 0 0 0 0 0 0 0 0 0 0 0 0.05 0.05 0.05 4 4 25 0.5 0 0.04 0.02 0 0 0 0 0 0 0 0
0];
```

```
Sugars = C(21,1);
Carbohydrates = C(21,14);
Proteins = C(21,15);
Lipids = C(21,16);
Cations = C(21,25);
Anions = C(21,26);

end

%Partial Pressure of Bioagas Contents
P_gas_h2o = 0.0313*exp(5290*((1/298.15) - (1/T)));
%Partial_Pressure_of_Water
P_gas_h2 = ((C(:,33)*R*T)/16);                    %Partial_Pressure_of_Hydrogen
P_gas_ch4 = (C(:,34)*R*T/64);                     %Partial_Pressure_of_Methane
P_gas_co2 = C(:,35)*R*T;
%Partial_Pressure_of_Carbon_Dioxide
P_n2 = P_atm - P_gas_h2o;                         %Partial_Pressure_of_Nitrogen
P_gas = P_n2 + P_gas_h2 + P_gas_ch4 + P_gas_co2 + P_gas_h2o;
%Total_Gas_Pressure

%Calculation of Gas Flowrate
q_gas = kp*(P_gas - P_atm).*(P_gas./P_atm);       %Gas_Flowrate (L/d)
k = find(q_gas<0);
q_gas(k) = 0;

%Methane Flowrate
CH4 = q_gas.*((P_gas_ch4./P_gas))/(OLR*V_liq);
%Methane_Yield_(L/kgVS)
Qch4 = CH4 * (OLR*V_liq);                         %Methane_Flowrate_(L/d)
toc

%Methane Flowrate vs Time Plot
plot(t,CH4)
```

```
plot(t,Qch4)
xlabel('Time (days)');
ylabel('Methane Yield (mL/gVS)');
legend('Reactor 1');

%Animation
h = animatedline;
for i=1:length(t)
addpoints(h,t(i),Qch4(i));
drawnow;
pause(0.1);
end
```